University of Padova

Department of Management and Engineering DTG

Master's Thesis in Product Innovation Engineering

Experimental and numerical analyses of a PCM latent thermal storage for air-conditioning applications

Supervisor
Prof.ssa Giulia Righetti

Co-supervisor
Ch.ssmo Prof. Claudio Zilio

Master Candidate
Alessandro Buosi

Student ID
1241988

Academic Year
2021-2022

Abstract

In this thesis a 18 kWh latent thermal energy storage (LTES) which uses the roll-bond technology to efficiently store and release cold energy thanks to the phase change of 300 kg of a bio-based PCM with a melting temperature of 9 °C (CRODATERM9.5) has been experimentally and numerically studied. This energy storage can be coupled with a chiller (AC system) to store cold energy for domestic air conditioning. The experimental tests were carried out by varying the flow rate and inlet temperature of the water in order to identify their effects on the energy stored and the temperature field inside the PCM. Also some numerical simulations were conducted, the first ones were used to validate the model so that the behaviour can be predicted through the simulations without the need for experimentally studying every possible combination of temperature and flow rate of water.

SOMMARIO

In questa tesi è stato studiato numericamente e sperimentalmente un accumulo termico latente di 18 kWh che utilizza la tecnologia dei roll-bond per caricare e scaricare "freddo" all'interno di circa 300 kg di un materiale di origine biologica a cambiamento di fase (PCM) che presenta una temperatura di fusione di circa 9 °C (CRODATERM 9.5). Questo accumulo termico può essere asservito ad un impianto ad aria condizionata per disaccoppiare la produzione dalla richiesta di "freddo" e quindi aumentare l'efficienza del sistema. Nell'introduzione sono illustrati i motivi principali per cui è necessario ridurre le emissioni di CO_2 e le principali tecnologie che permettono di farlo. Uno dei principali problemi dei PCM (come quello utilizzato in questo caso) è la bassa conduttività termica, in letteratura sono presenti molti studi per cercare di migliorare questo aspetto negativo. Le soluzioni sono solitamente molto costose e spesso non sono realizzabili per un accumulo con delle dimensioni come quello studiato. Quindi la tecnologia dei roll-bond in alluminio , che viene già utilizzata per realizzare gli evaporatori per i frigoriferi, è stata utilizzata per migliorare lo scambio termico tra l'acqua e il PCM senza aumentare eccessivamente i costi. Successivamente viene spiegato come è stato realizzato l'impianto sperimentale. Come prima cosa è stato deciso il numero e la posizione delle termocoppie per monitorare il campo di temperatura all'interno dell'accumulo. In seguito le termocoppie sono state collegate all'ice point reference (IPR) e al sistema di acquisizione. Poi è stato realizzato il programma LabView che viene utilizzato per salvare i dati con una frequenza di circa 0.15 Hz (ogni 6.5 secondi). Si è deciso di inserire 39 termocoppie all'interno del PCM, inoltre è stata monitorata anche la portata e le temperature dell'acqua in ingresso e in uscita. L'obiettivo della tesi è quello di studiare il comportamento dell'accumulo termico al variare delle condizioni operative, quindi questo è stato posto all'interno della camera climatica ed è stato collegato al circuito idronico di un chiller che permette di avere acqua alla temperatura e portata desiderata. Le prove sono state effettuate variando la portata d'acqua (sia per la fase di carica che per la fase di scarica), la temperatura dell'acqua (sia per la fase di carica che di scarica) e anche la circuitazione dell'acqua all'interno dei roll-bond. I dati sperimentali ottenuti sono poi stati elaborati, in questa fase è stata anche valutata l'incertezza sperimentale combinata. I parametri sono stati variati in base all'esperienza ottenuta grazie ai risultati che si ottenevano dalle prove precedenti.
In parallelo alle prove sperimentali sono state realizzate anche delle simulazioni numeriche tramite software Ansys Fluent. Il modello utilizzato è bidimensionale, è stata considerata una coppia di roll-bond e il PCM in mezzo ad essi. Le condizioni al contorno utilizzate sono di simmetria nella parte destra e sinistra, e di adiabaticità sopra e sotto. Come condizioni iniziali sono stati usati i dati sperimentali. Il modello è stato validato rispetto ai dati sperimentali, la differenza principale tra le simulazioni e i dati sperimentali è che numericamente non è possibile simulare il fenomeno del sottoraffreddamento che avviene nel PCM nella realtà. Grazie alle simulazioni è stato possibile studiare una differente configurazione dei roll-bond e i risultati sono stati confrontati con quelli sperimentali. Inoltre è stata valutata l'influenza sul tempo richiesto per la carica e la scarica al variare della distanza tra i roll-bond.
Le principali osservazioni sono:

- L'accumulo termico richiede più di 8 ore per essere completamente caricato, anche per la fase di scarica è richiesto molto tempo.
- È stato osservato che la temperatura di ingresso dell'acqua ha un'effetto maggiore rispetto alla portata.
- L'inversione tra ingresso e uscita dei condotti di alimentazione dell'acqua non porta a nessun beneficio.
- Invece il collegamento completamente in parallelo dei roll-bond aumenta l'energia immagazzinata per la prima ora.
- Il modello numerico bidimensionale permette di descrivere adeguatamente il sistema reale.
- Anche l'influenza della distanza tra i roll-bond sull'energia immagazzinata è stata numericamente studiata. È stato trovato che diminuendo questa distanza il tempo di carica e scarica diminuisce in modo significativo.

- Dai risultati sperimentali è stato osservato che nella parte inferiore dell'accumulo si forma una zona "fredda" dove il PCM impiega molto tempo a sciogliersi durante la fase di scarica.

Alcuni sviluppi futuri potrebbero essere:

- Misure sperimentali di viscosità e coefficiente di espansione termica in modo tale da migliorare l'accuratezza delle simulazioni.
- Ottimizzazione della geometria dell'accumulo termico (rapporto altezza-larghezza).
- Ottimizzazione della geometria dei roll-bond in modo tale da migliorare lo scambio termico tra l'acqua e il PCM.
- L'effetto delle distanza tra i roll-bond e il numero dei roll-bond stessi.
- Studiare il sistema complessivo, ovvero l'accumulo termico associato alla pompa di calore.

Contents

List of figures

List of tables

List of acronyms

3LC ..... Three-Layer Calorimetry
AI ..... Artificial Intelligence
AMI ..... Advanced Metering Infrastructure
BAS ..... Building Automation System
BICPV ..... Building-Integrated Concentrated Photovoltaic
COP ..... Coefficient of Performance
CSP ..... Concentrated Solar Power Plants
DSC ..... Differential Scanning Calorimetry
EMIS ..... Energy Management and Information Systems
EV ..... Electric Vehicles
GEB ..... Grid-interactive Efficient Buildings
GWP ..... Global Warming Potential or Greenhouse Warming Potential
HTF ..... Heat Transfer Fluid
HVAC ..... Heat,Ventilating and Air Conditioning
IEA ..... International Energy Agency
IoT ..... Internet of Things
IPR ..... Ice Point Reference
LTES ..... Latent Thermal Energy Storage
ML ..... Machine learning
PCM ..... Phase Change Materials
PV ..... Photovoltaic
TCES ..... Thermochemical Energy Storage
TES ..... Thermal Energy Storage
TIM ..... Transparent Insulation Materials
TTES ..... Tank Thermal Energy Storage
VRE ..... Variable Renewable Energy
ZEB ..... Zero Energy Buildings

1 Introduction

Nowadays, we are living a climate and energy crisis, as developing countries grow also their power consumption grows and therefore the emissions. In 2021 the global CO_2 emissions reached 37 Gt (gigatonnes) as reported by IEA [1]. As stated by IRENA [2] climate change has become one of the biggest concern of this century, the only way of solving this problem is an energy transformation in order to reduce the carbon emissions that cause climate change. The Paris Agreement, as stated by the United Nations (UN) [3] establishes a clear goal to limit the increase of global temperature to below 2 °C, and ideally below 1.5 °C, compared to pre-industrial levels, by the end of this century. The global energy production system is under pressure to change from fossil fuel energy production to renewable energy in order to alleviate this problem and in order to reach the climate goals agreed upon in Paris. The objective is the rapid substitution of conventional fossil fuel generation with low-carbon technologies. There are also other reasons to reduce the carbon emissions as shown in Figure 1.1. Another important objective is to improve the power grids efficiency and energy flexibility such that peak hours demand is more evenly distributed throughout the day. In recent years the cost for electricity from renewable generation has kept falling, considering all of the commercially available technologies. This is especially true for PV cost which fell 82% in the last decade, onshore wind fell 45% as reported by IRENA [2], and the price is expected to fall even further. An important aspect it is air pollution which is a major public health crisis, caused mainly by unregulated, inefficient and highly polluting energy sources. The switch to clean energy along with electromobility would improve the air quality and reduce illness caused by pollution, thus every dollar spent in transforming the global energy system potentially provides a payoff of more than 7 USD of savings in improved health and lowers the impact of climate change [2]. The transformation of the global energy system would lead to clean energy access for everyone because even today a large amount of people doesn't have access to energy. Renewable energy, as opposed to traditional technologies, can be set up even in rural areas bringing electrification to rural communities. Renewables can provide a secure alternative to fossil fuels, especially for countries which are heavily dependent on imported fossil fuels. The transition process itself will bring profound structural changes in labour markets, resulting in four types of job effects: job creation, elimination, substitution and transformation [2].

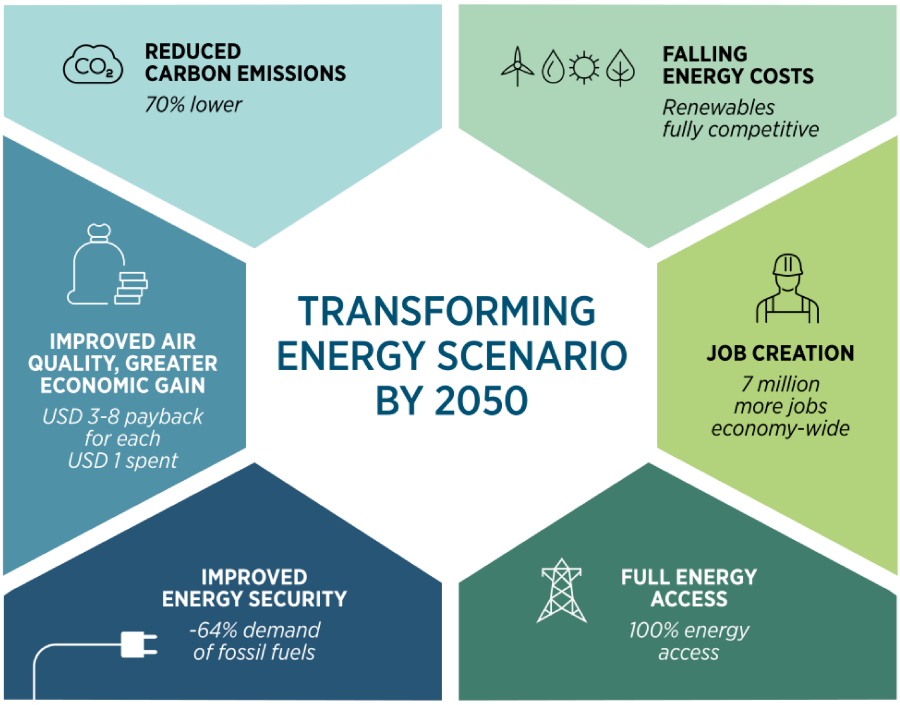

Figure 1.1: Pressing needs and opportunities, from IRENA

The five technology pillars for the future of energy are as follows:

- *Electrification*
- *Increased power system flexibility*
- *Conventional renewable resources*
- *Green hydrogen*
- *Foster innovation to address challenging sector*

Electrification

As described by IRENA [2] the price for renewable power generation technologies in the last decade have been falling despite lower renewable energy subsidies and slowing global GDP growth. In the Transforming Energy Scenario, electricity would become the central energy carrier by 2050, growing from 20% share of final consumption to an almost 50% share; as a result, gross electricity consumption would more than double. The rate of growth in the share of electricity usage is set to quadruple, an additional 1000 terawatts-hours (TWh) of electricity production has to be added to the electric grid every year on top of current plans, in order to satisfy the energy demand growth. This energy needs is equivalent to adding the entire electricity generation of Japan every year. To supply this additional renewable electricity demand, over 520 gigawatts (GW) of new renewable capacity would need to be added per year. In parallel, the share of renewable electricity in generation has to rise from 26% currently to 57% by 2030 and to 86% by 2050. This rise is being accelerated by declining costs: $\frac{4}{5}$ of solar PV and wind projects to be commissioned in 2020 will produce electricity cheaper than any fossil-fuel alternative [2]. The electrification

of end uses will drive increased power demand to be met with renewables. In the transport sector, the number of electric vehicles (EVs) will increase from around 8 millions in 2019 to over 1100 millions following the Transformation Energy Scenario by 2050. For the heating sector, heat pumps offer efficiency gains ranging from two to four times higher than conventional heating systems, and the number of heat pumps installed by 2050 would need to increase 10-fold. The shift to those highly efficient electrification technologies also brings increases in energy efficiency. In Figure 1.2 the steps required in the future in order to achieve the objective of the Transformation Energy Scenario by 2050 are shown.

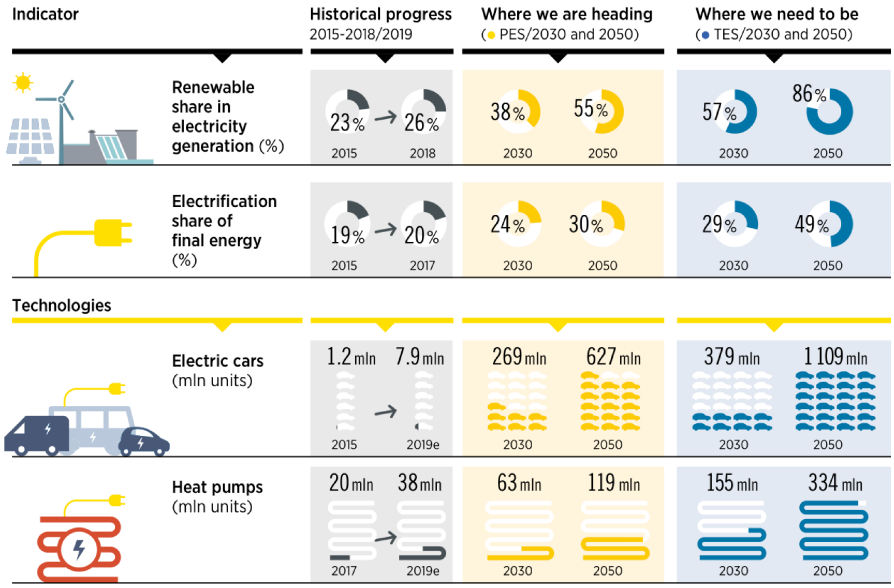

Figure 1.2: Steps for an increased electrified energy system

Increased power system flexibility

In order to have high shares of variable renewable energy connected to the power grid, systems need to be more flexible. Today, countries are integrating Variable Renewable Energy (VRE) at a share of over 30% on annual basis (and in some cases much higher), which means that instantaneous penetration of VRE can, at times, approach, or even exceed, electricity demand. In the Transforming Energy Scenario, 73% of the installed capacity and over 60% of all power generation would come from variable resources (solar PV and wind), up from 10% of power generation today. In order to achieve the necessary flexibility of power systems, both long term and short term storage technologies are essential, and the amount of stationary storage (which excludes EVs) would need to expand from around 30 gigawatts-hours (GWh) today to over 9000 GWh by 2050. When storage available to the grid from the EV fleet is included, this value will increase from 14000 GWh to 23000 GWh. However, most flexibility will still be achieved through other measures, including grid expansion and operational measures, demand-side flexibility and sector coupling. IRENA [2] estimates that smart solutions, such as smart charging EVs, can significantly facilitate the integration of VRE by leveraging storage capacity and the flexibility potential of the demand side. Investment in end-use electrification, power grids and flexibility will need to increase from USD 13 trillion in the

Planned Energy Scenario to USD 26 trillion in the Transforming Energy Scenario over the period to 2050.

Conventional renewable resources

As reported by IRENA [2] hydropower, bioenergy, solar thermal and geothermal renewable energy all have significant scale-up potential and represent over $\frac{1}{4}$ of the mitigation potential in the Transforming Energy Scenario. Two technologies that can play particularly important roles are hydropower and bioenergy. In the Transforming Energy Scenario, hydropower capacity would need to increase 25% by 2030, and 60% by 2050, while pumped hydro storage capacity would need to double. When including both types of hydropower, around 850 GW of newly installed capacity is required in the next 30 years - or roughly adding the entire power system capacity of the European Union in 2020. The synergies between hydropower and other renewable energy technologies in power system operation include the cost effectiveness of using hydropower to counteract the short-term variability of wind and solar generation, and seasonal complementaries in resource patterns. Multipurpose hydropower infrastructure also can provide co-benefits such as regulating river flows and reducing flooding. Increasing hydropower capacity does not specifically entail only building new dams: options also exist to upgrade turbines and systems in existing plants, utilise run-of-river designs and electrify non-power dams. However for new hydropower plants, planners need to consider local environmental impacts, and engage in discussions with communities in the impacted areas. Hydropower plants will also need operational changes that reflect changing power systems needs, including faster and more frequent ramping, and planning practices that include evaluating the impacts of climate change on water supply and reservoir storage requirements. Due to longer planning cycles for new hydropower construction, policy makers and planners need to start thinking about new projects now. For existing dams, investments are needed in order to modernise old hydro power plants [2]. Bioenergy will become increasingly vital in end-use sectors. Bioenergy makes up a large share of renewable energy use today and it's going to play a big role as a fuel for heat and power generation in industry and for the transport sector. The share of primary energy that is met with modern bioenergy (which excludes traditional uses of biofuel) will increase from 5% today to 10% in the Planned Energy Scenario. In the Transforming Energy Scenario, bioenergy plays an important role, especially in some sectors that are hard to electrify such as shipping and aviation and also for the industry sector, both for process heat and use as a feedstock. In the Transforming Energy Scenario, the share of primary energy met with modern bioenergy should increase to 23%. Meanwhile, traditional uses of bioenergy, which cover a large share of bioenergy demand today, must be phased out and replaced with cleaner options, inculding modern bioenergy and other renewables. Bioenergy must be produced in ways that are environmentally, socially and economically sustainable. The potential to produce bioenergy cost effectively and sustainably on existing farmlands and grasslands is enormous, likewise to use residues from existing production forests without encroaching upon rainforests. Bioenergy from such sources would make use of surplus crop potential and not threaten food production [2].

Green hydrogen

Hydrogen it is important for energy demands that are not easily electrified. Today around 120 megatonnes (Mt) (14 EJ) of hydrogen is produced per year, but almost all of it is produced using fossil fuels or from electricity generated by fossil fuels, with high carbon footprint obviously; less than 1% is "green" hydrogen. Nonetheless progress is being made and in early 2020 the world's largest green hydrogen production plant with 10 MW electrolyser capacity began operation in Japan. Green hydrogen means that it is produced using only renewable electricity, this is possible through the electrolysis process whose cost is steadily decreasing. Green hydrogen will become cost

competitive with "blue" hydrogen (produced using fossil fuels in combination with carbon capture and storage) in the next few years in locations with favourable low-cost renewable electricity. It's expected that green hydrogen will be cheaper than blue hydrogen in many locations within the next 5 to 15 years as costs keep falling. Some energy-intensive industries may in the future relocate to areas with good renewable energy resources to tap this potential to produce cheap green hydrogen. A plus of hydrogen is that it can be processed further in order to obtain hydrocarbons or ammonia, which can help reducing emissions in sectors like shipping and aviation. The natural gas industry is also looking at hydrogen as a promising solution for greening the gas system and extending the life of existing infrastructures. However, this approach must be viewed with caution in light of unclear prospects of actually being able to significantly reduce emissions of the gas system and the potential to lock in carbon-intensive infrastructures. Hydrogen can become the energy vector that allows to tap into ample remote, low-cost renewable energy resources, this could accelerate even more the demand for renewable power generation. The target of The Energy Transforming Scenario is to have 160 Mt (19 EJ) of green hydrogen annually produced by 2050. That amount, however, would only cover 5% of global energy demand today, with an additional 2.5% being met by blue hydrogen. Significant scale-up of electrolysers is required to produce the amount necessary by the Transforming Scenario, requiring additions of between 50 GW and 60 GW per year of new capacity from now until 2050.

Foster innovation to address challenging sectors

In the Transforming Energy Scenario, half of the energy demand could be supplied by electricity by 2050, but the remaining half must also be considered. Of the remaining energy demand $\frac{1}{3}$ is already supplied by end-use renewable sources, with the remaining $\frac{2}{3}$ by fossil fuels. Solutions to further reduce fossil-fuel use include increased direct use of renewable energy (bioenergy, solar thermal, geothermal heat), energy efficiency and structural changes that can reduce energy demand, and deeper electrification. However, more will still be needed, in particular for sectors such as shipping, aviation and heavy industry. To put it in prospective, $\frac{3}{4}$ of the remaining emissions in the Transforming Energy Scenario in 2050 are from the aviation, shipping and heavy industry sectors [2]. The Deeper Decarbonisation Perspective (DDP) includes the steps necessary to reduce the remaining emissions. The Deeper Decarbonisation Perspective is on top of the Transforming Energy Scenario, for challenging sectors such as freight, shipping, aviation and heavy industry. Advances in biofuels, synthetic fuels, new materials and the circular economy will all be necessary. Industry is the dominant energy consumption sector in many countries such as China, where this sector consumes around half of the final energy, an urgent solution need to be found for industry energy demand. Innovation is also needed to find zero CO_2 emission solutions for industrial process emissions and for non-energy uses in these sectors. Innovation will also continue to be crucial to address transport modes that are hard to electrify, namely aviation and shipping [2]. The Deeper Decarbonisation Perspectie shows how the remaining energy and industrial process-related CO_2 emissions in the Transforming Energy Scenario can be cut to zero. Renewable energy provide 60% of the reduction needed when including green hydrogen and renewables-based electrification; 37% of reductions come from energy efficiency and other structural and behavioral changes; and the remaining 3% of reductions come from carbon capture, utilisation and storage (CCUS) and nuclear. Overall, when considering reductions in energy and industrial process-related CO_2 emissions from the Baseline Energy Scenario to zero, renewables make up 43% of the reductions, energy efficiency 26%, EVs 12%, green hydrogen 9%, blue hydrogen and CCS/Carbon dioxide removal (CDR) 7%, behavioural changes 2%, and nuclear under 1% (EVs and behavioural changes could also be considered as part of the energy efficiency, or for

the case of EVs, renewables if powered by renewable electricity. However, to show their relative importance they are shown separately) [2].

1.1 Planning for the long term

As reported by IRENA [2] in order to achieve the Energy Transformation Scenario, energy-related CO_2 emissions need to fall by 3.8% per year until 2050. Annual energy-related CO_2 emissions would need to decline by 70% below today's level by 2050. Over half of the necessary reductions in emissions, by 2050, come from renewable energy, followed by around $\frac{1}{4}$ coming from energy efficiency. When including direct and indirect electrification (such as green hydrogen and technologies like EVs), the total reductions increase to over 90% of what is required. The Deeper Decarbonisation Perspective then describes how reducing the remaining emissions to zero - over $\frac{2}{3}$ of which come from challenging sectors such as aviation, shipping and heavy industry - will require additional renewable energy, electrification (both direct use and green hydrogen usage), energy efficiency, carbon management, and other structural and habit changes. Outside the energy sector, efforts also are needed to reduce emissions from non-energy use, emissions from land use, land-use change and forestry, and fugitive gases in the coal, oil and gas industries. In Figure 1.3 the different scenario for CO_2 emissions reduction can be seen.

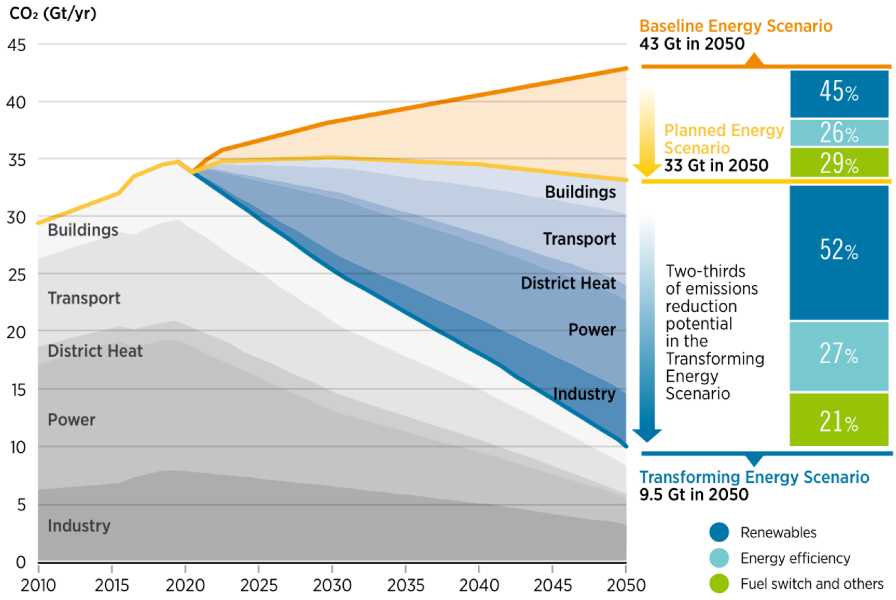

Figure 1.3: Different scenarios for CO_2 emissions reduction

1.2 Space cooling

As reported by IEA [1] space cooling accounted for nearly 16% of building sector final electricity consumption in 2020 (about 1885 TWh). The International Energy Agency [1] reported that demand for space cooling has risen at an average pace of 4% per year since 2000 and CO_2 emissions more than doubled to nearly 1 Gt from 1990 to 2020. This data is important because Air Conditioning (AC) systems can be straining for the electric grid especially during peak demands hours and in extreme heat events. China, the United States and Japan combined account for $\frac{2}{3}$ of the AC market with more than 1 billion units sold here, although in the last few years AC demand rose more quickly in India and Indonesia with a yearly increase installation of 10% since 2010. While AC ownership exceeds 90% in the United States and Japan, it remains under 5% in sub-Saharan Africa and less than 10% in India even though the number of cooling degree days* is much higher in this latter regions. Rising living standards, population growth, and more frequent and extreme heatwaves are expected to create unprecedented cooling demand in the next decade, therefore the number of ACs installed could increase by another 40% by 2030 as declared by the IEA [1]. As disclosed by Adom et. al. [4] about Africa, which has lots of developing countries and unexploited opportunities, that in any economy the carbon dioxide emissions are strictly related to social, economic and industrial factors, this makes it clear that there is a big potential market growth and with that CO_2 emissions will grow as well. One of the main way to reduce the emissions is to improve the efficiency of AC systems, more efficient systems are already available on the market and could cut in half the energy demand if widely diffused, the market is also transitioning towards the usage of refrigerants with a lower Global Warming Potential (GWP)† indeces.

1.3 Different approaches to energy reduction

As already stated, huge amount of energy is being used for space cooling in households around the world and the demand it is only going to increase in the near future. If the target is to reduce the energy used while maintaining the thermal comfort of the people inside the house, there are different approaches possible, such as:

1. Reduce the energy required by the building;
2. Improve the efficiency of the AC system;
3. Others approaches.

*A cooling degree day (CDD) is a measurement to quantify the demand for energy needed to cool buildings. It is the number of degrees that a day's average temperature is above 18 °C. Usually when the outside temperature reaches that level, people inside no longer want the building heated, but instead begin to consider cooling the building

†GWP it's a measure of how much energy the emission of 1 ton of refrigerant (or gas in general) will absorb over a given period of time, relative to the emission of 1 ton of CO_2 emissions

1.3.1 Reduce the energy required by the building

This approach is much broader and does not apply only for cooling, but it is essential to reduce the energy required for heating during the winter months. As stated by Cabeza and Chàfer [5] Zero Energy Buildings (ZEB) can be defined as a reference to achieve the balance between needs and self-sufficiency for a building under service conditions, to achieve it there are two main strategies, the reduction of energy demand using energy saving techniques and the increase of energy supply implementing renewable energy systems. As stated by Cabeza and Chàfer [5] there are many different technologies that can help reduce the energy usage in cooling/heating of buildings, as can be seen in Figure 1.4 [5].

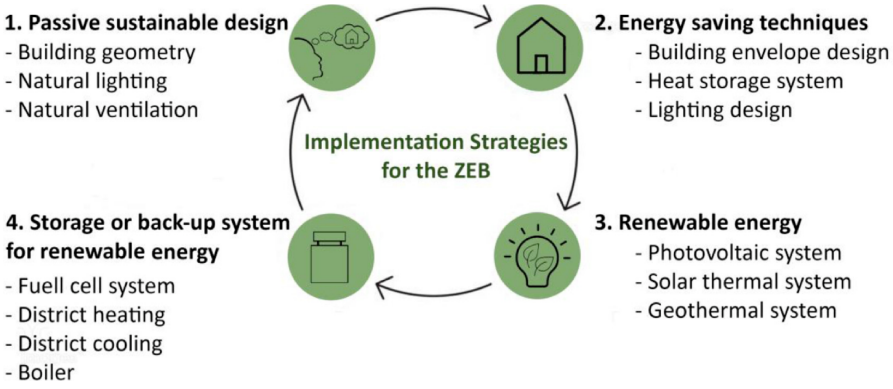

Figure 1.4: Passive and active strategies to achieve zero energy buildings

Bioclimatic architecture objective is to increase comfort levels of a building in any season and/or climate at the same time to reduce the need for heating, cooling, lighting and ventilation. One way to reduce the energy usage in a building is to control and reduce its envelope air leakages namely increasing its air tightness, the heat lost due to air leakages has been quantified to represent up to 40% of the total heat loss from buildings. The first choice to reduce thermal needs of building is to improve the building envelope therefore decreasing the heat transfer coefficient, this can be achieved with different types of materials. Newer materials such as transparent insulation materials (TIM) have the advantages of insulating materials but being transparent they allow the usage of daylight in order to improve the visual comfort of the building. A more interesting approach is to increase the thermal mass of the building envelope[‡], this can be achieved by using materials with high density such as concrete, rammed earth or PCMs. The main advantage of this technique is that buildings with high thermal inertia have a reduced and delayed reaction to external ambient temperature, the drawback of high thermal inertia is that it will require more time for the building to reach the comfort temperature. The shading systems are equally as important because a well designed system can drastically reduce the building peak heat gain and cooling requirements and can also improve the natural lighting quality of the building interiors, the effectiveness of the shading systems will depend on the solar orientation of a particular building facade. It was found that active shading systems can save from 12%-50% of the building cooling electricity consumption. Passive walls are another way to reduce the energy required by a building, for example the facade can have a double skin with a ventilated air layer between the

[‡]thermal mass is defined as a material ability to absorb, store, and release heat

two and this provides a thermal buffer zone. Other solutions are available, like the usage of greenery both on roofs and on facades, also the usage of high albedo material[§] or coatings on roofs to provide a reduction of the solar heat gain in the building increasing the solar reflectance of the surface. Evaporative cooling is another approach for dissipating heat by using water as a sink, this is probably the oldest air conditioning technology, it works by increasing the water vapor content of air and thus the temperature decreases. With this technique the minimum reachable temperature is the wet-bulb temperature of outside air, the indirect evaporative cooling and the radiant cooling are both present in systems like roof ponds.
About 60% of the heat loss of a building is due to glazed areas because the thermal conductivity in these areas is much higher compared to the rest of the building. Innovative solutions are available, like solar absorbing windows, reversible windows, switchable electrochromic windows etc. and the type of glazing can be either static or dynamic, with the first one having fixed thermal and optical properties and the latter one has changeable properties thanks to different kind of switching devices. The usage of geothermal heat pumps jointly with renewable energy production is an excellent option to use energy more efficiently. In this case the ground is used as a heat sink, it is the cold side (evaporator) during the winter and becomes the hot side (condenser) during the summer cycle, the inversion is simple and can be achieved using a valve. The advantage of using geothermal energy is that the ground deeper than 1.5 meters presents an almost constant temperature of 14 °C all year round, this allows to improve the coefficient of performance (COP) of the system in both cold and hot seasons. The two main configurations of geothermal are with the poles arranged vertically or horizontally. In the first case is required less surface for the plant, on the other hand very long poles are needed and to plant them a specialized machinery is required hence this process is expensive. The other option is to arrange the poles horizontally, this has the drawback of requiring a lot of free surface to be realized but the depth required is not that big, this configuration goes well when it is realized at the same time as, for example, the parking lot of a shopping mall.

1.3.2 Improve the efficiency of the AC system

The maximum efficiency of an AC system is the one of the Carnot cycle, but this is unobtainable. The efficiency of the Carnot cycle is $COP = \frac{T_1}{T_1 - T_2}$, T_1 is the temperature of the hot heat sink, instead T_2 is the temperature of the cold heat sink. Carnot cycle is an ideal cycle and one hypothesis is that the heat exchanging phases (both cold and hot) happens at the same temperature as the heat sinks, but in order to exchange heat there must be a difference in temperatures between the two sources and usually this difference is at least 2 °C or greater. It is clear that a real cycle will always have a smaller COP compared to the Carnot cycle, furthermore if the temperature difference between the two heat sinks decreases the efficiency of the cycle increases. This means that for an hypothetical AC system it is better to work during the night, when the hot heat sink is much cooler compared than during the day, this way the efficiency it's higher, but obviously the cooling it's required during the day and not as much during the night. To solve this problem a Phase Change Material (PCM) Latent Thermal Energy Storage (LTES) can be used with the AC system in order to shift the working hours of the system from day to night.

[§] albedo is a measure of the reflectivity of a surface

1.3.3 Other approaches

Some other approaches are possible, as stated by Pinto et. al. [6] Grid-interactive Efficient Buildings (GEB) are important for the energy transition and will benefit building owners, inhabitants and the electric grid. GEB use new technology such as Internet of Things (IoT), real time monitoring and control, peer-to-peer energy. In order to boost the number of GEBs in the smart grid some countries are planning a mass deployment of Advanced Metring Infrastructure (AMI). Smart meters, Artificial Intelligence (AI) and connectivity can be very useful in order to improve power demand and generation forecasts, and also to extract energy usage patterns. The increasing number of sensors in smart buildings has given access of an unprecedented availability of long term data monitoring about energy performance and indoor quality of buildings [6]. Hence databases of buildings are more available than ever before, these open up the opportunity to define energy behaviour and optimization of buildings. An effective tool in order to extract useful information from the databases is Machine Learning (ML) and can be applied in different applications of the building to improve its performance and inhabitant comfort and health. Some promising applications for building energy management are: the prediction of energy demand required for the efficient operation of a building, the optimization of building operation, the detection and commissioning of operational failures of building equipment, the energy benchmarking analysis, the characterisation of energy demand profiles, and the assessment of the impact of user behaviour [6]. The building sector it is starting to use ML with the introduction of Energy Management and Information Systems (EMIS), which improve the functionalities of traditional Building Automation Systems (BAS) in order to analyse and control energy use and system performance. As stated by Chiesa et. al. [7] a large part of energy is used for the lighting of buildings, especially in offices, even though most of the time outdoor light goes beyond the required lighting threshold for most of the day. If used properly outdoor light can help reduce the electrical consumption for indoor lighting which represents $\frac{1}{3}$ of the electricity needs in buildings. For the summer season the management of an active shading is more complicated because it is easy to overheat the building if too much light is being let in. Having smart homes it is just the beginning, in order to optimise these systems advanced control methods are required, advanced HVAC control can reduce between 13% and 28% of the energy consumption, as stated by Ján Drgoňa et. al. [8].

1.4 TES

As declared by the international renewable energy agency (IRENA) [9] a big step in reducing the CO_2 emissions is switching to renewable energy such as solar and wind. To achieve the climate targets planned by the Paris Agreement [3] every year more renewable energy is added to the electric grid, mainly solar PV and wind, which are also called Variable Renewable Energy (VRE) because their biggest limitation is daily and seasonal variability, TES can help making more stable and flexible energy systems. In Figure 1.5 are reported different TES technologies used for different temperatures and time spans. It's expected that the quantity of TES will increase dramatically from 234 GWh installed by the end of 2019 to over 800 GWh in 2030 [9]. If we consider the power sector the TES technology is used for load shifting, capacity firming and ancillary services. For this sector the most common technology is molten salts because it is a known technology and are already used with Concentrated Solar Power (CSP) plants. Instead, if we consider the space cooling sector over 13.9 GWh of TES capacity are used for cooling in buildings and district cooling systems. However this value can increase swiftly in the coming years as emerging

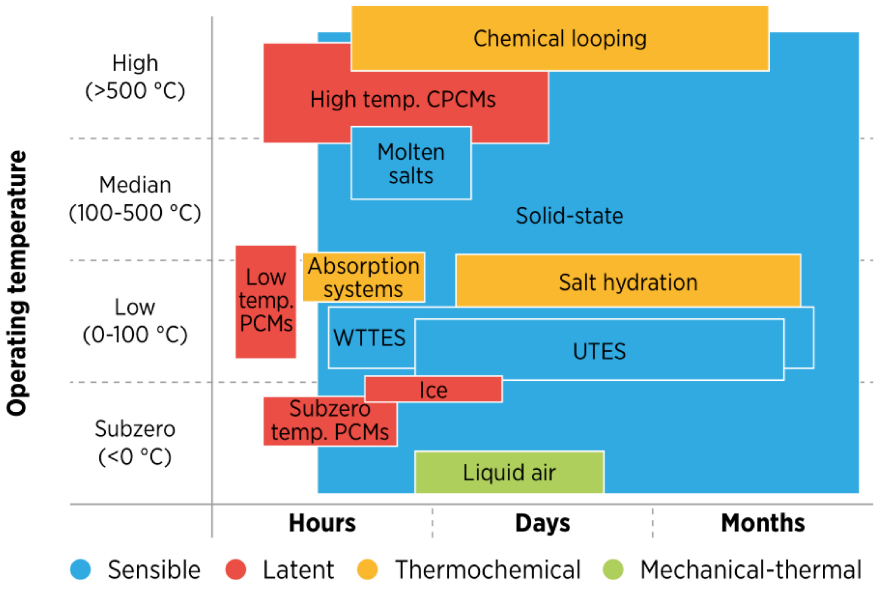

Figure 1.5: Operating temperatures and time ranges for different TES technologies

economies develop and demand for space cooling increases, even because in this countries the temperature is already pretty high and it is still increasing due to climate change. Instead if we examine the district heating sector we find that around 199 GWh of TES capacity is already in use, making this sector the largest share of TES in use [9]. The cold chain[¶] sector extensively uses TES systems in some fields such as the transportation of frozen products. A technology that is already being used is water Tank TES (TTES), usually the capacity is between 100 and 1000 litres of water which can be cooled or heated during periods of off-peak electrical demand or excess electricity from PV panels. The sensible thermal energy can be later used during peak demand, this technology has already been used around the world and was found to help the local electricity network by reducing residential peak demand [9]. In Figure 1.6 are reported the applications of TES (adapted from Jouhara et. al. [10]), usually the objective is to increase the flexibility and energy efficiency of the systems by balancing energy demand and supply.

[¶] the cold chain refers to the supply chain required to bring products, that must be stored at low temperature, from the producer to the consumer

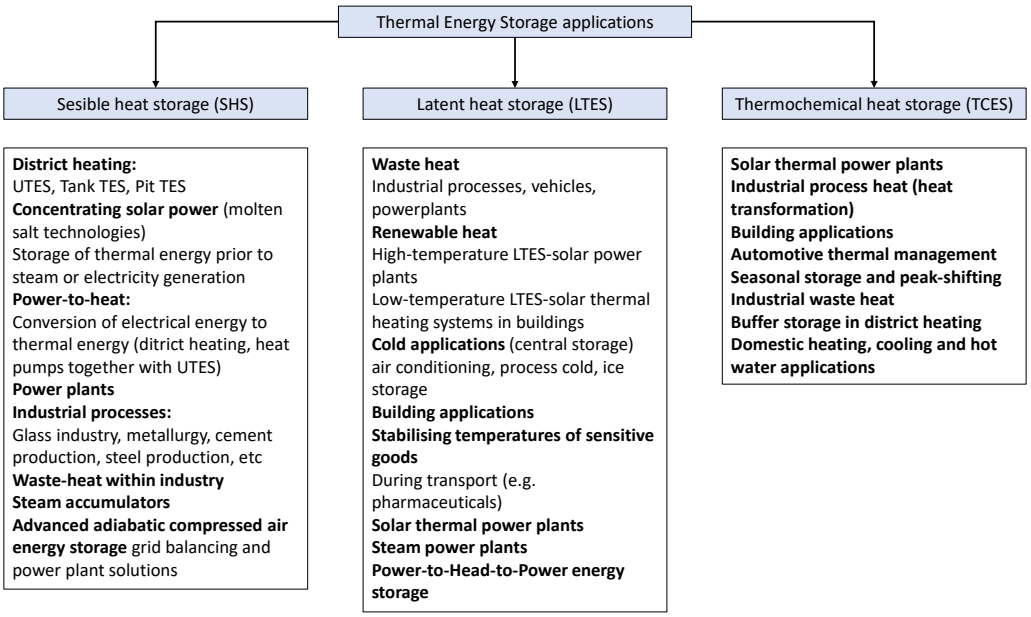

Figure 1.6: Applications of sensible, latent and thermochemical energy storage

1.5 PCMs

As reported by IRENA [9] several phase change materials are already used in commercial applications, in particular low temperature PCMs with phase-change temperatures from 0 up to 120 °C. As regards organic materials, paraffin is the most commonly used, formed of wax at room temperature and chemically consisting of hydrocarbons with alkanes C_nH_{2n+2}, the melting point increases as the number of carbons increase inside the molecule. Laboratory-grade paraffin waxes, tetradecane and hexadecane and their binary mixtures are mainly used. As regards inorganic materials, salt hydrates such as strontium bromide ($SrBr_2.xH_2O$) have already been commercialised for domestic heating [9]. Encapsulation or using shape-stabilisation (prepared by PCM integration into supporting material and micro encapsulating PCMs in shell) are the most common forms of paraffin used. Recently emerging integration of PV and PCM system concepts for temperature control offers an opportunity to extend its usage to buildings-integrated concentrated photovoltaic (BICPV) systems. Employing PCMs passively keeps the BICPV unit's temperature within a safe operating range and can also collect rejected heat for possible regeneration [9]. As stated by Chandel and Agarwal [11], PCMs are materials that absorb or give back a considerable amount of heat during the phase change by increasing or decreasing the internal molecular energy, this happens at almost constant temperature. The heat exchanged while changing phase is called latent heat because the temperature doesn't change, instead sensible heat it is when there is a temperature change in the medium. Examples of sensible heat storage are water, pebbles, rocks, concrete and sand etc. Phase transition can be: solid-liquid, liquid-gas, solid-gas, solid-solid. The most used are the ones with the solid-liquid transition, considering that they offer a wide range of temperatures therefore are suitable for more applications, as well as high storage capacities and little volume changes during phase transition [11]. The PCM with liquid-gas phase change have

the problem of large volume change during transition whilst having big capacities too. Instead PCMs with solid-solid transition store energy as a result of a change in the crystalline state and they are very interesting because a container is not necessary. A big weakness of these transformation is that the storage capacity is much lower than the other kinds of phase transition [11]. As reported by Oró et. al. [12], the main characteristics required for a good PCM are:

- Thermophysical properties
    - Melting temperature in the desired operating temperature range
    - High latent heat of fusion per unit volume
    - High specific heat to provide additional significant sensible heat storage
    - High thermal conductivity of both solid and liquid phases
    - Small volume change on phase transformation and small vapor pressure at operating temperature
    - Congruent melting of the phase change material for a constant storage capacity of the material with each freezing/melting cycle
    - Reproducible phase change

- Nucleation and crystal growth
    - High nucleation ratio to avoid subcooling of the liquid phase during solidification, and to assure that melting and solidification process occurs at the same temperature
    - High rate of crystal growth, so that the system can meet the demand for heat recovery from the storage system.

- Chemical properties
    - Complete reversible freeze/melt cycle
    - No degradation after a large number of freeze/melt cycles
    - No corrosiveness to the construction/encapsulation materials
    - Non-toxic, non-flammable and non-explosive

- Economics
    - Abundant
    - Available
    - Cost effective
    - Easy recycling and treatment
    - Good environmental performance based on Life Cycle Assessment (LCA).

A possible classification of PCMs based on their chemical nature is as follow [11]:

1. Organic
2. Inorganic
3. Eutectic

1.5.1 Organic

These include paraffins which are saturated compounds of carbon and hydrogen such as alkans, fatty acids and vegatable oils. They can be linear, cyclic or branched structures. Their advantages are: high latent heat capacity, non-reactive, long term stability is good because they do not undergo segregation with melt/freeze cycles, super cooling is limited in fact they have good nucleation properties. However they suffer of low thermal conductivity and they are flammable. Paraffin wax are a kind of organic PCM, typically is a greyish black sludge, and it is the last product obtained from the petroleum refining process, bleaching agents and other chemicals are used in order to convert it into paraffin wax. Paraffin waxes are the most widespread organic PCM and are suitable for about 1500 cycles, the two main factors affecting the melting and freezing points are the molecular mass and the chain length of these compounds. Hence these two aspects should be modified in order to obtain the desired melting temperature, the storage density is also a function of these two parameters [11]. Vegetable based oils are completely safe when ingested because are food grade unlike paraffin wax. However they have a lower flash point and higher flame propagation rates compared to paraffins. They are obtained from vegetable feed stocks which is a much greener way than petroleum refinement and nearly carbon free. Pure vegetable oil based waxes are non-toxic. Fatty acids are long hydrocabon chains with a terminal carboxyl group. Usually glycerides or phospholipids are used to obtain fatty acids and they usually have an even number of carbon atoms ranging from 4 to 28. These are found to be inflammable and corrosive and they stink, these factors limit their application in buildings. Last but not least important is the economic aspect, fatty acids are twice or thrice as costly as the paraffin wax [11].

1.5.2 Inorganic

Inorganic PCMs can be metal or salt hydrates. Their main advantages are the very high latent heat storage capacity, non-inflammability and sharper phase transition. Instead the drawbacks segregation and super cooling which limit their use in some applications. Hydrated salts are inorganic compounds that, when in contact with water, undergo a change in their structures, thus the water associated is called the water of hydration or water of crystallization, some examples are Na_2SO_4, $10H_2O$, $CaSO_4$, $6H_2O$ etc. Salt hydrates are very attractive as a PCM because they have a high thermal conductivity, high latent heat capacity, high specific heat capacity and low cost but they have some drawbacks like super cooling due to the poor nucleating ability and phase segregation due to their incongruent melting. Incongruent melting is a phenomenon that reduces the reversibility of the phase change process, thus the heat storage capacity is reduced, this effect can be limited by using gelling agents which bind the PCM in a three-dimensional network. Long term stability is not good, in fact after several cycles the hydrated mass decreases and the system degrades. If salt hydrates are used as PCM studies of its thermal properties

like phase change temperature, sub-cooling, nucleation rate and enthalpy are necessary, these properties should be evaluated before and after repeated heating and cooling cycles. They usually are non-toxic but they can cause skin or eye irritation and respiratory problems if not handled properly [11].

1.5.3 Eutectic

Eutectics are a mixture of two or more compounds and they have a lower melting temperature compared to that of the compounds alone. When this happen the composition is called eutectic composition and the corresponding temperature as eutectic temperature. They do not suffer from segregation during melting and freezing, they have a sharp phase change temperature. Some eutectics of fatty acids have been synthesized and have attractive properties, some of them have bad smells thus their use in buildings is limited. Their toxicity depends if the constituent materials are organic or inorganic [11].

1.6 PCMs Flaws

As stated by Chandel and Agarwal [11], paraffin wax have poor thermal conductivity, large volume change during phase transition, oxidation may sometime occur, thus some form of containment is required, is non-corrosive to most of the materials except for those with chemical similarity like plastic materials especially poly-olefins. Commercial paraffin wax contains volatile compounds like formaldehyde and vinyl chloride, these two are carcinogenic if subjected to long exposures. The U.S. Environmental Protection Agency (EPA) found some toxins in paraffin wax such as: benzene, toluene, naphthalene. This means they are flammable and thus some precautions must be taken. Paraffin wax are also non-biodegradable so their disposal is an issue [11]. Flammability of PCMs is the main reason for their limited usage in buildings applications, flame retardants must be used but should not affect the PCM properties in a detrimental way. Fire retardants works in different ways depending on the type, they can prevent the burning of the PCM, diluting the gas phase below the minimum oxygen concentration by forming inert gas, release of chain terminating radicals, separating the flame from the surface [11]. There is a lack of studies in literature about fire retardants for PCM, however halogenated compounds pose significant health hazards and will be banned. Phosphorus and nitrogen based flame retardants seems to be the best solution, nano-silica appears promising as well, graphite is still under research [11]. Hydrated salt usually corrode the metal container, therefore a proper encapsulation method is required, stainless steel was found to be the most corrosion-resistant. There are different types of corrosion in metals such as oxidation or fretting, crevice corrosion, erosion and pitting corrosion [11]. Pitting corrosion is very problematic because can happen in a very short period of time and the rate can increase further due to galvanic effect. Some ways to avoid these problems can be coating the container with a more reactive metal in order to protect the container material, anodic and cathodic protection or galvanizing the container. The usage of gelling agents, used for avoiding incongruent melting, may affect the properties of the the salt hydrates. Salt hydrates are not suitable for buildings until a proper encapsulation method is found [11]. In literature there is not much data about thermophysical properties of eutectics, this because their synthesis, property determination and testing is costly and time consuming [11]. Another problem of PCMs is the subcooling (or super cooling), this phenomenon is when the material does not solidify immediately when reaching the solidification temperature, but keeps cooling far below this temperature, as reported by Oró et. al. [12].

1.7 Heat transfer enhancement

As reported by Veerakumar and Sreekumar [13], one common problem of LTES is their low thermal conductivity, especially when using organic PCMs. This problem can lead to partial melting/freezing cycles, therefore the energy stored is lower than the theoretical storable energy. Several techniques have been studied like inclusion of nano-structures, filling materials and extended surface. As stated by Fan and Khodadadi [14], the low thermal conductivity limit the energy charging/discharging rates of the system using the PCM.

1.7.1 Extended surface

Due to the low thermal conductivity of PCMs the conductive heat transfer is very small, instead, when liquid, convective heat transfer is dominant. Thus the logical approach to improve the overall heat transfer is to increase the heat transfer surface, as studied by Al-Maghalseh and Mahkamov [15]. Fins are useful because they increase the heat transfer surface and thus increase the heat transfer rate. The fins configuration must be studied specifically for each application, the main aspects that affect the heat transfer rate are as follows: dimensions, numbers and location of the fins [15]. Sivasamy et. al. [16] studied a fin array system in order to identity the effects of fin spacing, module thickness, vertical or horizontal orientation and temperature difference. The charging and discharging process can be significantly reduced if the fins configuration is optimized to promote the heat transfer between the Heat Transfer Fluid (HTF) and PCM. Another approach is by using metal foam, it was found that the overall heat transfer rate increased by 5-20 time during solidification and 3-10 times during the melting process. The usage of metal beads can also accelerate the solidification and melting processes, in this case the factors influencing the performance are the diameter and number of the metal beads [16].

1.7.2 Filling materials

The definition of composite PCMs is: base phase change material used in combination with high thermal conductivity materials, called filling materials, like graphite, expanded perlite etc. [16]. Graphite has good thermophysical properties, high thermal conductivity, high electrical conductivity and high absorbability. Three main types of graphites are used like graphite flakes, expanded natural graphite and ground expanded natural graphite [16]. As reported by Al-Maghalseh and Mahkamov [15], metal foams and matrix materials can also be used, usually a decrease in porosity entail an increase in the melting rate as well as in the convection flow of liquid PCM. Instead a decrease in the porosity means there is less PCM inside, therefore the energy storage capacity is reduced.

1.7.3 Multiple PCMs

In this approach PCMs are arranged in such a way that their melting temperature are in the decreasing order, this way allows to maintain nearly a constant temperature during the melting process and to increase the energy efficiency. Thus the heat flux to the PCM is also nearly constant. Instead for the discharging process if the flow direction of the HTF is reversed than the PCMs are still in the increasing order of their melting points [16]. Obviously the PCMs to use must be chosen carefully.

1.7.4 Encapsulation

Encapsulation is a useful technique because it helps to avoid leakage problems and interactions between the PCM and the outside environment, and at the same time it can increase the heat exchange area between the PCM and HTF. PCM can either be macro or micro encapsulated [11]. As stated by Veerakumar and Sreekumar [13] the container should have qualities such as thermal stability, corrosion resistance, strength and flexibility and must prevent PCM from mixing with the HTF.
Macro encapsulation is when PCM is held inside shells, tubes, pouches, spheres and thin plates etc. This way the PCM is protected from environmental degradation, and it allows for easy integration of PCM inside buildings. However macro encapsulation suffers from poor heat transfer, thermal stratification and leakage [11].
Micro encapsulation technique is used to form capsules of micrometer size, this is possible by coating the PCM with a very thin layer of a material such as polymer. This method allows to avoid leakage, volumetric changes during melt freeze cycles, block the interactions between PCM; encapsulation can also increase the heat transfer area. Micro encapsulation can be achieved either with physical or chemical techniques. Physical techniques are cheaper but the capsules have non uniform sizes, they have imperfect properties and the smallest size that can be produced is about 100 microns. Instead chemical encapsulation produces particles with well defined structures and properties, on the other hand they are costlier and more complicated compared to physical techniques [11].
As stated by Al-Maghalseh and Mahkamov [15], nanoparticles can also be used to enhance the properties of the PCM.
As reported by Oró et. al. [12], there are also bulk systems of encapsulation which consists of using tank heat exchangers, in this case there is the need of large heat transfer surface.

1.8 Roll bond

In this work a tank filled with PCM has been used, obviously the low thermal conductivity of the PCM poses a big problem for storing and releasing the thermal energy. Usually the approaches found in literature are expensive and complicated to realise, especially when the system is as big as it is in this case. To avoid this problem the roll-bond technology was used, this technology is already used in the refrigeration sector. Roll-bond means a plate with a small thickness (about 3 mm) and a circuit where usually a refrigerant flows and evaporates in such a way to cool down the inside of the fridge. In the system presented in this thesis, instead, there is water that flows inside the roll-bond.

2

System description

As already stated the focus of this work is to study the PCM system, the setup used has been specifically built for this purpose. The system is made up of the tank, the roll-bonds and the PCM itself. In figure 2.1 a schematic view is reported. There is a chiller which can be set at any temperature wanted, the minimum temperature used was 2 °C because if it goes lower the water would start to freeze and glycol needs to be added. Instead the flow-rate is controlled by varying the electric frequency of the pump. The tank contains about 300 kg of bio-based PCM, and 16 roll-bond connected to the water manifolds, the tank can be seen in Figure 2.2. The tank is a parallelepiped shape with internal dimensions of 1400 mm × 710 mm × 650 mm, the walls are 5 cm in thickness

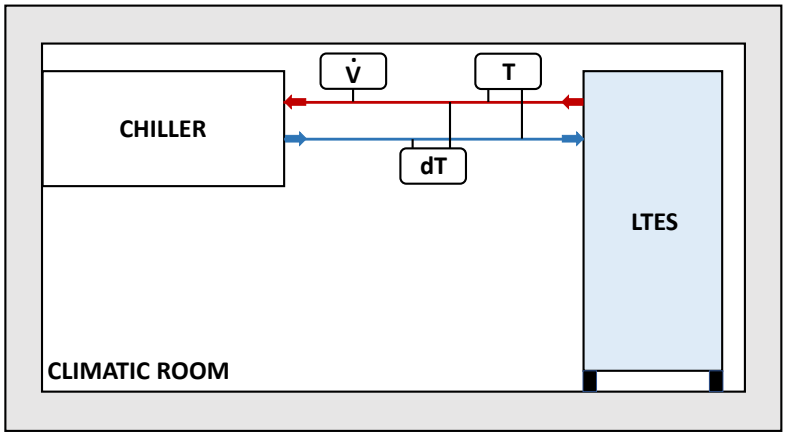

Figure 2.1: Plant scheme

Figure 2.2: LTES Tank inside the climatic room, CAD model to illustrate the insides of the tank with the roll-bonds

all around. Inside the walls there is insulating material to limit heat loss as much as possible. To reduce even more the heat losses, the tank was placed inside a climatic room set at 9 °C. The flow rate is measured by an Endress + Houser Promag H electromagnetic flow meter, this kind of flow meter works based on the Faraday's law of electromagnetism. Repeatability tests were conducted for some operating conditions. The maximum percentage difference is below $\pm 2\%$.

2.1 Acquisition system

First of all in order for the thermocouples to precisely measure the temperature they need an Ice Point Reference (IPR). The thermocouples used are T-type (copper-constantan) and are connceted to a Kaye $K^{-1}70$ Ice Point Reference as can be seen in Figure 2.3. The thermocouples are made with very thin wires covered with red and blue plastics for insulation, and they go from the tank to the Kaye (left of Figure 2.3). From the IPR the analogic signal is taken, with some wires (left of Figure 2.3), to the acquisition system Keysight 34970A (right of Figure 2.3). At the Keysight the signal is acquired with a sampling frequency of 0.15 Hz (every 6.5 seconds) and converted from analogical to digital, finally the signal goes straight into the labview program.

Inside the data acquisition system there are 3 acquisition cards, like the one seen in Figure 2.4, each one of them has 20 channels, thus 3 are needed.

Figure 2.3: Back of Kaye $K^{-1}70$ Ice Point Reference (left), and data acquisition system Keysight 34970A on top of the Kaye (right)

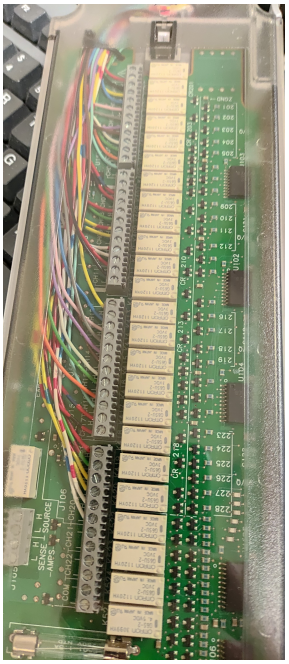

Figure 2.4: Acquisition card

3
Experimental setup

3.1 Thermocouples

In Figure 3.1 the tank is reported without two sides for ease of viewing, the two holes on the side are for the water manifolds and are useful as a reference. In order to properly study the system, 39 thermocouples (TCs) were inserted inside the tank, their position can be seen in Figure 3.1. In order to avoid using too many thermocouples it has been decided to put them in a certain pattern. The TCs were attached to a stainless steel rod with a zip tie, paying close attention to bend the junction of the thermocouples a little bit outwards. The different colours of the circles are used to identify a different amount of TCs as can be seen in Figure 3.1, the yellow colour mean that the rod has only 3 TCs, instead green means it has 5. The TCs are equally spaced from each other along the rod, by doing this 5 planes of TCs are obtained, as already seen in Figure 3.1. In order to easily identify every thermocouple, to every rod a letter has been assigned, and a number has also been assigned based on the height where the TC is placed on the rod. This way every thermocouple is identified by a letter followed by a number, i.e. plane 1 contains only TC with the number 1 of every rod, instead plane 2 contains only the TCs of rods A,F,M (see Figure 3.1).

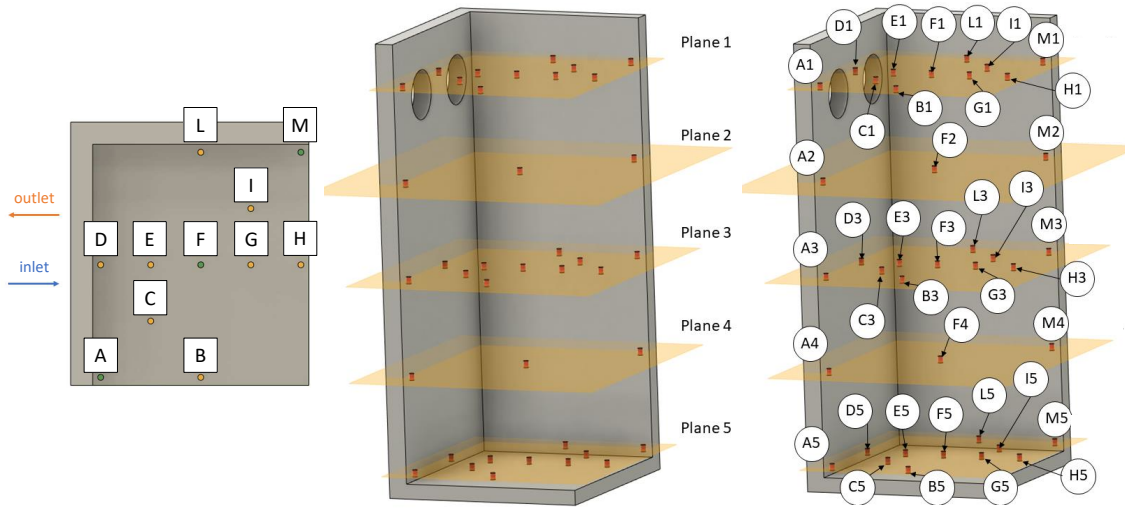

Figure 3.1: Thermocouples positions

3.2 PCM used

The tank was filled with about 300 kg of bio-based CRODATERM 9.5 PCM purchased from Croda, it is derived from plant-based feedstock and has the form of crystalline wax or oily liquid.

Property	Value	Unit
density at 2 °C	963	$kg\,m^{-3}$
density at 20 °C	858	$kg\,m^{-3}$
flash point	195	°C
specific heat capacity (solid)	2.2	$kJ\,kg^{-1}K^{-1}$
specific heat capacity (liquid)	2.1	$kg^{-1}K^{-1}$
thermal conductivity (solid)	0.24	$W\,m^{-1}K^{-1}$
thermal conductivity (liquid)	0.15	$W\,m^{-1}K^{-1}$
peak melting temperature	9	°C
peak crystallisation temperature	5	°C
total stored heat from 1 to 16 °C	220	$kJ\,kg^{-1}$
total stored heat from 16 to 1 °C	216	$kJ\,kg^{-1}$

Table 3.1: PCM thermophysical properties (stated by manufacturer)

Its properties are reported in Table 3.1, the phase change temperature peak is at 9 °C and the latent heat is about 220 kJ/kg.
Peak melting/crystallisation temperatures and latent melting/crystallisation heats are measured using Three-Layer Calorimetry (3LC). 3LC is an industry standard technique for determining the heat capacity of a PCM that uses a much larger amount of sample ($\sim$ 100 ml) compared to Differential Scanning Calorimetry (DSC). With 3LC, the thermal response of the PCM within an insulated compartment is measured as the ambient temperature is cycled between temperature limits chosen to ensure full melting and crystallisation of the PCM (normally over 30 °C range). Depending on the application, 3LC can give a much better representation of the "real world" behaviour of a PCM, because of the larger sample quantity, compared to DSC technique. The rate of temperature change of the PCM during measurement is also lower than is often possible by DSC (the average temperature change rate is 0.3 °C/minute). The output from 3LC is the total heat capacity (latent heat and sensible heat) within the temperature range is reported. In addition, the heat capacity as a function of temperature, reported in 1 °C intervals, is also provided.

3.3 Roll-bond

The term roll-bond means an aluminium plate with a conduit, in reality this term refers to the production process. The production process consists of different phases, it starts with two thin plates of aluminium, they are annealed in order to remove the oil stains from previous processes. The next step is to roughen up one side of the aluminum plate, after this there is the printing process of the graphite on the rough side of the plate. As the next stage the other plate is placed on the roughened side of the previous one, then the rolling stage starts. The two mated plates pass through flat rollers that applies enough pressure to bond them together, this can happen at room temperature or in a furnace. The graphite previously placed prevents the bonding of the plates through the line printed. Finally the roll-bond is inflated with hydrogen at around 8-10 MPa using the hole at the top, this deforms the alluminium along the graphite line forming a pipeline. Some control steps are executed to detect if there are any leaks in the system, this is especially important for the refrigeration sector in order to avoid leakage of gases. As already anticipated in Chapter 2, inside the tank with the PCM there are also 16 roll-bonds. As can be seen in Figure 3.2 the roll-bonds are placed vertically in the tank with a distance of about 31 mm from each other. The design of the roll-bond can also be seen, there is the main conduit that divides into several ones.

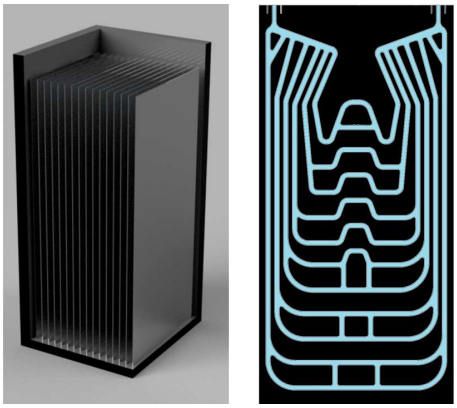

Figure 3.2: Roll-bond design

3.3.1 Roll-bond temperature field

In Figure 3.2 the water circuiting inside the roll-bond can be seen. At first glance it seems to be a bad design because the flow rate is divided in 6 different paths. Furthermore the length of the paths are of diverse length, thus the pressure drops are different. In Figure 3.3 the roll-bond and its temperature field are reported. A thermocamera

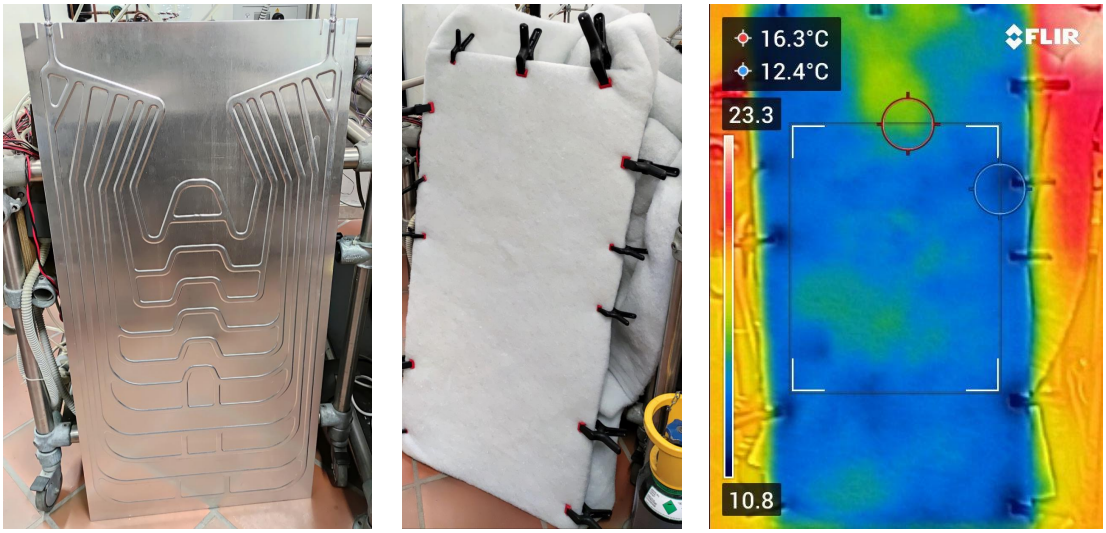

Figure 3.3: Temperature field of the roll-bond

has been used to visualize the temperature field, an insulating blanket was wrapped around the roll-bond because the aluminium reflects the electromagnetic waves. It can be seen that overall the temperature is homogeneous on the roll-bond, thus all channels are properly fed with water, contrary to expectation.

3.4 Data acquisition

In order to record the data a labview program was specifically made, the program can be seen in Figure 3.4.

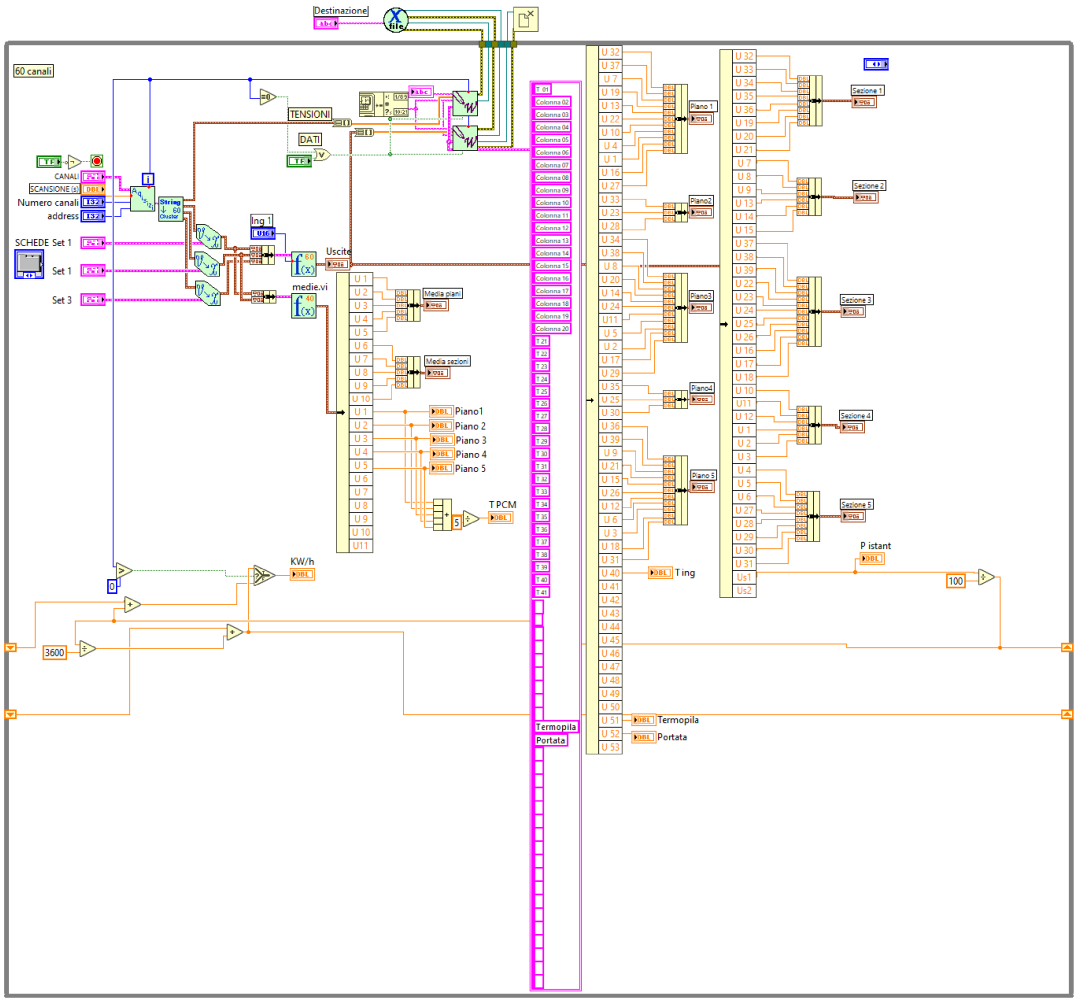

Figure 3.4: Labview program

This program allows to read the data from the acquisition system and perform some data manipulation like temperature graphs, energy graphs and setting up the output excel file with all the data subdivided in columns. In Figure 3.5 are reported the graphs of the temperatures in real time of each TC, the graphs are divided into 5 different planes as already seen in Figure 3.1. There is also a graph with the average temperature of each plane (bottom right of Figure 3.5, this is useful to see at a glance what is happening inside the PCM. Instead in Figure 3.6 the most useful parameters are reported to quickly see how the system is behaving. In Figure 3.6, starting from the left side, the power exchanged can be seen (in 6.5 seconds time steps increments), below the difference in temperature, flow rate and inlet temperature can also be seen. Moving to the center of the figure there are two

graphs, one is to see the energy stored, and the second one is for the average temperature of the PCM. Finally on the right there is a diagram with the average temperatures of each plane.

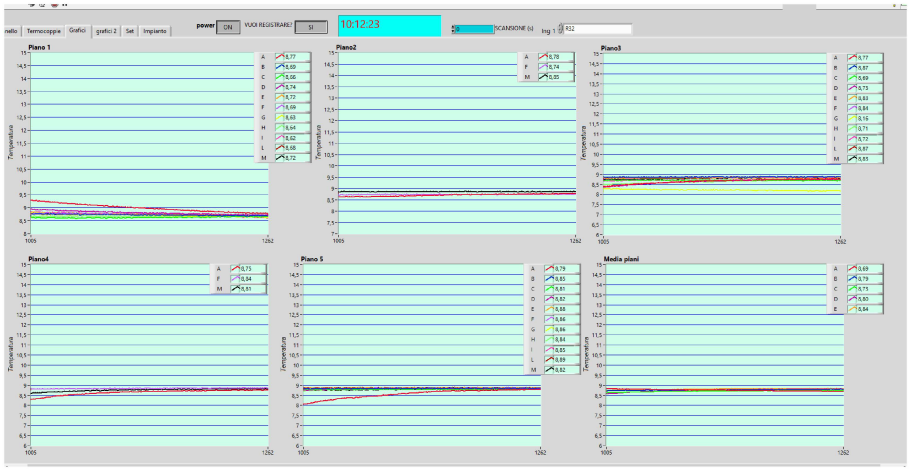

Figure 3.5: Real time temperatures

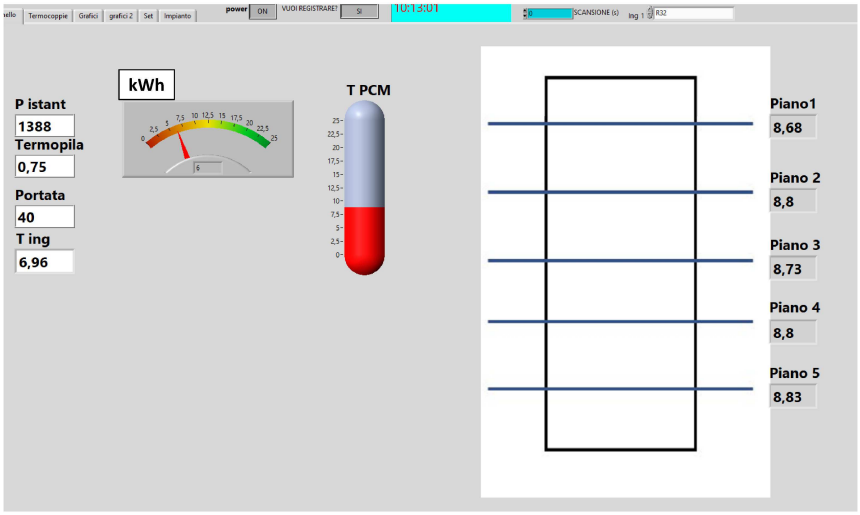

Figure 3.6: Overview data

3.5 Water circuiting

3.5.1 Parallel of series

The water circuiting inside the roll-bonds is not straight forward, as can be seen in Figure 3.7 on the left. The water flows from the inlet manifold inside the first roll-bond, then, instead of going to the outlet manifold, it goes inside the second roll-bond and only then it goes to the outlet. Thus with this configuration we have a parallel of 8 groups, each group is a series of two roll-bonds. This configuration has been used until test 26.

3.5.2 Parallel

For the last few test the configuration has been changed to complete parallel, each roll-bond works as reported in Figure 3.7 on the right. The water from the inlet manifold enters the roll-bond and exits directly after following the design paths of the roll-bond.

In order to change the configuration the connections between the water manifolds and the roll-bonds had to be changed. In Figure 3.8 the new connections are reported, there is also a pressure gauge that was used to detect if there were any leakages before starting the test with the new configuration.

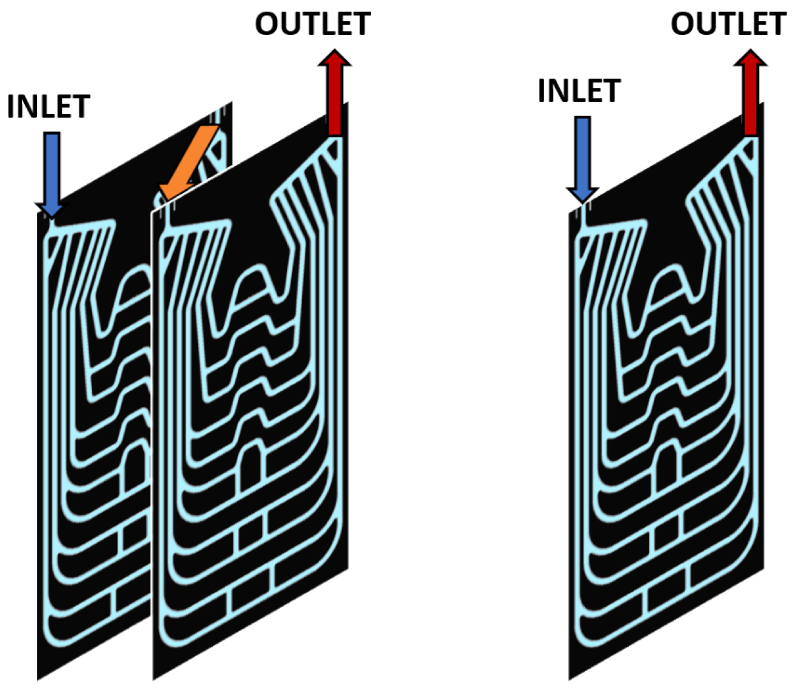

Figure 3.7: Water configurations, parallel of series (left) and complete parallel (right)

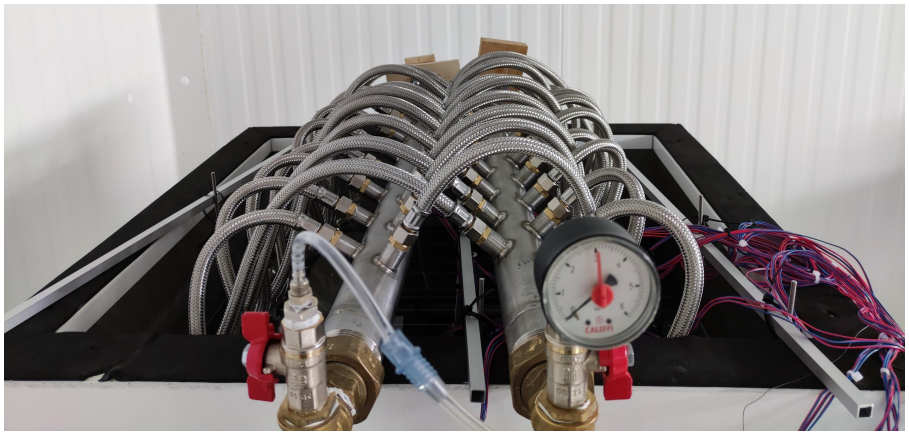

Figure 3.8: New manifolds connections

4

Experimental test description

In order to correctly study the system a lot of tests were carried out, the type of test was decided based on what happened in the previous ones. To compare the tests some assumptions had to be made.

Charging phase

Charging phase mean when the PCM changes from liquid to solid or decreases its temperature, thus the water comes out at a higher temperature than the inlet temperature. This phase is considered to start when the average temperature inside the PCM hits 14 °C during the cooling phase. Also the stored energy starts to be measured from this temperature. Instead the ending is considered when the circulating pump is turned off in order to change the temperature set point of the chiller for the discharging phase.

Discharging phase

The discharging phase starts as soon as the circulating pump is switched on after the chiller reaches the set temperature. As opposed to the previous phase, the discharge is considered concluded when the average temperature of the PCM reaches 14 °C.
Usually the tests were carried out within a day, there are some exceptions especially for the longer tests like the complete charges and discharges which were done in subsequent days, for this tests the climatic room was left turned on during the night. Furthermore the climatic room was always turned on with a temperature set point of 9 °C, which is very close to the theoretical phase change temperature of the PCM and was specifically chosen. The parameters changed during the tests are: water inlet temperature and water flow rate during the charging and discharging phases. The water circuiting has also been changed, the inlet and outlet were swapped and the roll-bond configuration was changed. All data was saved by the labview program to excel files automatically, for the first half-hour the data is useless because this time is required for the IPR (Kaye) to reach equilibrium. It was

found that the best way to change from charging to discharging was setting the temperature in the chiller while the circulation pump was turned off, and only after the water reaches the temperature that was set (this requires about 5 minutes) the circulating pump can be turned back on and the discharging phase can start.

5 Experimental data redaction

5.1 Tests performed

In Table 5.1 all the tests carried out on the tank are reported, also the parameters like flow rate and water temperature are written.

Table 5.1: Tests performed

Number of the test		**Date**	**Flow rate** [l/min]	**Inlet water temperature** [°C]	**Test duration** [hours]
1	Charging	27/01	40	6.5	7
	Discharging	27/01	40	14	4.5
2	Charging	3/02	40	6.5	7
	Discharging	3/02	40	14	4.7
3	Charging	9/02	20	6.5	7
	Discharging	9/02	40	14	4.3
4	Charging	10/02	40	6.5	7
	Discharging	10/02	40	19	3.5
5	Charging	15/02	40	6.5	4
	Discharging	15/02	40	14	4
6	Charging	17/02	40	6.5	4
	Discharging	17/02	40	19	2.6
7	Charging	18/02	40	6.5	4
	Discharging	18/02	40	24	2

Table 5.1: *Continued* Tests performed

Number of the test		Date	Flow rate [l/min]	Inlet water temperature [°C]	Test duration [hours]
8	Charging	21/02	10	6.5	4
8	Discharging	21/02	10	19	2.5
9	Charging	21/02	18	2	2.5
	Discharging	22/02	18	14	5.4
10	Charging	23/02	10	2	4
	Discharging	23/02	10	19	2.9
11	Charging	14/03	17	2	complete
	Discharging	15/03	17	16	complete
12	Charging	16/03	30	6.5	5
	Discharging	16/03	18	29	0.4
13	Charging	17/03	17	2	step
	Discharging	17/03	17	16	step
14	Charging	21/03	8.5	2	4
	Discharging	21/03	8.5	16	5
15	Charging	22/03	18	2	step
	Discharging	22/03	18	16	step
16	Charging	23/03	18	2	step
	Discharging	23/03	18	16	step
17	Charging	24/03	18	2	step
	Discharging	24/03	18	16/19	step
18	Charging	28/03	17	2	complete
19	Discharging	29/03	17	16	step
20	Discharging	30/03	17	16	step
21	Charging	4/04	17	2	step
	Discharging	4/04	17	16	step
22	Charging	7/04	18	2	4
	Discharging	7/04	18	16	5
23	Charging	11/04	10	4	7 (14.5 kWh stored)
24	Discharging	12/04	34	16	5
25	Charging	13/04	18	2	6 (14.5 kWh stored)
26	Discharging	14/04	8.5	16	6
27	Charging	5/05	18	2	4
28	Charging	9-10/05	18	2	complete
	Discharging	11/05	18	16	complete

5.2 Theoretical storable energy

A quick calculation has been done in order to estimate the storable energy inside the PCM, the result is about 18.6 kWh of energy can be stored. Inside there are more or less 330 kg of PCM, the latent heat (declared by the manufacturer) is about 186 $\frac{\text{kJ}}{\text{kg}}$. The specific heat for the solid is $C_p = 2.2\ \frac{\text{kJ}}{\text{kg}\,^\circ\text{C}}$, instead for the liquid is $C_p = 2.1\ \frac{\text{kJ}}{\text{kg}\,^\circ\text{C}}$. It has been estimated that about 18.6 kWh of energy can be stored in the PCM, also the sensible energy has been considered during the cooling from 14 °C to 9.5 °C, and 9.5 °C to 6 °C in addition to the latent energy stored.

5.3 Formulas used

5.3.1 Energy stored

The energy exchanged and consequently stored is calculated starting from the power exchanged.

$$Q = \dot{m} \cdot C_p \cdot (t_{in} - t_{out}) \tag{5.1}$$

where $\dot{m}$ is the water flow rate measured, C_p is the specific heat of water, t_{in} is the water inlet temperature, t_{out} is the water outlet temperature.

$$Q = \frac{\text{kg}}{\text{sec}} \cdot \frac{\text{kJ}}{\text{kg} \cdot \text{K}} \cdot \text{K} = \text{kW} \tag{5.2}$$

From this the energy can be calculated

$$E = Q \cdot time = \text{kW} \cdot \text{sec} = \frac{\text{kJ}}{\text{sec}} \cdot \text{sec} = \text{kJ} \tag{5.3}$$

$$E_{stored} = \sum E \tag{5.4}$$

Thus the energy stored is the sum of the energy exchanged for every period of time (see Equation 5.4), the period of time is 6.5 seconds long due to the system acquisition sample frequency. The Kline and McClintock method (see Equations 5.6, 5.7, 5.8, 5.9) was used in order to evaluate the uncertainty of the total energy stored (maximum 3.4%, average 1.5%).

5.3.2 Specific heat

An attempt was made to estimate the specific heat of the PCM.

$$C_p = \frac{E}{m \cdot \Delta T} \tag{5.5}$$

where E is the energy exchanged with the water (see Equations 5.1, 5.3), it was assumed that all the energy from the water goes to teh PCM without heat losses, m is the mass of the PCM and ΔT is the average temperature

difference between the final and initial conditions of the PCM. The values calculated are reported in Table 5.2, this was calculated only for the first few tests because the value obtained is inside the margin error with the one given by the manufacturer.

Test	C_p	Unit
1	2.6	kJ kg^{-1} K^{-1}
2	2.56	kJ kg^{-1} K^{-1}
3	2.63	kJ kg^{-1} K^{-1}
4	2.35	kJ kg^{-1} K^{-1}
5	2.61	kJ kg^{-1} K^{-1}

Table 5.2: Values of C_p estimated

For the calculation of the C_p only the data where it is certain there is only liquid phase were used, in fact only the data where all thermocouples were above 10°C were considered. For each test only a small part could be used. Furthermore the temperature was measured about halfway between the two roll-bonds, thus it is likely that some solid has already formed on the roll-bond.

5.3.3 Kline-McClintock for experimental uncertainty

The Kline-McClintock method was used in order to evaluate the experimental uncertainty, where $i\dot{m} = \pm 0.2$ l/min is the uncertainty on the measurement of the water flow rate, instead iC_p is the uncertainty of the specific heat of the PCM, $i\Delta T = \pm 0.05$ °C is the uncertainty of the thermopile, for the single thermocouple $it = \pm 0.1$ °C, and the uncertainty on the mass estimation of the PCM is $im_{PCM} = 20$ kg.

$$iE = \sqrt{i\dot{m}^2 \cdot \left(\frac{\partial f}{\partial m}\right)^2 + iC_p{}^2 \cdot \left(\frac{\partial f}{\partial C_p}\right)^2 + i\Delta T^2 \cdot \left(\frac{\partial f}{\partial \Delta T}\right)^2} \tag{5.6}$$

$$iE = \sqrt{i\dot{m}^2 \cdot \left(C_p \cdot \Delta T\right)^2 + iC_p{}^2 \cdot \left(\dot{m} \cdot \Delta T\right)^2 + i\Delta T^2 \cdot \left(\dot{m} \cdot C_p\right)^2} \tag{5.7}$$

$$iT = \sqrt{it^2 \cdot \left(\frac{1}{39}\right)^2 \cdot 39} \tag{5.8}$$

$$iC_p = \sqrt{iE^2 \cdot \left(\frac{1}{m_{PCM} \cdot \Delta T_{PCM}}\right)^2 + im_{PCM}{}^2 \cdot \left(-\frac{E}{m_{PCM}{}^2 \cdot \Delta T_{PCM}}\right)^2 + i\Delta T_{PCM}{}^2 \cdot \left(\frac{E}{m_{PCM} \cdot \Delta T_{PCM}}\right)^2} \tag{5.9}$$

iT is the uncertainty on the average temperature of the PCM.

The uncertainty on the energy stored has also been calculated, for test 11 a total energy of 18 kWh of energy was stored, the uncertainty is $iE = \pm 0.6$ kWh which is 3.37% of the energy.

6
Experimental data results

6.1 Experimental tests

In this chapter some tests are presented in chronological order. Not all the tests are presented but only the most meaningful, some of them are left out and others were used to verify the measures repeatability or to study some working conditions discarded in a latter moment.
At the end of the tests presented, some evaluations of the influence of some working parameters such as inlet water temperature, flow rate and type of circuiting are studied.

6.1.1 Test 1

This is the first experiment that was carried out, the energy stored was $\sim$ 9.7 kWh in 7 hours, as reported in Figure 6.1. The time is very long and not appropriate for household applications. The flow rate is 40 l/min and the inlet temperature are 6.5 °C and 14 °C for the charging and discharging phases respectively. For the first test the temperatures of the thermocouples for each plane are also reported throughout the experiment, as can be seen in Figures 6.3, 6.4, 6.5, 6.6, 6.7.

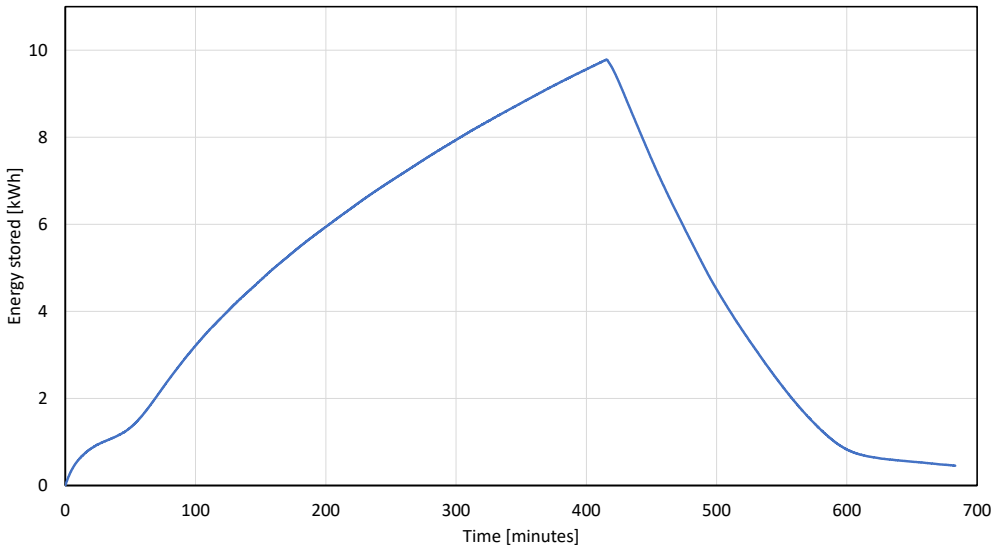

Figure 6.1: Graph of the energy stored with a flow rate of 40 l/min and water temperature of 6.5 °C for the charging phase and 14 °C for the discharging phase.

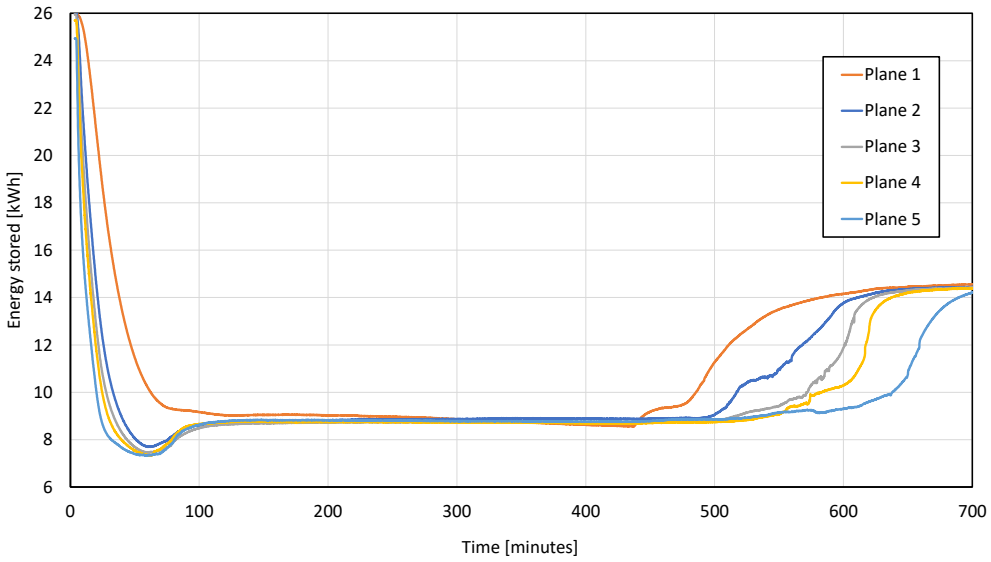

Figure 6.2: Average temperatures of the planes during the test with a flow rate of 40 l/min and water temperature of 6.5 °C for the charging phase and 14 °C for the discharging phase

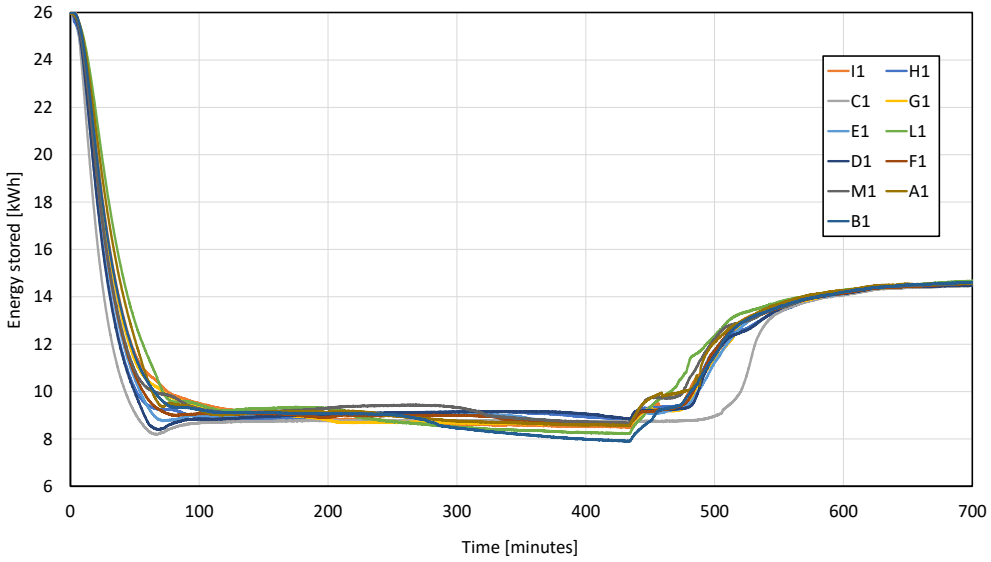

Figure 6.3: Temperatures of plane 1, flow rate of 40 l/min, water temperature of 6.5 °C for the charge and 14 °C for the discharge.

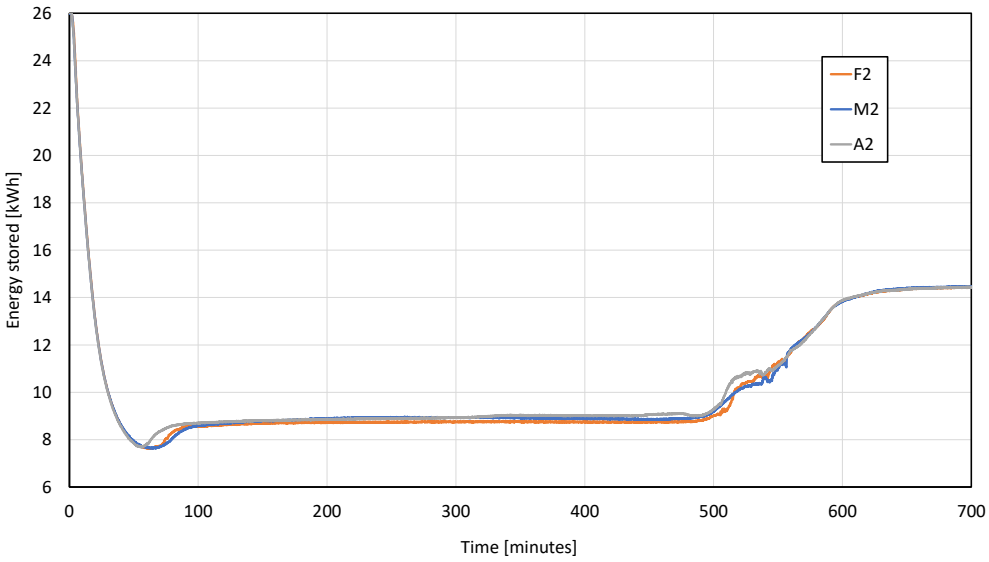

Figure 6.4: Temperatures of plane 2, flow rate of 40 l/min, water temperature of 6.5 °C for the charge and 14 °C for the discharge.

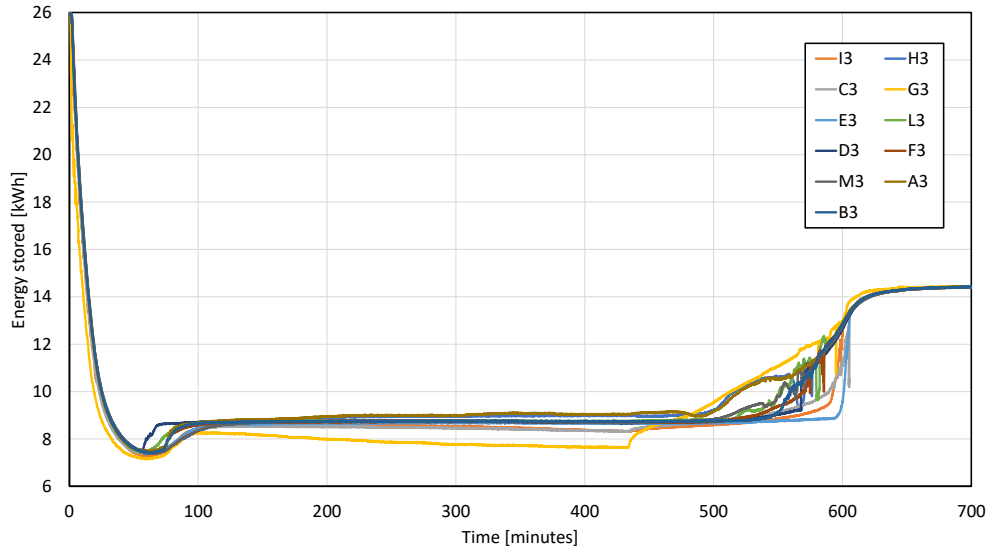

Figure 6.5: Temperatures of plane 3, flow rate of 40 l/min, water temperature of 6.5 °C for the charge and 14 °C for the discharge.

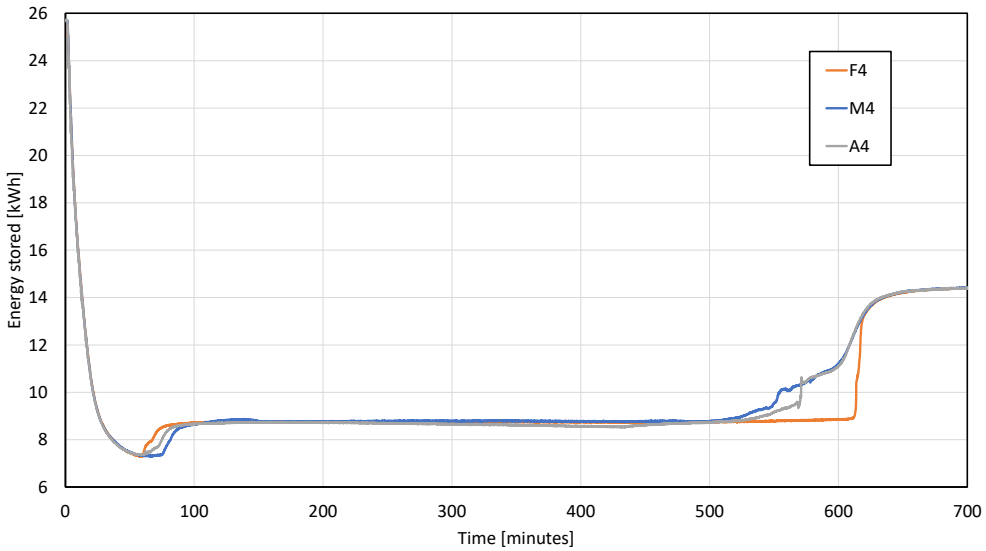

Figure 6.6: Temperatures of plane 4, flow rate of 40 l/min, water temperature of 6.5 °C for the charge and 14 °C for the discharge.

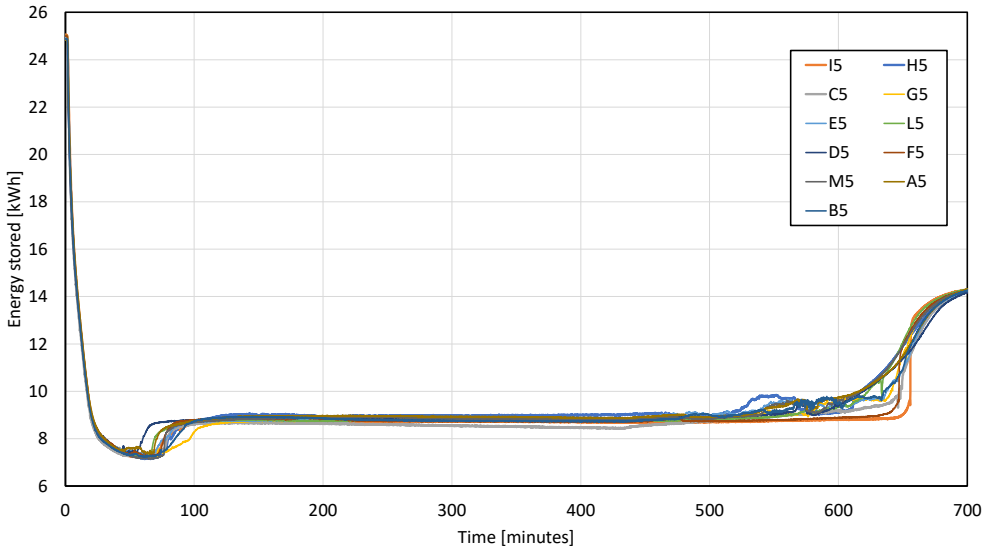

Figure 6.7: Temperatures of plane5, flow rate of 40 l/min, water temperature of 6.5 °C for the charge and 14 °C for the discharge.

For the other tests only the energy graph and the average temperature of the planes graph are reported. During the charging phase the temperatures of the planes are similar, see Figure 6.2, instead during the discharge the difference is much bigger. The subcooling phenomenon also occurs during the charging phase.

6.1.2 Test 5

From this experiment onwards it has been decided to limit the length of the charging phase to 4 hours, this was done in order to have shorter tests. As can be seen in Figure 6.8 the energy stored is almost 7 kWh in about 4 hours. The parameters are: flow rate 40 l/min, inlet temperature for the charge 6.5 °C and 14 °C for the discharge.

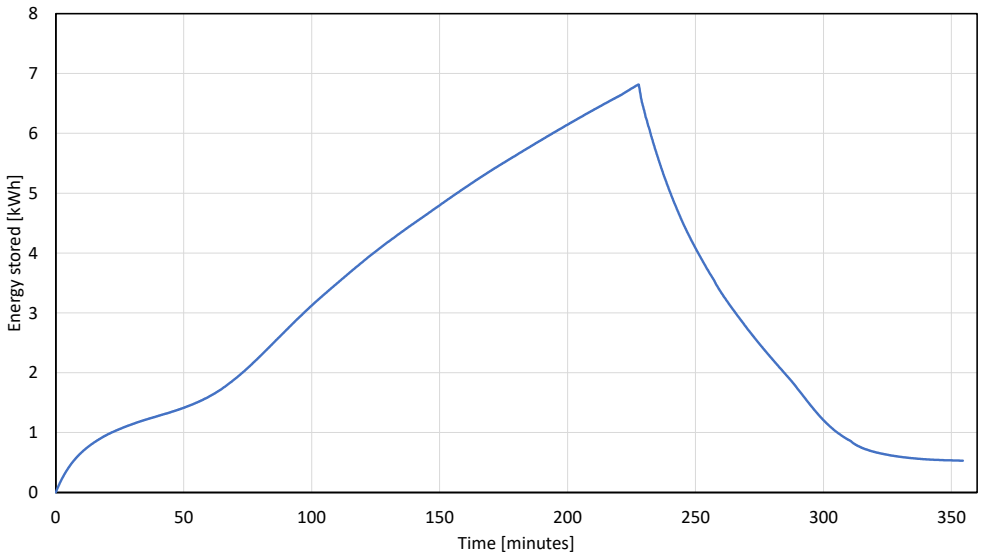

Figure 6.8: Graph of the energy stored with a flow rate of 40 l/min and water temperature of 6.5 °C for the charging phase and 14 °C for the discharging phase.

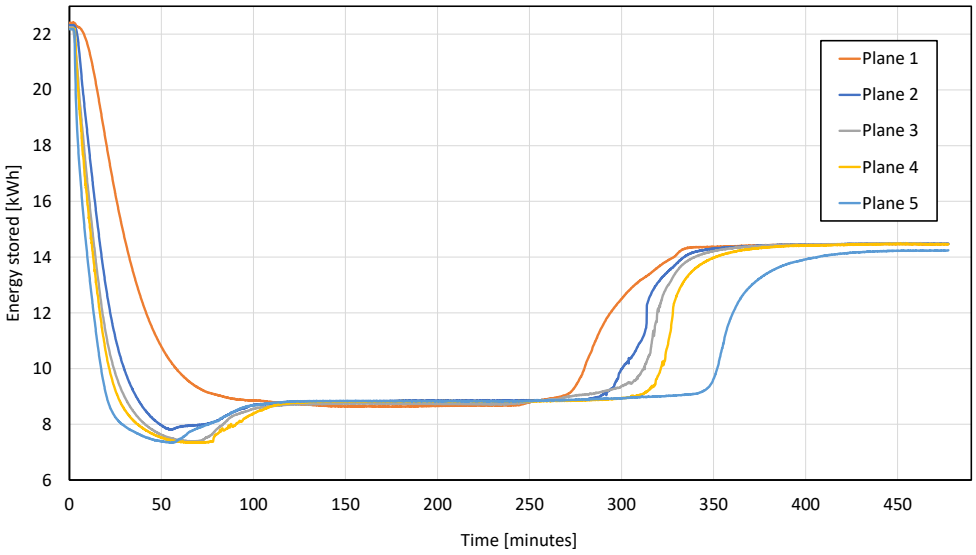

Figure 6.9: Average temperatures of the planes during the test with a flow rate of 40 l/min and water temperature of 6.5 °C for the charging phase and 14 °C for the discharging phase

6.1.3 Test 8

In this test the flow rate was set to 10 l/min with a water temperature of 6.5 °C for the charge and 14 °C for the discharge. The energy stored is much lower than the previous experiments, as can be seen in Figure 6.10. Obviously with a lower flow rate the system stores the energy slower.

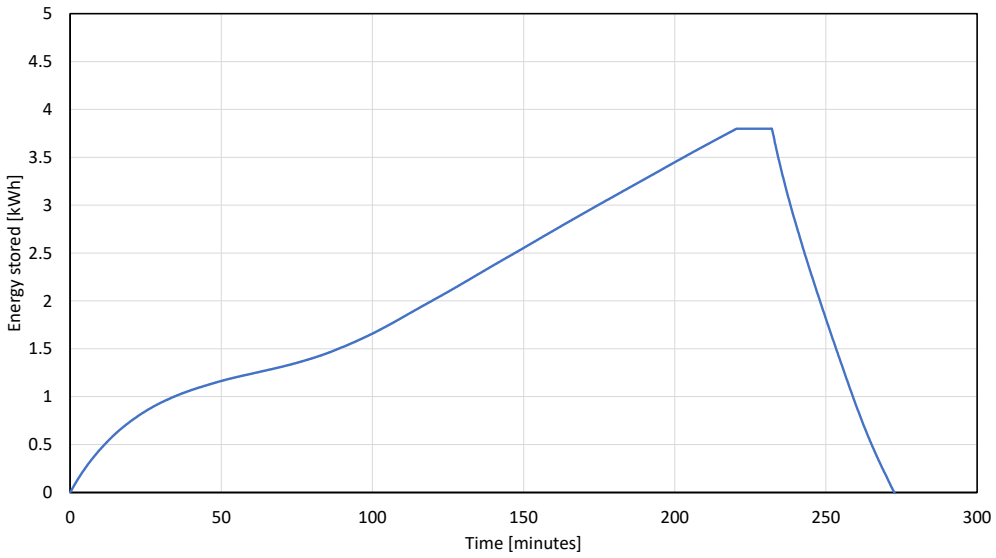

Figure 6.10: Graph of the energy stored with a flow rate of 10 l/min and water temperature of 6.5 °C for the charging phase and 14 °C for the discharging phase.

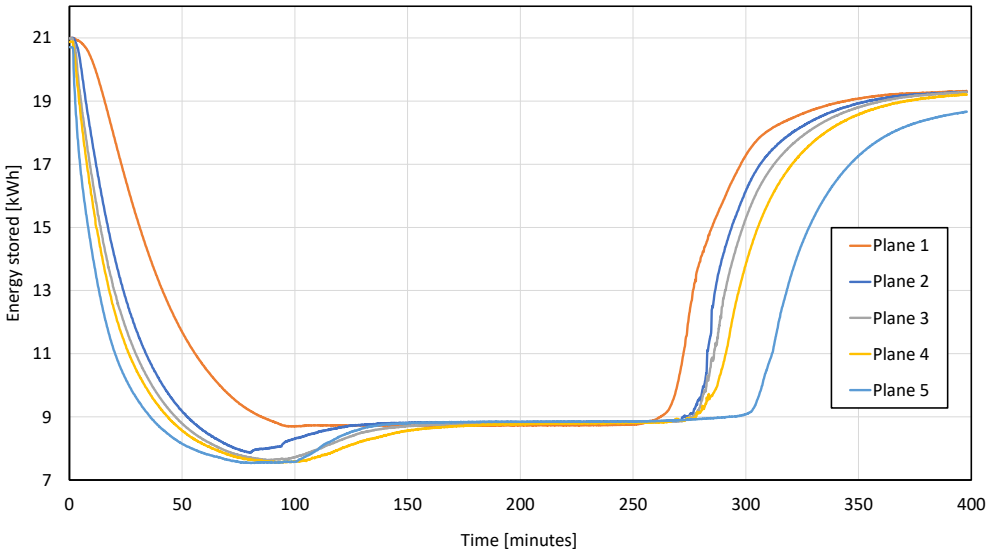

Figure 6.11: Average temperatures of the planes during the test with a flow rate of 10 l/min and water temperature of 6.5 °C for the charging phase and 14 °C for the discharging phase

6.1.4 Test 9

For this test, during the charging phase the flow rate was 10 l/min with an inlet temperature of 2 °C for the water. The charging was done in the afternoon after test 8, it lasted for 2.5 hours and 9.6 kWh of energy were stored, as reported in Figure 6.12 which is a lot when compared to previous tests in a very short time. For lack of time the discharging phase was carried out the following day.

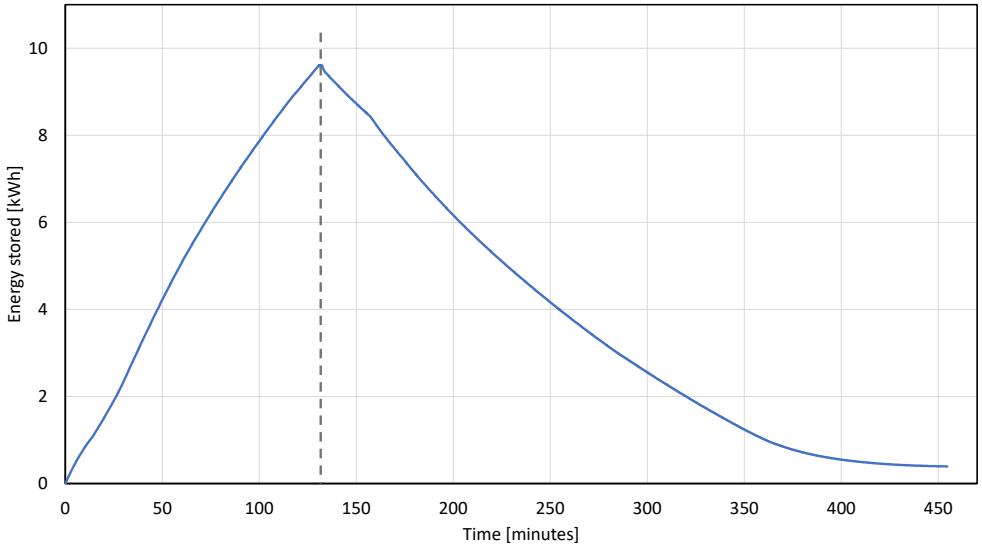

Figure 6.12: Graph of the energy stored with a flow rate of 10 l/min and water temperature of 2 °C for the charging phase and 14 °C for the discharging phase.

Having divided the two phases in two different days lead to temperature redistribution during the night as can be seen in Figures 6.13, 6.14, 6.15, 6.16, 6.17, 6.18.

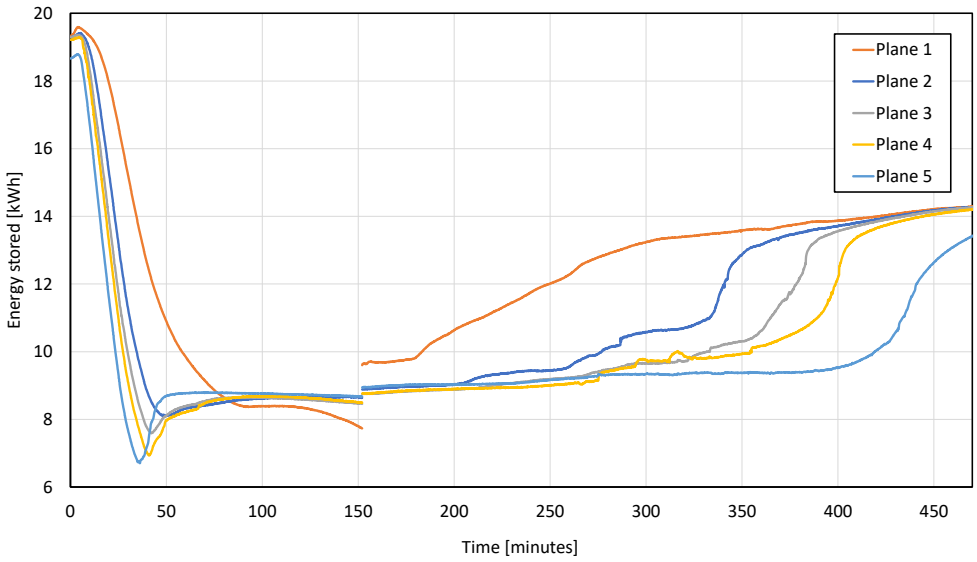

Figure 6.13: Average temperatures of the planes during the test with a flow rate of 10 l/min and water temperature of 2 °C for the charging phase and 14 °C for the discharging phase

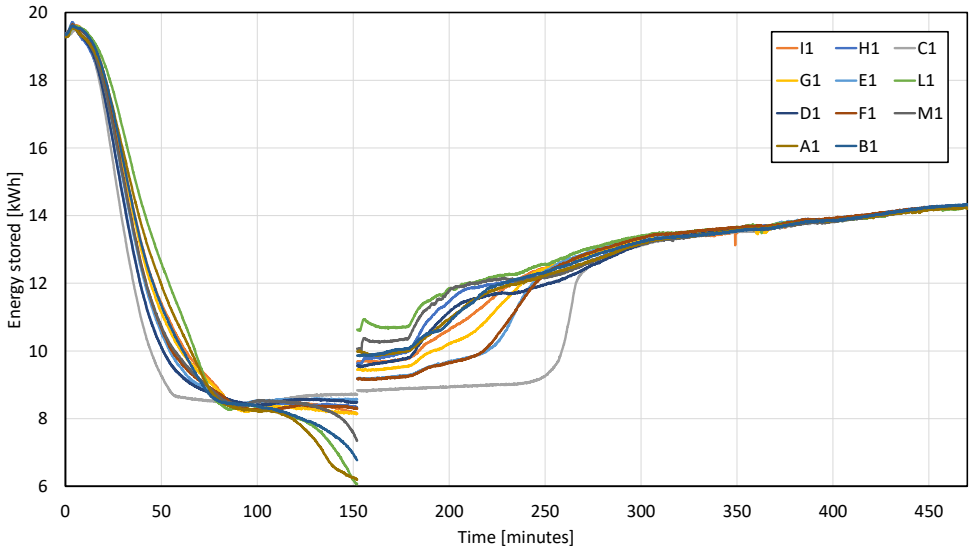

Figure 6.14: Temperatures of plane 1, flow rate of 10 l/min, water temperature of 2 °C for the charge and 14 °C for the discharge.

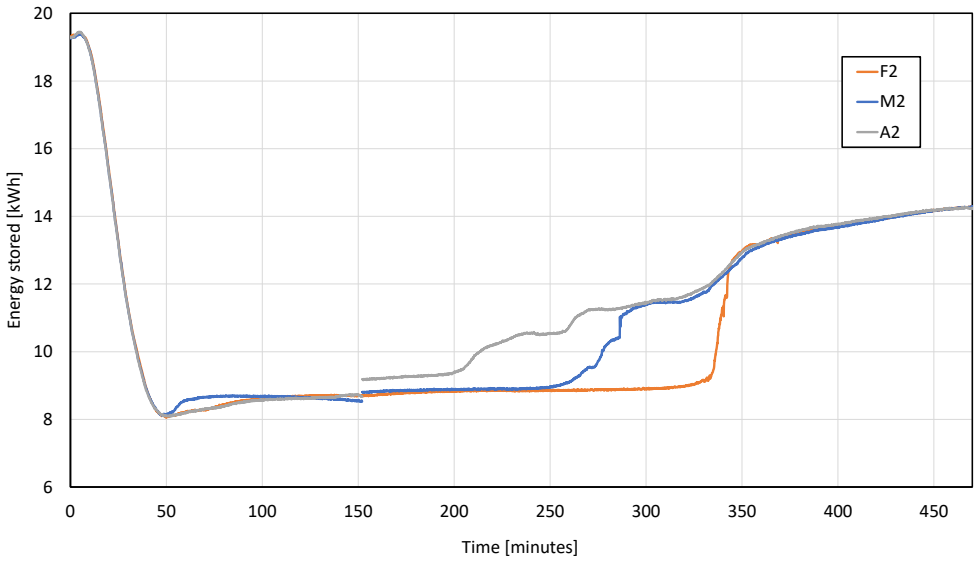

Figure 6.15: Temperatures of plane 2, flow rate of 10 l/min, water temperature of 2 °C for the charge and 14 °C for the discharge.

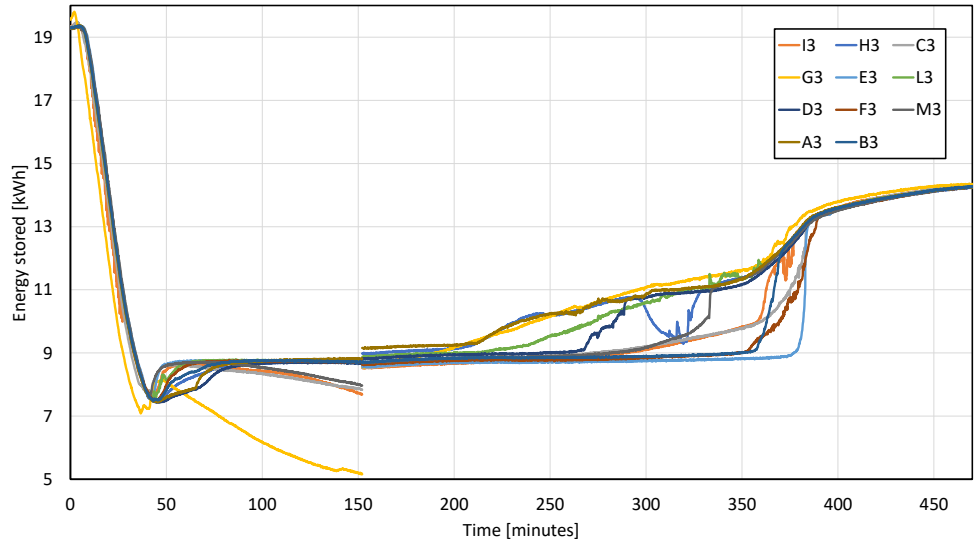

Figure 6.16: Temperatures of plane 3, flow rate of 10 l/min, water temperature of 2 °C for the charge and 14 °C for the discharge.

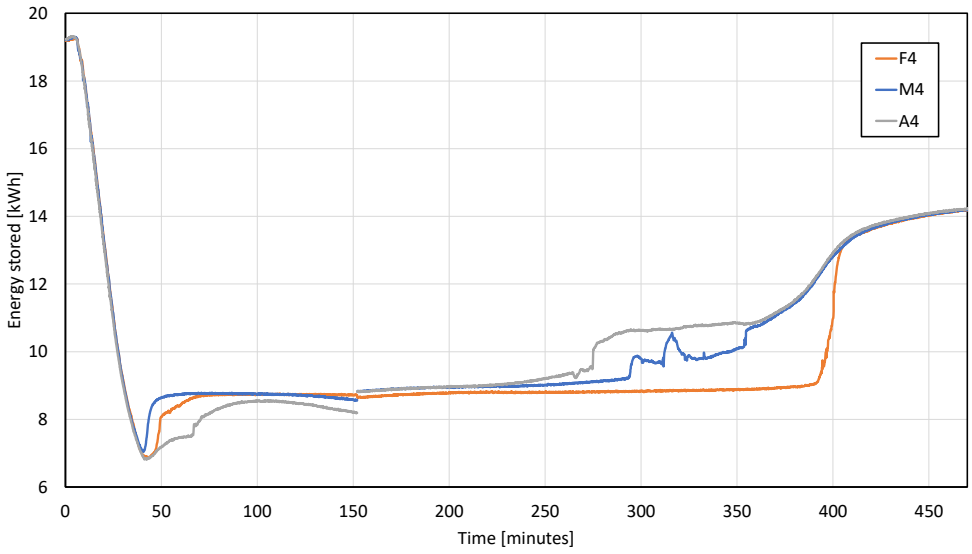

Figure 6.17: Temperatures of plane 4, flow rate of 10 l/min, water temperature of 2 °C for the charge and 14 °C for the discharge.

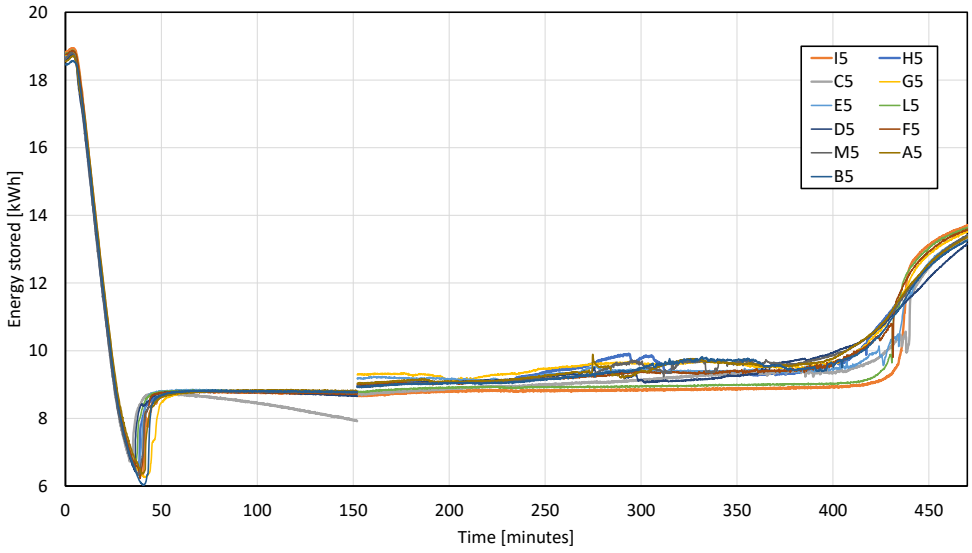

Figure 6.18: Temperatures of plane 5, flow rate of 10 l/min, water temperature of 2 °C for the charge and 14 °C for the discharge.

6.1.5 Test 11 (complete)

Test number 11 was a complete charge and discharge, the energy stored throughout the test is reported in Figure 6.19. Due to the time required to do a complete test the discharging phase was carried out the day after the charging phase. The data collected during the night was removed, the climatic room was left turned on at 9 °C in order to minimize the thermal losses of the PCM.

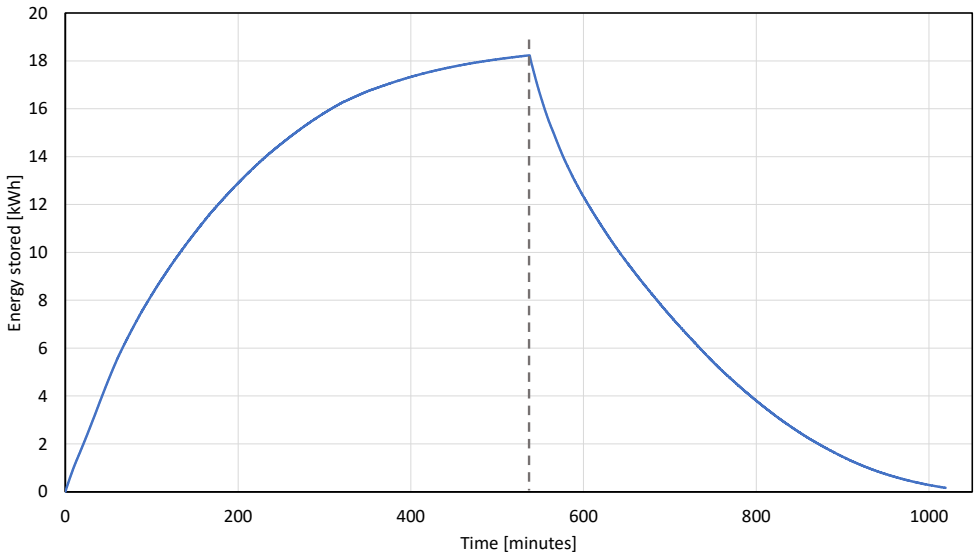

Figure 6.19: Graph of the energy stored with a flow rate of 17 l/min and water temperature of 2 °C for the charging phase and 16 °C for the discharging phase.

Instead in Figures 6.20 and 6.21 the energy stored for every hour of each phase is reported. The energy exchange is almost symmetric between the charging and discharging phases. As can be seen in Figures 6.20 and 6.21 the energy exchanged each hour decreases a lot, this means the heat transfer efficiency is also decreasing. It takes almost 9 hours to charge about 18 kWh of energy, but after 5 hours 16 kWh of energy are already stored. Thus it is inconvenient to use this system at maximum capacity, because the time required for storing and releasing the last few kWh of energy is too long when it is almost completely charged or discharged.

As already explained in Chapter 3, the TCs are zip tied to stainless steel rods which are placed between the roll-bonds. Thus, their positioning is not perfect, some of them may be closer or further away from the roll-bond. In Figure 6.22 the average temperatures of the planes are reported. This test was carried out with a flow rate of $\sim$ 17 l/min and inlet temperature of $\sim$ 2 °C of the water for the charging phase.

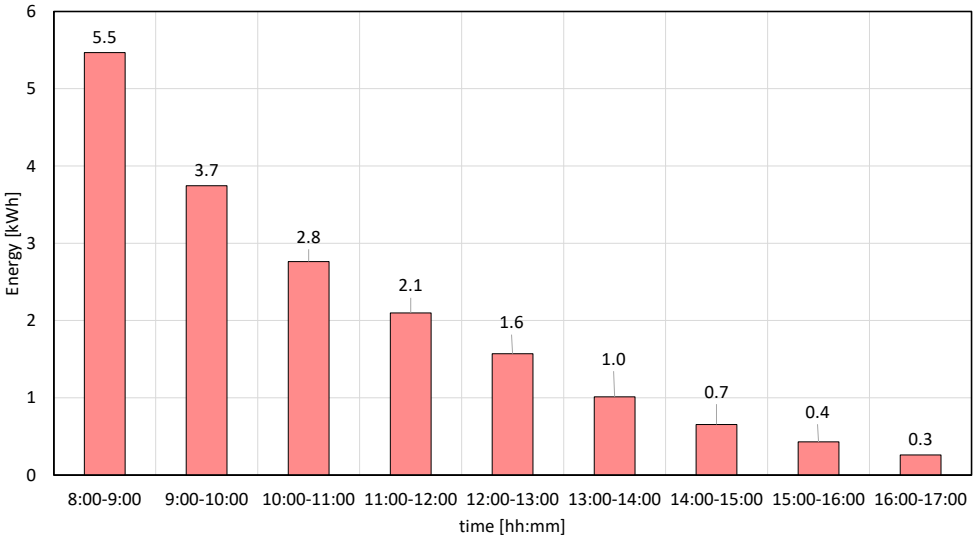

Figure 6.20: Energy stored every hour of the charging phase

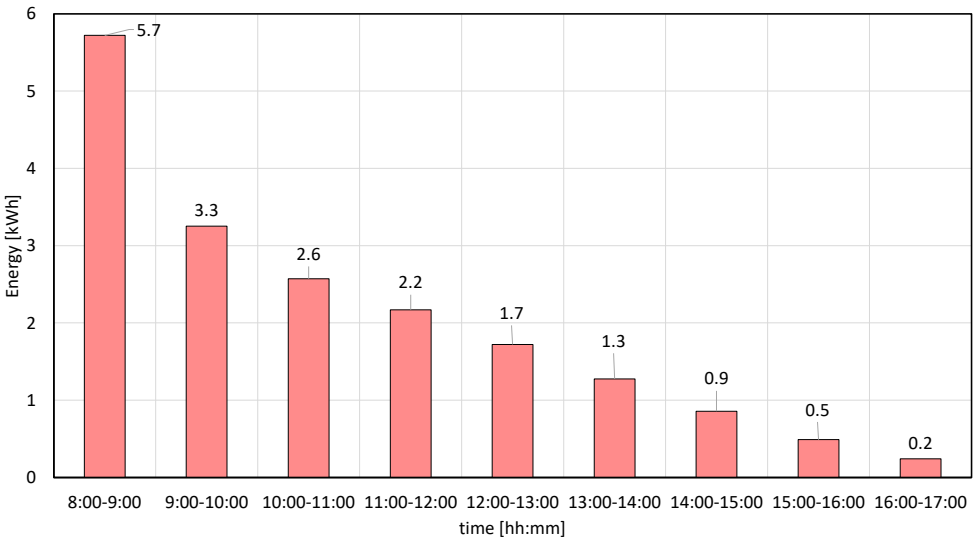

Figure 6.21: Energy released for every hour of the discharging phase

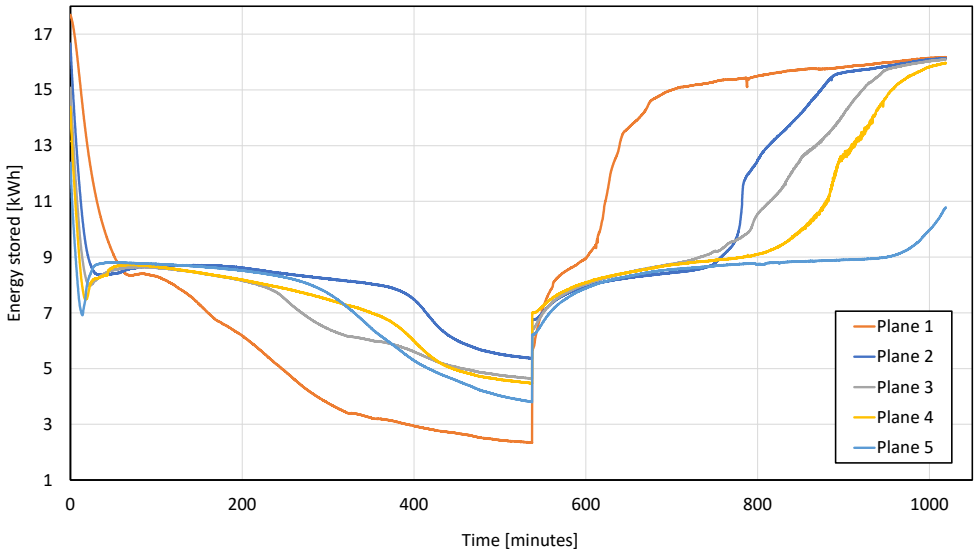

Figure 6.22: Average temperatures of the planes during the test with a flow rate of 17 l/min and water temperature of 2 °C for the charging phase and 16 °C for the discharging phase

At the beginning of the test the temperatures of the planes are closer to each other, this means that the temperature inside the PCM it is pretty homogeneous. During this phase the subcooling (or supercooling) phenomenon arises, in fact the lowest average temperature reached by plane 5 is about 6.9 °C before changing phase. Subcooling can be problematic, especially if it lasts for longer periods of time, this is not the case for this test. This phenomenon is necessary in order to start the nucleation of the first crystals of solid inside the liquid phase. Then the phase change starts and the temperatures climb and settles around 8.7 °C, until the PCM is all solid and then they can go lower. A temperature spike during the night can be seen, this is probably due to thermal losses from the PCM to the climatic room, even though the temperature inside the room is set to 9 °C there is still a relevant temperature difference between the inside (PCM) and the outside (climatic room). The next day the discharge process was started, the flow rate it is still $\sim$ 17 l/min and the water temperature is $\sim$ 16 °C. During this phase there is a clear temperature stratification inside the PCM. The plane 1 has a continuous temperature rise with no sign of phase changing of the PCM. Instead planes 2,3,4 are pretty close to each other. Plane 5 takes about 2 hours longer than plane 4 to melt, this may be due to the design of the tank, in fact the roll-bonds do not reach the bottom, but are placed inside some rails in order to keep them in place. Thus a cold zone forms at the bottom and it takes more time to melt completely. Instead the TCs of plane 1 looks like they are not inside the PCM when it melts due to the volume shrinkage during the solidification process, as can be seen in Figure 6.23. Therefore plane 1 is not representative of the behaviour of the PCM.

In Figure 6.22 the temperatures of plane 1 are shown, it can be seen that there is a big difference in temperature between the TCs (the biggest difference is 5 °C).

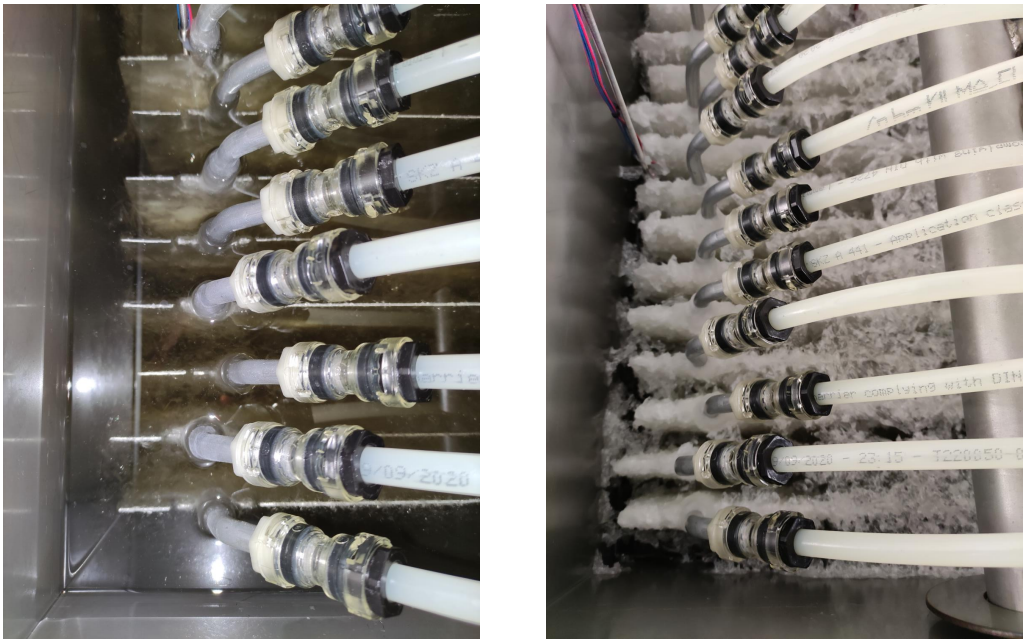

Figure 6.23: Volume shrinkage during the solidification process

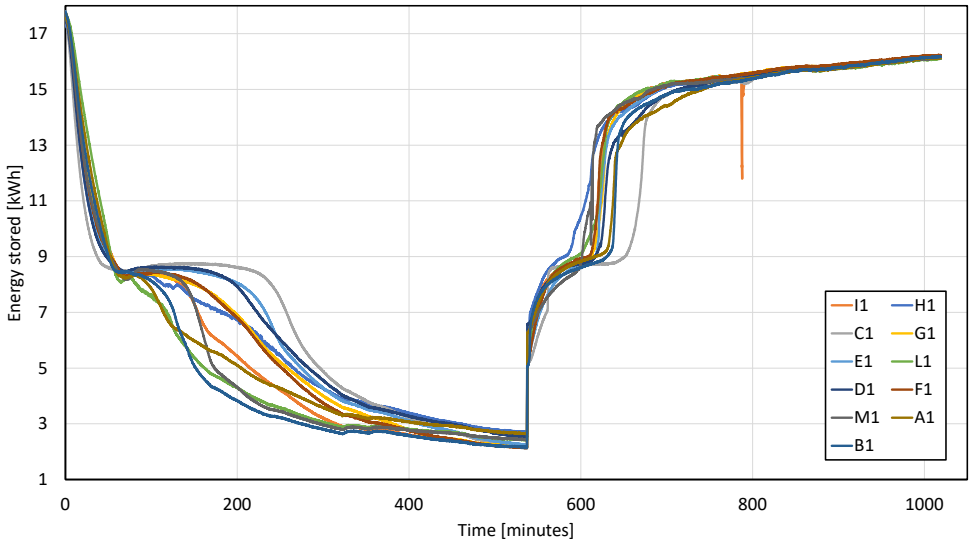

Figure 6.24: Temperatures of plane 1, flow rate of 17 l/min, water temperature of 2 °C for the charge and 16 °C for the discharge.

Considering the TCs of plane 2, reported in Figure 6.25, there are only 3 TCs on this plane due to the positioning decided. The behaviour is very similar to the average temperature reported in Figure 6.22. The difference could be due to the different positions of the TCs in relation to the roll-bond design, or their distance from the

roll-bond.

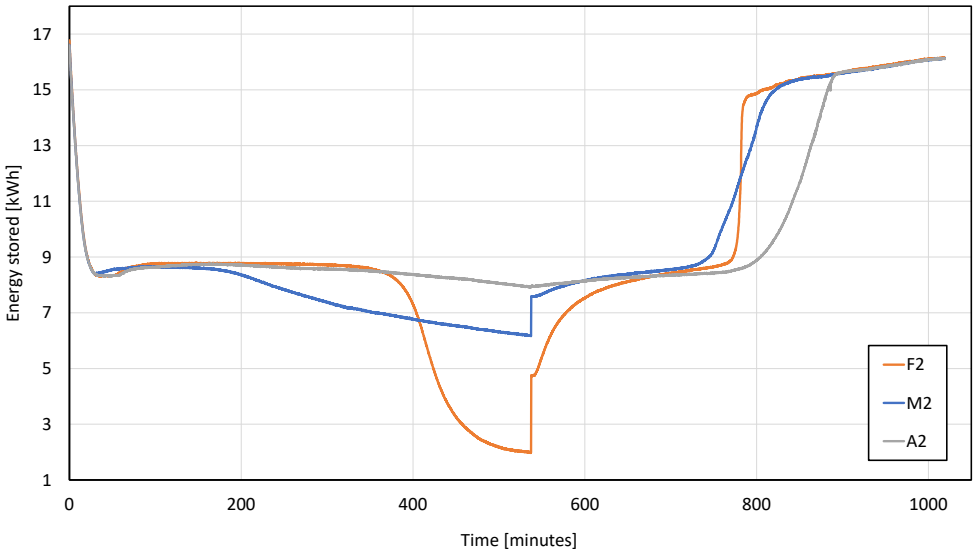

Figure 6.25: Temperatures of plane 2, flow rate of 17 l/min, water temperature of 2 °C for the charge and 16 °C for the discharge.

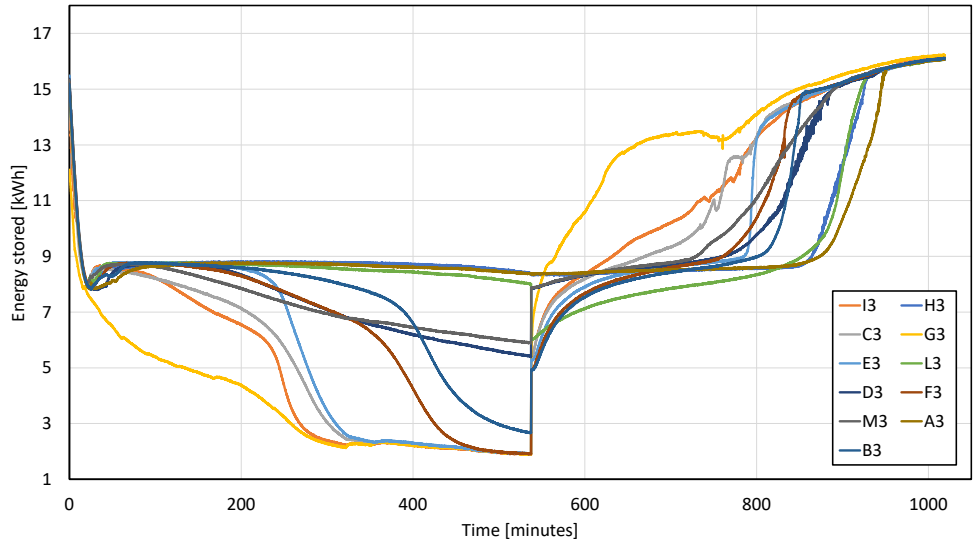

Figure 6.26: Temperatures of plane 3, flow rate of 17 l/min, water temperature of 2 °C for the charge and 16 °C for the discharge.

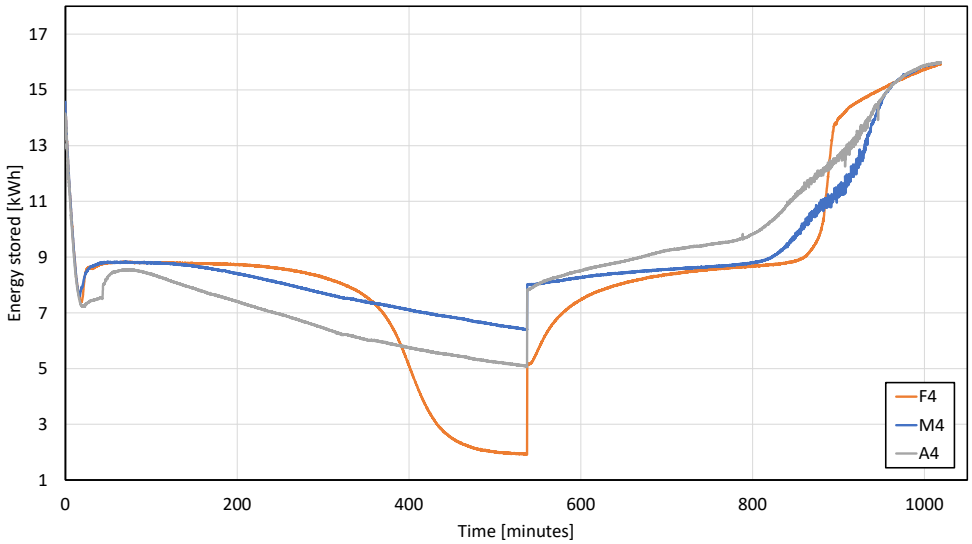

Figure 6.27: Temperatures of plane 4, flow rate of 17 l/min, water temperature of 2 °C for the charge and 16 °C for the discharge.

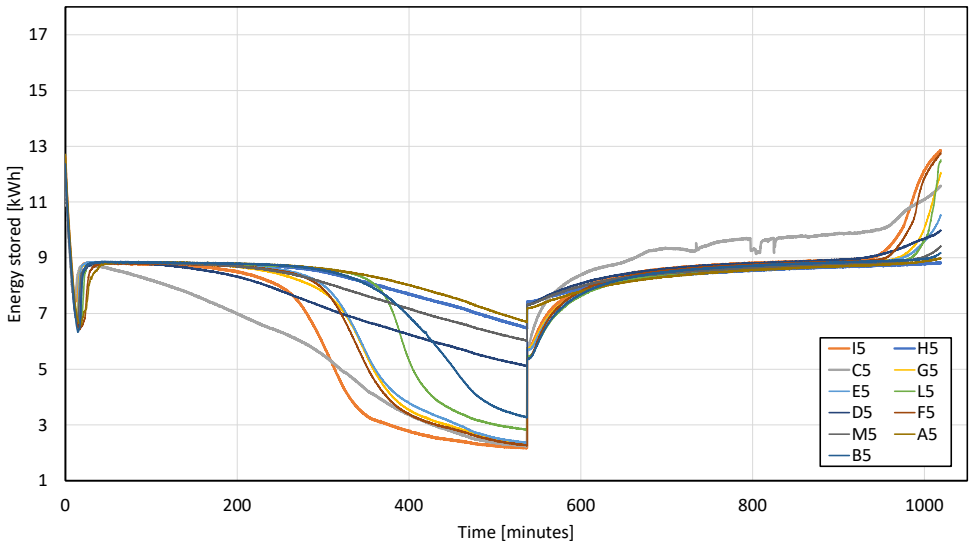

Figure 6.28: Temperatures of plane 5, flow rate of 17 l/min, water temperature of 2 °C for the charge and 16 °C for the discharge.

During the charging phase the heat transfer is quite good, as reported in Figure 6.20. Indeed the natural convection inside the PCM may help, as the liquid cools down and solidifies its density increases, thus the colder liquid builds up at the bottom.
Instead for the discharging process the natural convection is detrimental for the heat transfer. As the solid melts,

the liquid having lower density, moves upwards. The problem is the bottom part that takes ages before melting, here the phase change is probably achieved only through conduction heat transfer thus the long time required, this can be seen in Figure 6.22 near the end.

Matlab program

In order to better visualize the temperature field inside the tank it has been decided to realize a matlab program. This program gets the data from the excel file and returns a 3D image of the temperatures inside, the visualization is done through 5 planes, the same used in the experimental tests. In order to have a light program not all the data was used, but only one tenth of data was considered (every minute or so). It has been decided to realize a 4D matrix, the experimental data has been used and placed inside this matrix. The fourth dimension is time, so basically is a 3D matrix (X, Y, Z) and its dimensions are the same as the real dimensions of the tank. Each data point of the experiments was placed in the matrix in the position corresponding to the real position of the tank, then for symmetry reasons some data was duplicated in different position (data in A', C', M', I') as reported by Figure 6.29. Then a linear interpolation was done for the 3D matrix, using the meshgrid command in Matlab, and this was repeated in the fourth dimension which is time. A linear interpolation was used in order not to make the program too heavy to run.

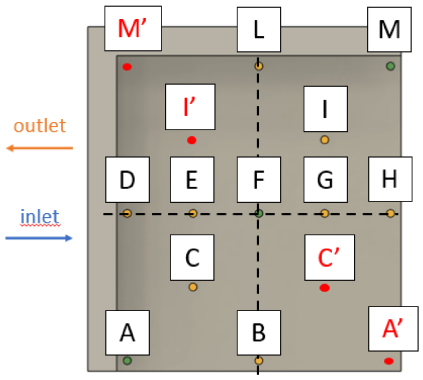

Figure 6.29: Symmetry used for the Matlab program

In Figure 6.30 (left to right) the charging phase is reported. The behaviour is the same as the one reported in Figure 6.22, the coldest point during the charging phase is the bottom of the tank probably due to the convection of the liquid. On the right of Figure 6.30 it can be seen that plane 1 is colder than the planes below, this suggests that this plane is not representative of the PCM behaviour because the TCs are outside the PCM (as already seen in Figure 6.23).

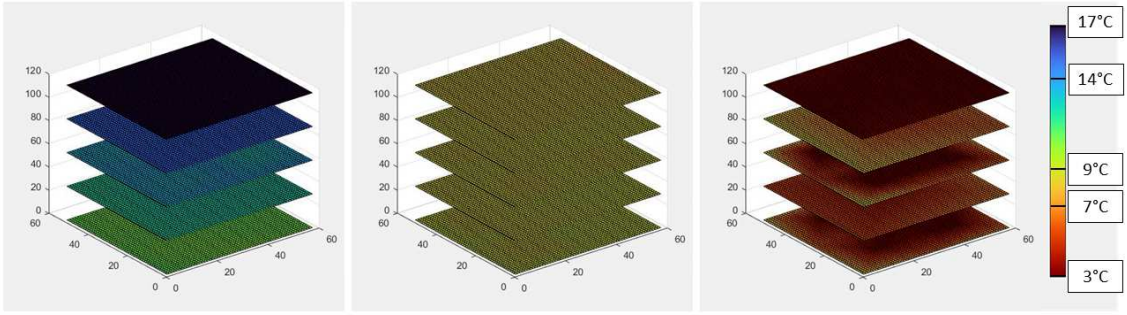

Figure 6.30: Temperature field during the charging phase

In Figure 6.31 (left to right) the discharging phase is reported. The bottom plane takes longer to melt (see right side of Figure 6.31) like already reported in Figure 6.22.

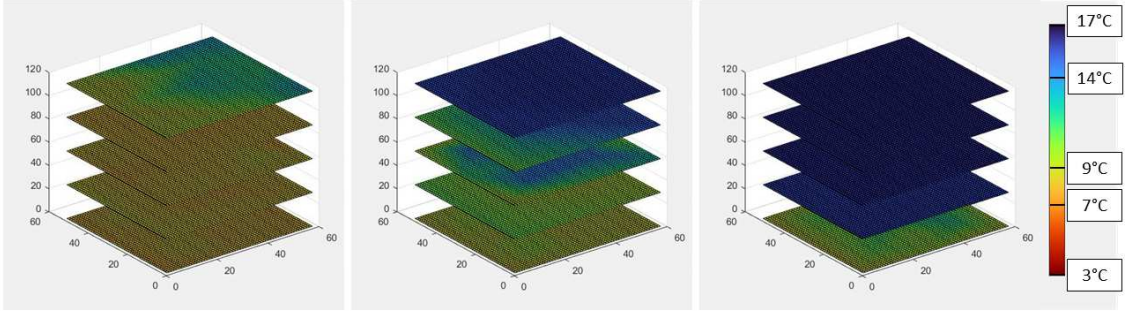

Figure 6.31: Temperature field during the discharging phase

6.1.6 Test 13

Considering a real application of this system it was concluded that a typical usage scenario is not a complete charge and discharge as studied till now. Thus it has been decided to do some intermittent tests with step charges and discharges. The flow rate used was 17 l/min and the water temperature was 2 °C for the charges and 16 °C for the discharges. In Figure 6.32 the stored energy is reported. The first charge has a duration of about 2 hours, after this there is 1 hour of discharge. After that the system is charged again for 1 hour and then completely discharged. It can be seen that the energy profile behaves symmetrically 6.32.

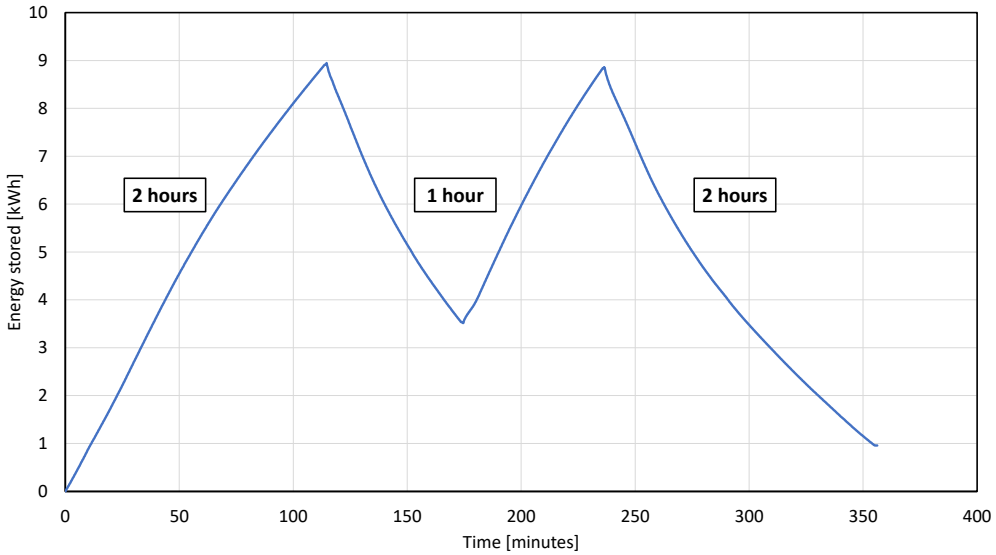

Figure 6.32: Graph of the energy stored for a discontinuous test, with a flow rate of 17 l/min and water temperature of 2 °C for the charges and 16 °C for the discharges.

In Figure 6.33 the average temperatures of the planes are reported. As already stated plane 1 is not representative of the behaviour because its thermocouples may be outside the PCM due to the volumetric shrinkage of the PCM.

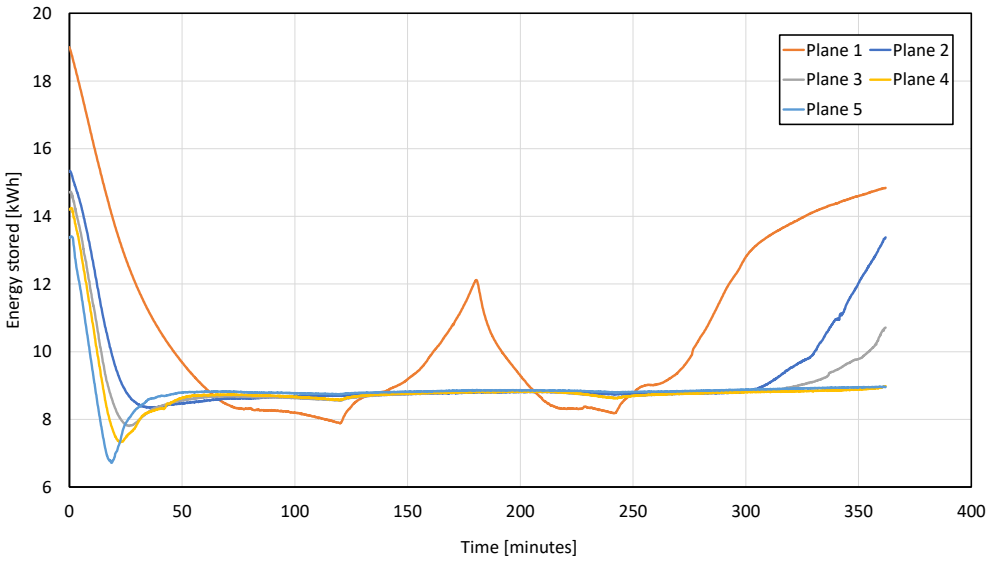

Figure 6.33: Average temperatures of the planes for a discontinuous test, with a flow rate of 17 l/min and water temperature of 2 °C for the charges and 16 °C for the discharges.

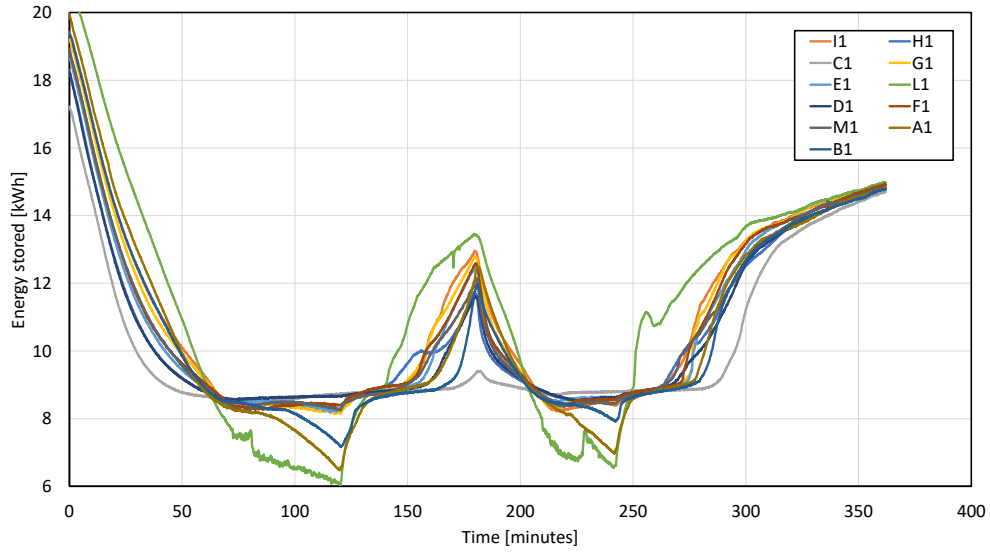

Figure 6.34: Temperatures of plane 1 for a discontinuous test, with a flow rate of 17 l/min and water temperature of 2 °C for the charges and 16 °C for the discharges.

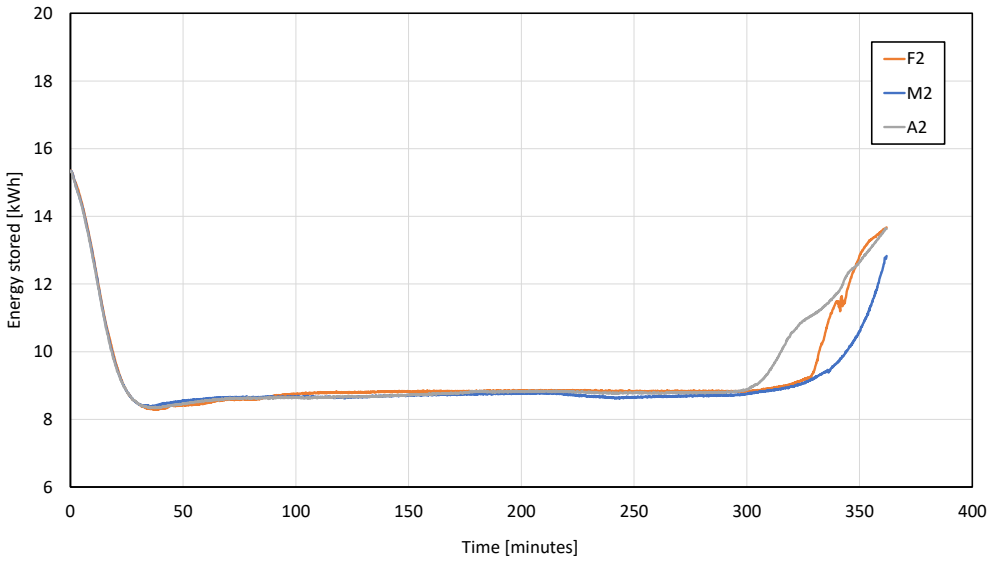

Figure 6.35: Temperatures of plane 2 for a discontinuous test, with a flow rate of 17 l/min and water temperature of 2 °C for the charges and 16 °C for the discharges.

The thermocouple G3 has a strange behaviour, as can be seen in Figure 6.36, this may be because the TC is touching the roll-bond.

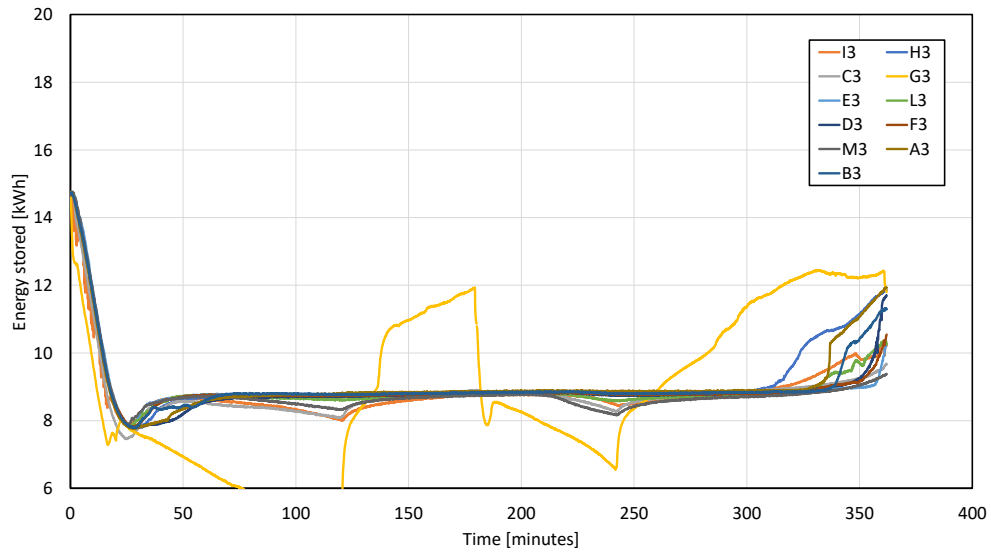

Figure 6.36: Temperatures of plane 3 for a discontinuous test, with a flow rate of 17 l/min and water temperature of 2 °C for the charges and 16 °C for the discharges.

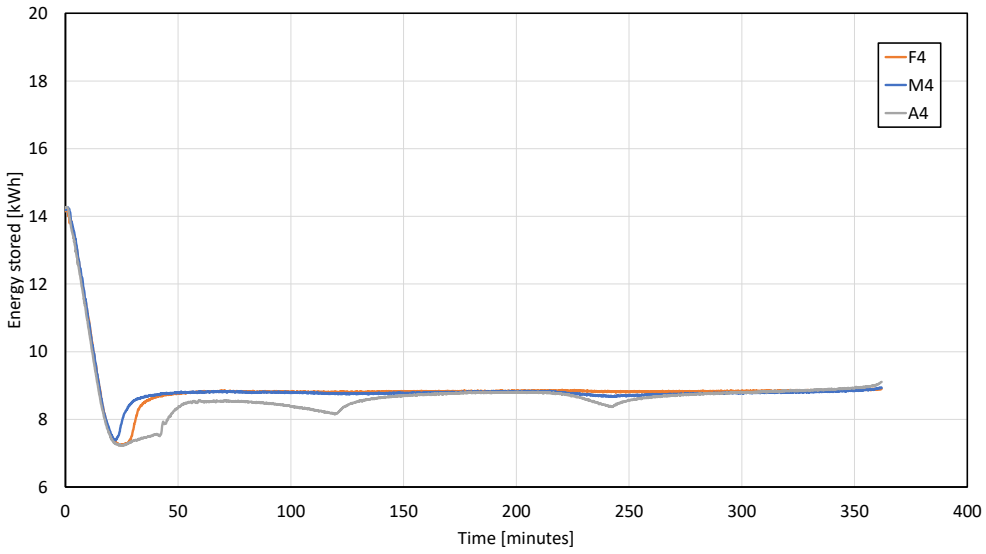

Figure 6.37: Temperatures of plane 4 for a discontinuous test, with a flow rate of 17 l/min and water temperature of 2 °C for the charges and 16 °C for the discharges.

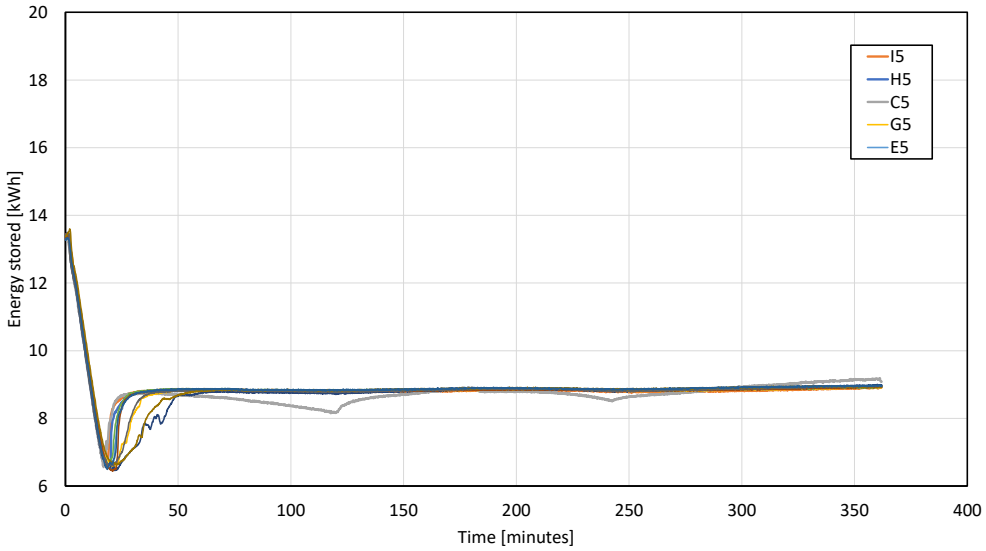

Figure 6.38: Temperatures of plane 5 for a discontinuous test, with a flow rate of 17 l/min and water temperature of 2 °C for the charges and 16 °C for the discharges.

6.1.7 Test 15

In this test a 30 minutes pause has been introduced compared to test 13. The flow rate and the inlet water temperature are still the same as test 13, flow rate is about 17 l/min, water temperature is 2 °C for the charge and 16 °C for the discharge. For the final discharge the water temperature was set to 24 °C to finish the test quickly. In Figure 6.39 the energy profile is reported. The first charge lasts for 2 hours, the discharge lasts 1 hour with a pause of 30 minutes. The second charge lasts 1 hour and after this there is a complete discharge of the system.

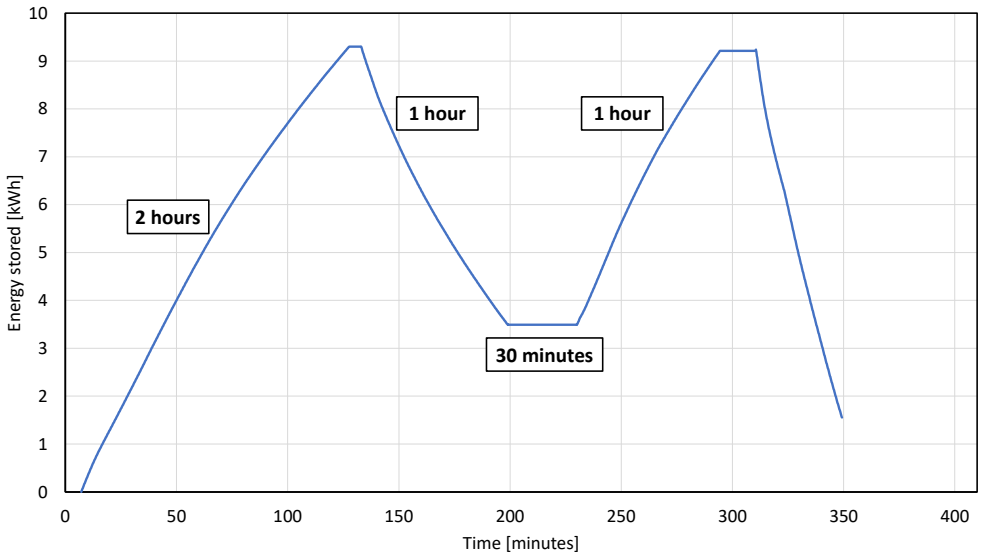

Figure 6.39: Graph of the energy stored for a discontinuous test (pauses with different duration), with a flow rate of 18 l/min and water temperature of 2 °C for the charges and 16 °C for the discharges.

As reported in Figure 6.40, the only plane affected by the 30 minutes pause is the first plane. But the TC of this plane are not reliable because they might be outside the PCM (as can be seen in Figure 6.23).

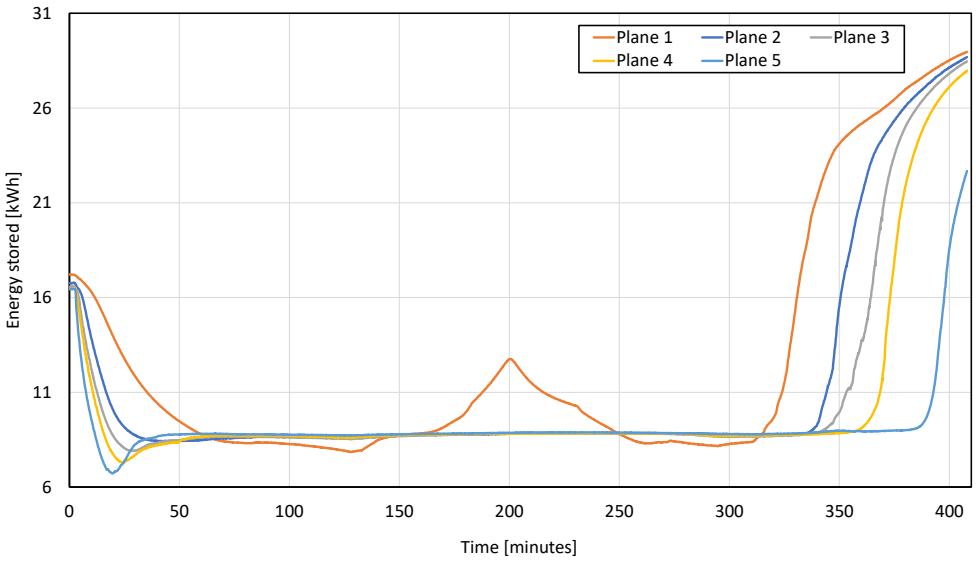

Figure 6.40: Average temperatures of the planes for a discontinuous test (pauses with different duration), with a flow rate of 18 l/min and water temperature of 2 °C for the charges and 16 °C for the discharges.

6.1.8 Test 16

In Figure 6.41 is reported the energy profile of the test. In this case the 40 minutes pause was placed just before the final discharge.

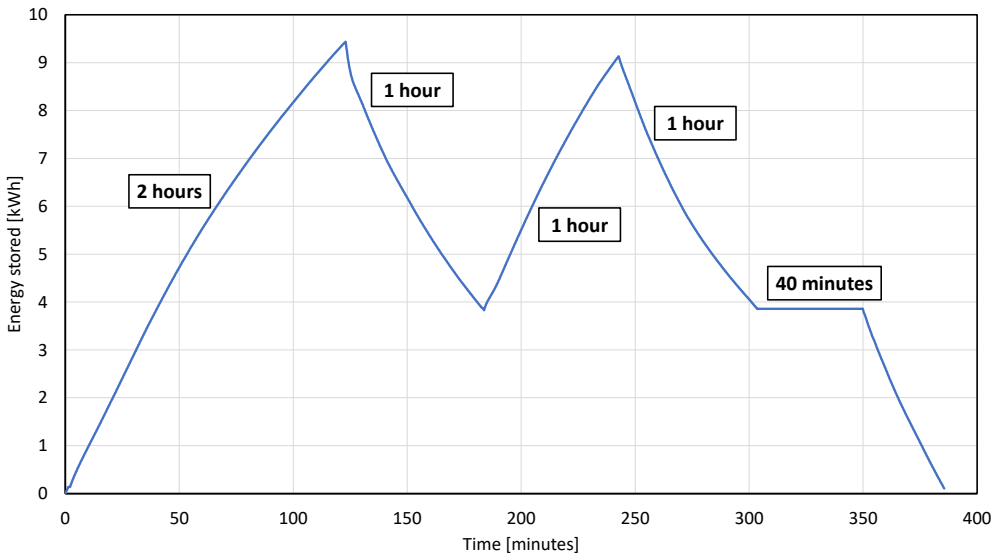

Figure 6.41: Graph of the energy stored for a discontinuous test (pauses with different duration), with a flow rate of 18 l/min and water temperature of 2 °C for the charges and 16 °C for the discharges.

Only the average temperature of plane 1 is affected by the pause (see Figure 6.42), but as already stated this plane is not representative.

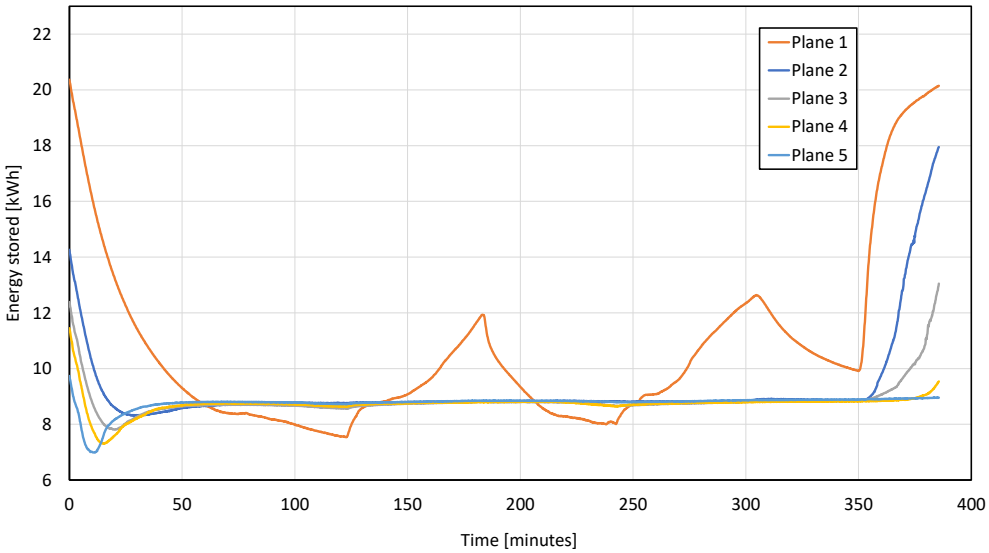

Figure 6.42: Average temperatures of the planes for a discontinuous test (pauses with different duration), with a flow rate of 18 l/min and water temperature of 2 °C for the charges and 16 °C for the discharges.

6.1.9 Test 17

For this test the 40 minutes pause is before the last charge, as can be seen in Figure 6.43.

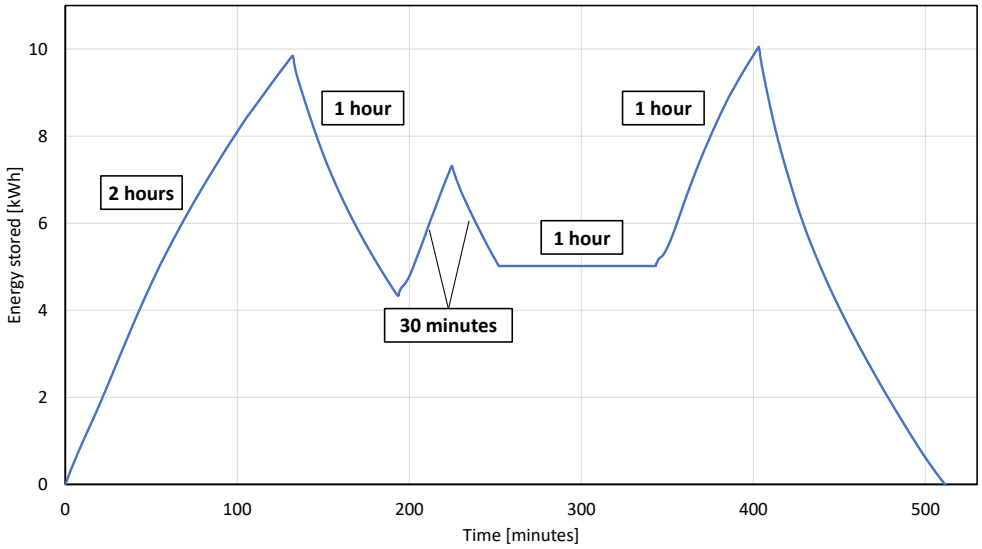

Figure 6.43: Graph of the energy stored for a discontinuous test (pauses with different duration), with a flow rate of 18 l/min and water temperature of 2 °C for the charges and 16/19 °C for the discharges.

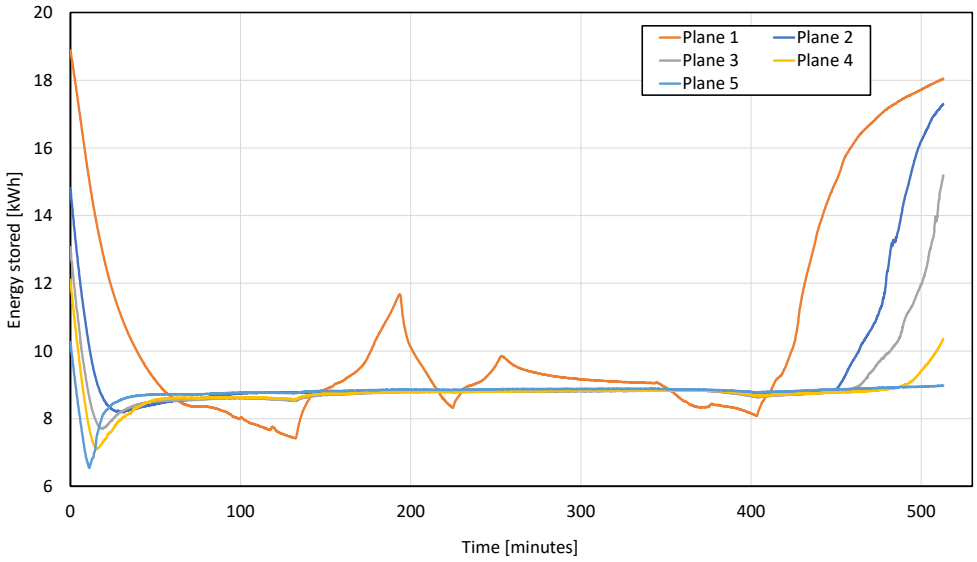

Figure 6.44: Average temperatures of the planes for a discontinuous test (pauses with different duration), with a flow rate of 18 l/min and water temperature of 2 °C for the charges and 16/19 °C for the discharges.

In Figure 6.45 the energies of the charging phases for test 13, 15 and 17 are reported. The difference between these three tests is the length of the pause, for test 15 is 30 minutes, for test 17 is 1 hour, instead test 13 is the reference with no pause whatsoever. The difference between these 3 energy curves is negligible, thus the pause and its length has no significant effect on the rate of energy stored.

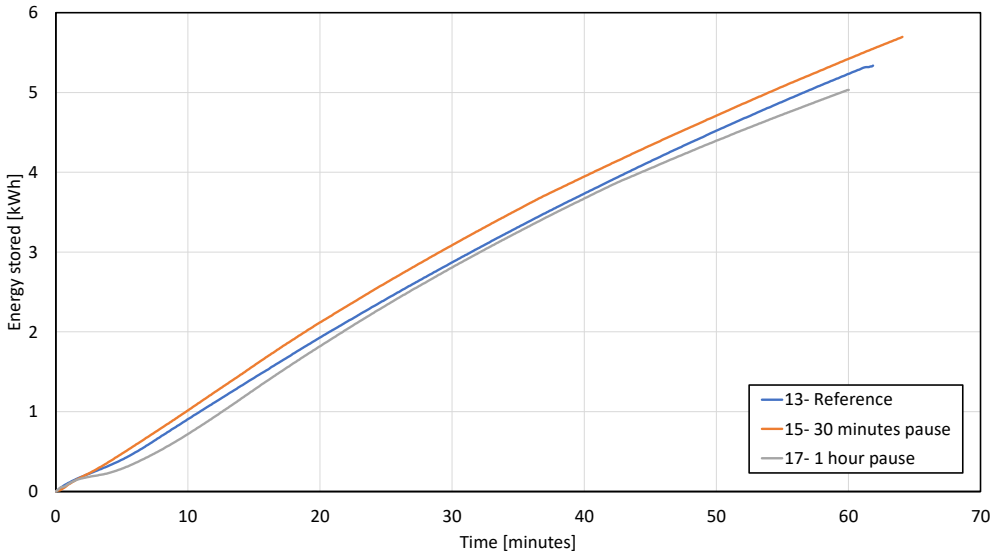

Figure 6.45: Charge comparison between charges of test 13, 15 and 17

6.1.10 Test 18-19-20

As seen in previous tests the pauses bring no convenience for tests of short duration. Thus it was decided to do a complete step discharge with pauses of different length. In Figure 6.46 the energy graph is reported. This test consists of three different experiments, the first one (test 18) is the charging phase with a flow rate of 17 l/min and water temperature of 2 °C. The second one (test 19) is the first step-discharging phase, the last one is a step-discharge as well (test 20). In both the discharging phases the flow rate was 17 l/min with a a water temperature of 16 °C. Obviously these tests were carried out in successive days due to the long time required for each one of them.

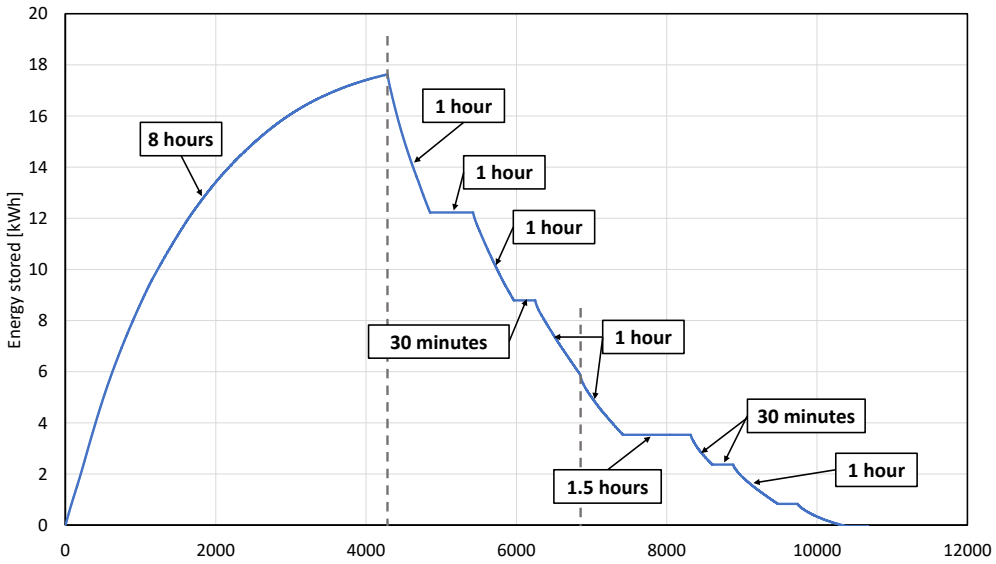

Figure 6.46: Graph of the energy stored with pauses of different length during the discharge, flow rate of 17 l/min and water temperature of 2 °C for the charges and 16 °C for the discharges.

In Figure 6.47 the average temperatures of the planes are reported. Near the end of the test, when the liquid fraction is high, there are temperature spikes likely due to convective motion of the liquid.

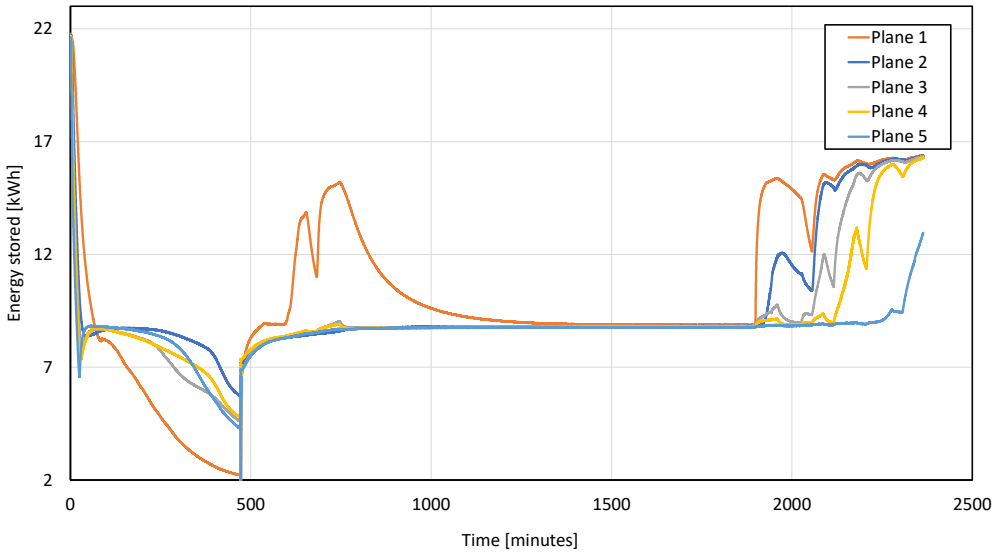

Figure 6.47: Average temperatures of the planes with pauses of different length during the discharge, flow rate of 17 l/min and water temperature of 2 °C for the charges and 16 °C for the discharges.

In Figure 6.48 the average temperatures of the planes and the energy stored in the PCM during the discharging phase are reported.

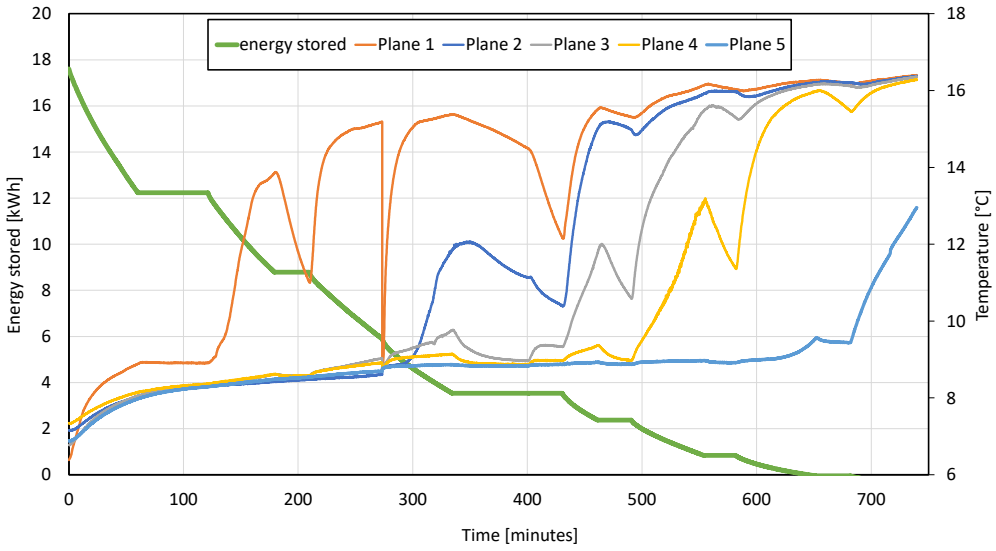

Figure 6.48: Energy during the discharge compared to the average temperatures of planes with pauses of different length during the discharge, flow rate of 17 l/min and water temperature of 2 °C for the charges and 16 °C for the discharges.

This graph is interesting because it shows that when the PCM is almost completely charged with energy the pauses have no effect on the temperatures of the planes. Instead when the system is less than 50% charged the

effect on the average temperatures of the planes can be seen, in fact the temperatures drop during the pauses. However the lower the plane is in the tank, the smaller the effect is on the plane, indeed plane 5 at the bottom is not affected at all. This behaviour can be explained with the liquid fraction inside the tank. If the liquid fraction is low, this means the PCM is almost completely solid, the temperature redistribution is low because the heat is exchanged only through conduction and the PCM has a very low thermal conductivity coefficient. Instead if the liquid fraction is high the convection can happen which is a much more efficient heat transfer system.

In Figure 6.49 a comparison between the discharging phase of test 11 and the discharge of tests 19-20 is reported.

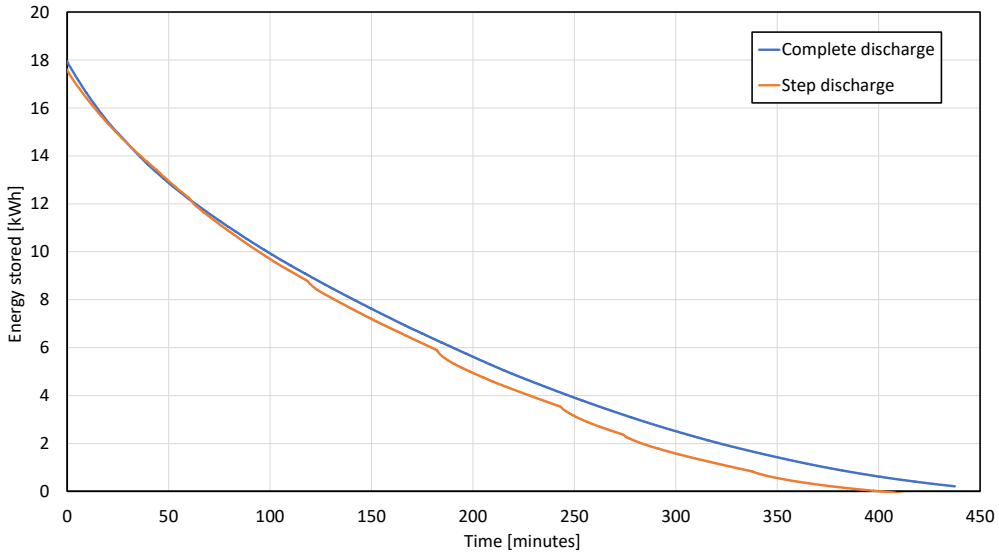

Figure 6.49: Comparison between continuous discharge (test 11) and step discharge (test 19-20)

Both the discharges were carried out with a flow rate of 17 l/min and a water temperature of 16 °C, the energy stored for both tests is almost the same so the confrontation is fair. The pauses have no effect if the liquid fraction is low, instead if it is higher the effect can be seen but it is still marginal. Overall the test 19-20 with the pauses is, at best, 40 minutes quicker than the normal discharge over a 7 hour long experiment. However the graph in Figure 6.49 is reported without the pauses, otherwise it would obviously be much slower.

6.1.11 Test 22

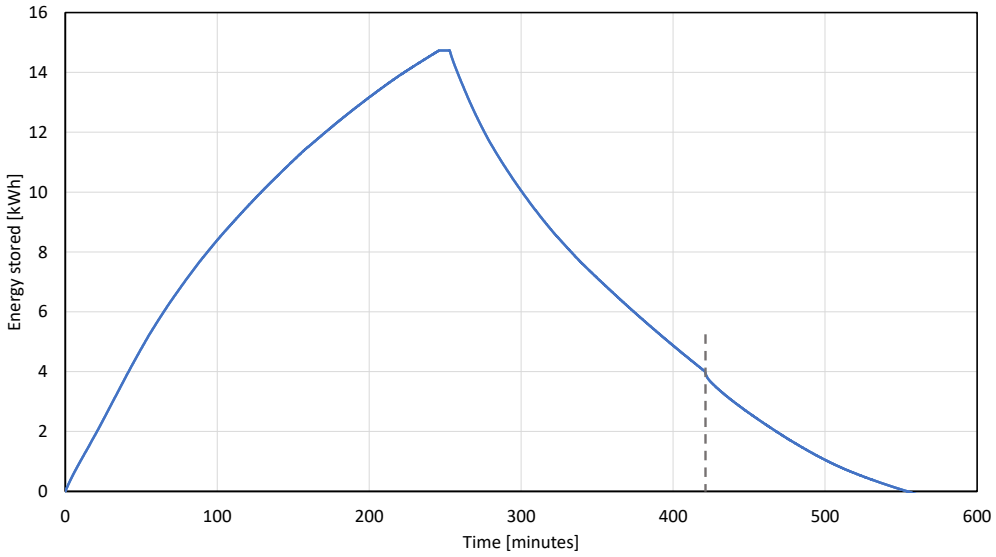

Figure 6.50: Graph of the energy stored with inlet and outlet swapped, flow rate of 17 l/min and water temperature of 2 °C for the charges and 16 °C for the discharges.

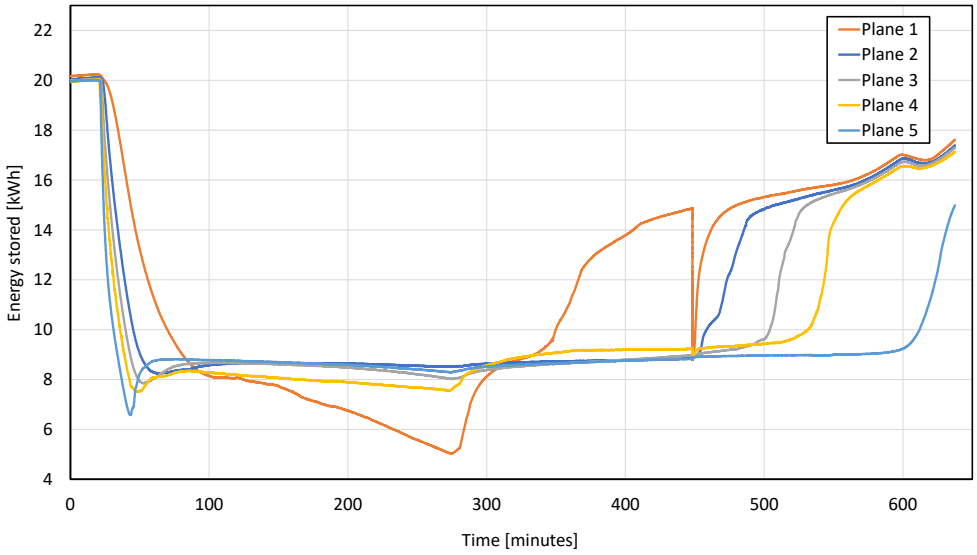

Figure 6.51: Average temperatures of the planes with inlet and outlet swapped, flow rate of 17 l/min and water temperature of 2 °C for the charges and 16 °C for the discharges.

For this test the configuration has been changed, particularly the inlet and outlet were swapped. The parameters were kept the same, flow rate of 17 l/min and water temperature of 2 °C and 16 °C for the charge and for the discharge respectively. In Figure 6.50 the energy graphs is reported.

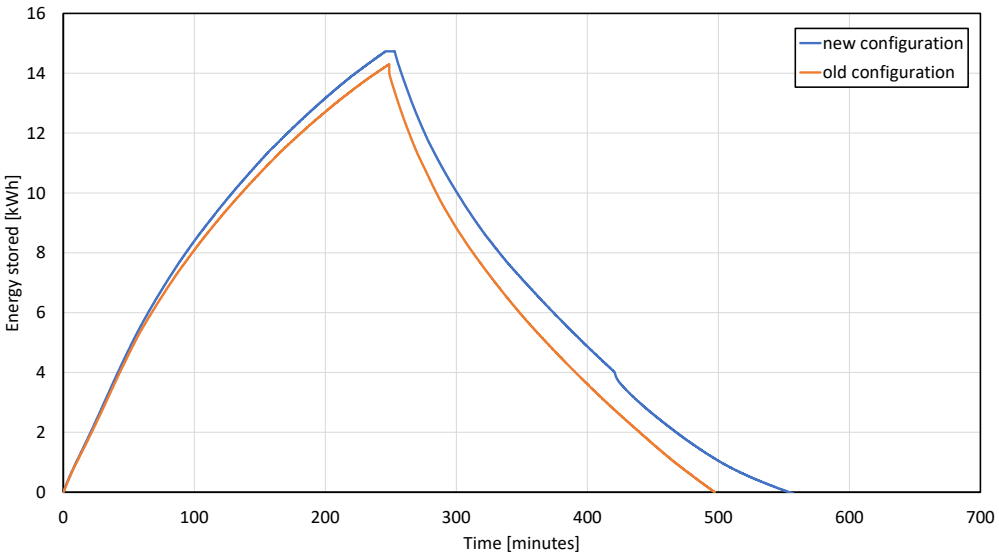

Figure 6.52: Comparison between old configuration (test 11) and new configuration of test 22 (inlet and outlet swapped)

The average temperatures are reported in Figure 6.51. The discharging phase was divided in two days, in fact the temperature of plane 1 has a huge drop in temperature, this is because when the PCM solidifies the TCs of this plane are outside the PCM. The swapping of the inlet and outlet manifolds was done before receiving the roll-bond design from the manufacturer, thus a big difference was expected between the two tests. As reported by Figure 6.52 the difference is very small, this was later confirmed also by the roll-bond design which is symmetrical.

6.1.12 Test 28

In this test the configuration of complete parallel of the roll-bonds is used, as reported in Chapter 3 in Figures 3.7, 3.8. A complete charge and discharge of the of the system was carried out, as reported in Figure 6.53.

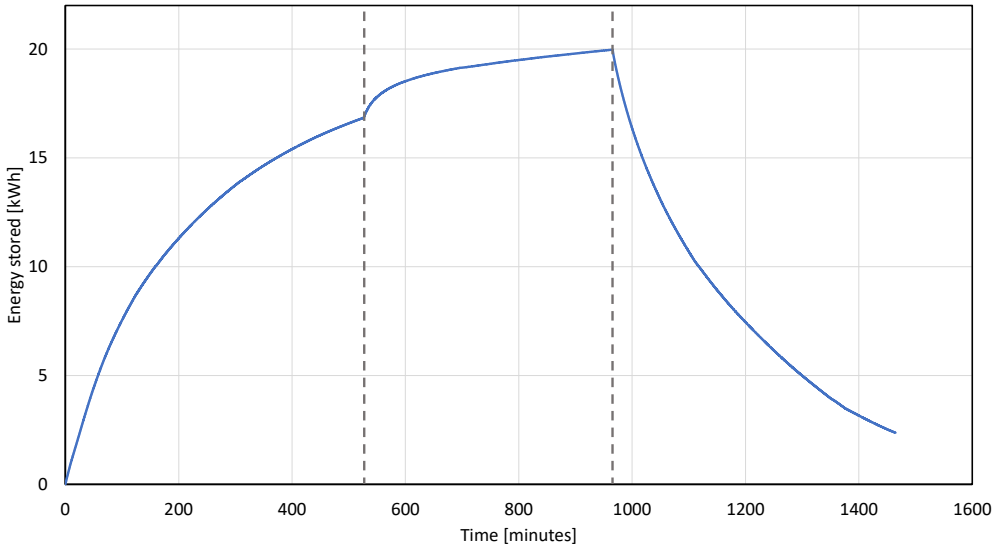

Figure 6.53: Graph of the energy stored with the new complete parallel configuration of the roll-bond, flow rate of 17 l/min and water temperature of 2 °C for the charges and 16 °C for the discharges.

The test was divided in three days. The first day the system was charged up to 16.8 kWh, for the night the climatic room was turned off and therefore the PCM lost some energy. Thus the following day it had been decided to do another charging phase to make sure the PCM was completely charged (this is the slope change in the charging phase visible in Figure 6.53). Finally the third day the discharging phase was done. In Figure 6.54 the average temperatures of the planes are reported. The temperatures fluctuations are due to the nights where the temperature has been redistributed and when switching from charging to discharging phase and vice versa.

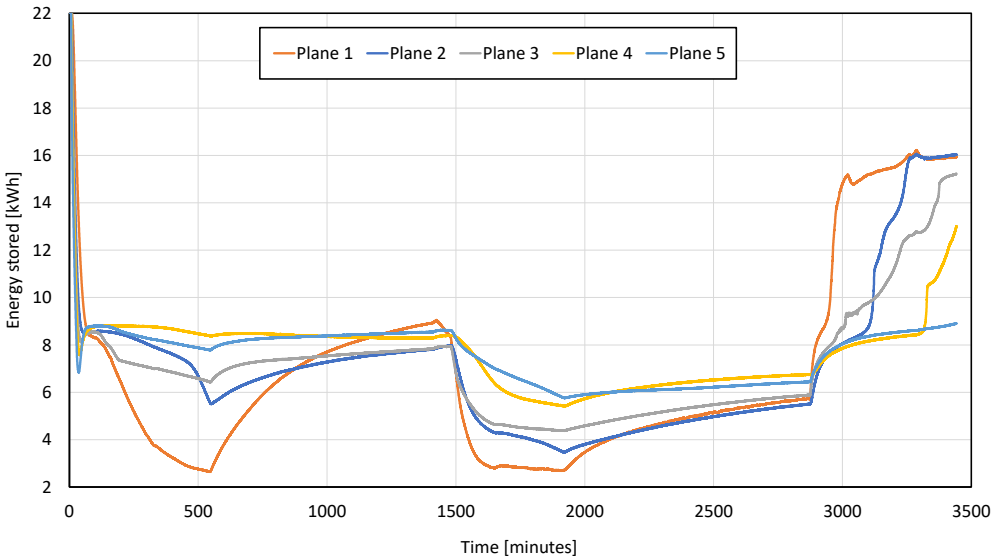

Figure 6.54: Average temperatures of the planes with the new complete parallel configuration of the roll-bond, flow rate of 17 l/min and water temperature of 2 °C for the charges and 16 °C for the discharges.

6.2 Flow rate influence

6.2.1 Comparison between tests 10-11-14

In Figure 6.55 the energy stored during different tests can be seen. In detail, the comparison between test 10, 11 and 14 is presented. The inlet water temperature was kept constant for the three tests, only the flow rate was changed. In test 10 the flow rate was 10 l/min, in test 11 was 17 l/min and finally in test 14 was 8.5 l/min. It can be seen that the higher the flow rate, the higher the energy stored. In detail, by doubling the flow rate, the energy stored in 4 hours increases by 30%, that is less than linear.

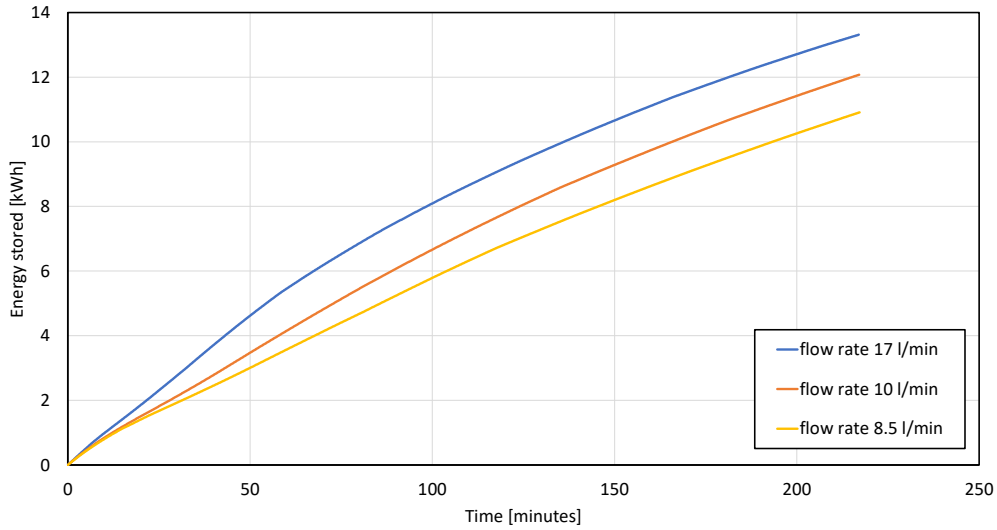

Figure 6.55: Flow rate influence during the charging phase. Tests run with flow rates equal to 17,10 and 8.5 l/min, inlet water temperature of 2 °C.

In addition, in Table 6.1 the times required to store 10 kWh of energy for each test are reported. As expected, higher flow rate tests required less time to store the same amount of energy.

Test	Flow rate [l/min]	Time required to store 10 kWh [minutes]	Difference
11	17	136	
10	10	166	18% slower
14	8.5	193	30% slower

Table 6.1: Time required to store 10 kWh with different flow rates (17, 10 and 8.5 l/min) and same water temperature of 2 °C

6.2.2 Comparison between tests 3-5-8-12

In Figure 6.56 the energy stored during tests collected at different flow rates are reported, all of them have the same inlet water temperature, fixed at 6.5 °C. The flow rate is 20 l/min for test 3, 40 l/min for test 5, 10 l/min for test 8 and 30 l/min for test 12.

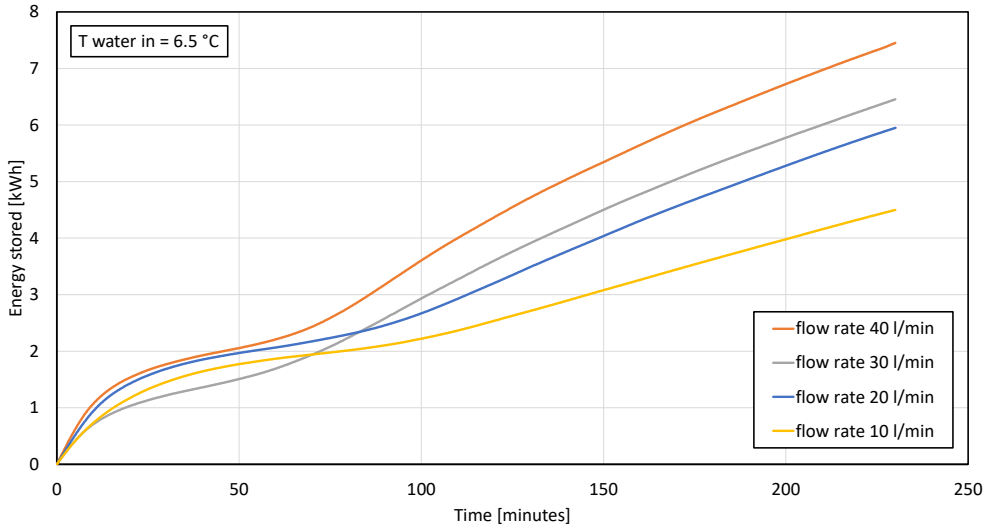

Figure 6.56: Flow rate influence during the charging phase. The comparison is between: test 3 (flow rate 20 l/min), test 5 (flow rate 40 l/min), test 8 (flow rate 10 l/min), test 12 (flow rate 30 l/min); the water temperature was 6.5 °C.

In Table 6.2 the time required to store 4 kWh of energy at different flow rates is reported. In this case, the inlet water temperature was set at 6.5 °C, so the results differ from the ones presented in Table 6.1 : the energy stored is lower due to the higher water temperature used during the charging phase.
If the two Figures 6.55 and 6.56 are compared the flow rate influence can be evaluated, in fact if the flow rate is halved the system is about 30% slower.

Test	**Flow rate** [l/min]	**Time required to store 4 kWh** [minutes]	**Difference**
5	40	110	
12	30	133	17% slower
3	20	150	26% slower
8	10	200	45% slower

Table 6.2: Time required to store 4 kWh at different flow rates and same inlet water temperature 6.5 °C

6.3 Temperature influence

6.3.1 Charging phase

In Figure 6.57 the energies profiles for three tests with different water temperatures are reported. The flow rate was kept constant at about 10 l/min, instead the water temperature was varied. For test 23 the temperature was 4 °C, for test 8 was 6.5 °C and for test 10 was 2 °C.

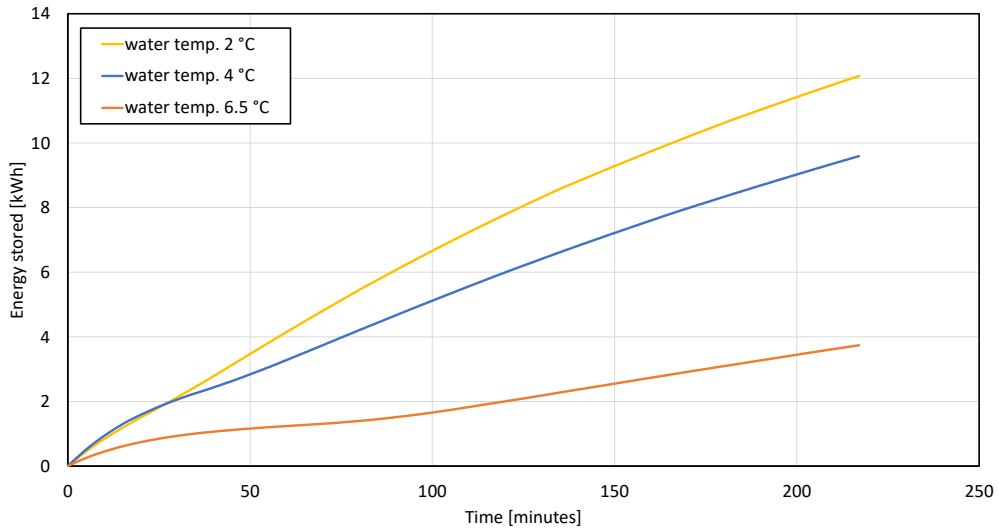

Figure 6.57: Temperature influence on the energy stored. The comparison is between: test 10 (water temperature 2 °C), test 23 (water temperature 4 °C), test 8 (water temperature 6.5 °C); the flow rate was kept constant at 10 l/min.

In Table 6.3 the energy stored in the three test after 200 minutes is reported. It was set this time span because test 8 is too slow to be compared to the other two. The temperature difference strongly influences the test duration, especially when very small ΔT are applied. It can be clearly seen Table 6.3 how the water temperature at 6.5 °C is not cold enough and the system is extremely slow to store energy. Thus it has been decided to compare the other two tests.

Test	Water inlet temperature [°C]	Energy in 200 minutes [kWh]	Difference
10	2	11.44	
23	4	9	21% lower
8	6.5	3.5	70% lower

Table 6.3: Energy stored after 200 minutes at different inlet water temperatures, the flow rate was kept constant at 10 l/min

In Table 6.4 a comparison between test 10 (inlet water temperature = 2 °C) and 23 (inlet water temperature

= 4 °C) is reported. Test 23 is about 25% slower in storing energy when compared to test 10 which was chosen as a reference.

Test	Water inlet temp. [°C]	Time to store 4 kWh [minutes]	Difference
10	2	58	
23	4	76	24% slower
Test	**Water inlet temp [°C]**	**Time to store 8 kWh [minutes]**	**Difference**
10	2	125	
23	4	171	27% slower

Table 6.4: Time required to store 4 kWh and 8 kWh at different inlet water temperatures, the flow rate was kept constant at 10 l/min

6.3.2 Discharging phase

In Figure 6.58 the energy profiles of the discharging process at different temperatures (14, 19 and 24 °C) are reported. All the tests were collected at the same flow rate of 40 l/min. In test 5 (water inlet temperature is equal to 14 °C) the PCM average temperature reaches the final temperature asymptotically. This is probably due to the lower plane that remains 6 or 7 °C lower than others, thus there is a colder zone at the bottom of the tank that endures also at the end of the test, as reported in Figure 6.22.

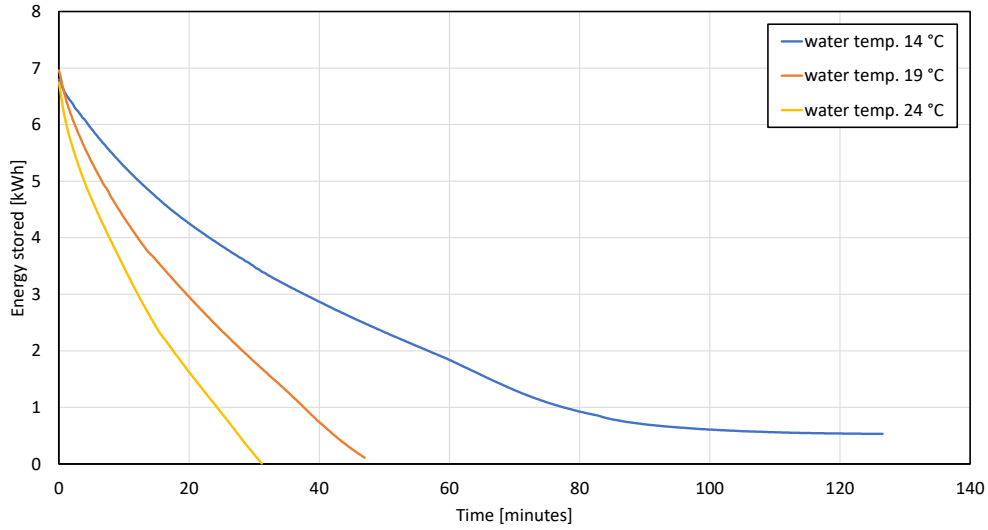

Figure 6.58: Discharges at different water inlet temperatures, 14 °C for test 5, 19 °C for test 6 and 24 °C for test 7; the flow rate was kept constant at 40 l/min.

In Table 6.5 the times required to discharge the system with different water temperatures (14, 19 and 24 °C; flow rate was kept constant at 40 l/min) are reported. As reported in this table a higher water inlet temperature ($\Delta T = 14$ °C $+41\%$) reduces the time required to discharge the system (-76%).

Test	**Water inlet temperature** [°C]	**Discharge duration** [minutes]	**Difference**
5	14	127	
6	19	47	63% faster
7	24	31	76% faster

Table 6.5: Time required for the discharge with different water inlet temperatures

6.4 Parallel configuration

In order to evaluate the effectiveness of the parallel configuration a comparison between test 11 (flow rate 17 l/min), 14 (flow rate 8.5 l/min), 27 (flow rate 8.5 l/min) and 28 (flow rate 17 l/min) was done, the inlet water temperature was kept constant at 2 °C. The difference in these tests is the configuration used (parallel of series or complete parallel, see Figure 3.7) and the water flow rate used. In Figure 6.59 the energies during the charging phase of the four tests are reported. Both test 11 and 14 had the old water configuration (parallel of series), instead, the configuration was changed to complete parallel for tests 27 and 28.

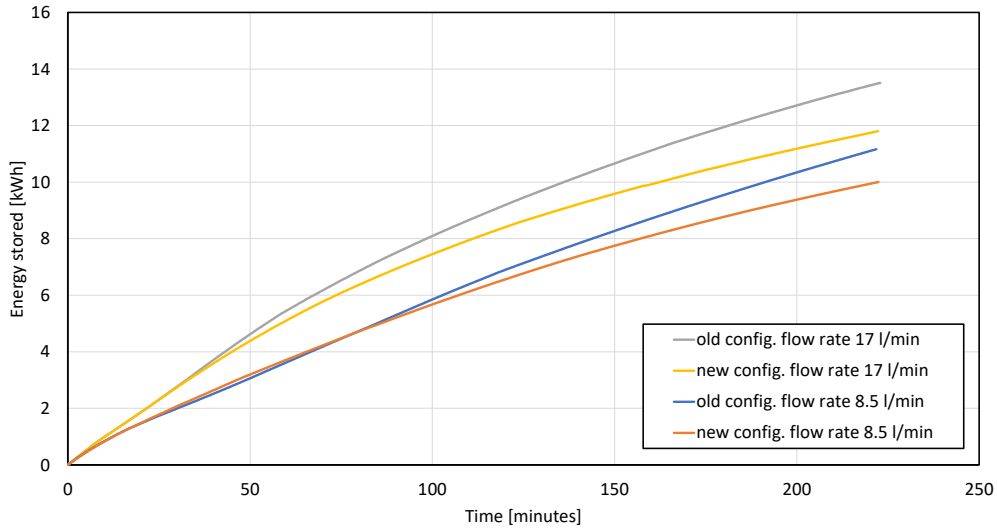

Figure 6.59: Influence of the configuration on the energy stored at different flow rates. Test 14 uses the old configuration and a flow rate of 8.5 l/min. Test 11 uses the old configuration and a flow rate of 17 l/min. Test 27 uses the old configuration and a flow rate of 8.5 l/min. Test 28 uses the old configuration and a flow rate of 17 l/min.

The comparison was done between these four tests to have the possibility to compare the same actual flow rate inside the single roll-bond. In fact with the configuration of parallel of series the flow-rate coming from the inlet manifold is splitted in 8, because there are 16 roll-bonds and they are connected in parallel of pairs, the roll-bonds of each pair are connected in series. Instead with the complete parallel configuration the flow rate is splitted in 16. Thus with the old configuration the flow rate passing thorough a single roll-bond is twice as much compared to the new configuration, for this reason test 28 (with 17 l/min of flow rate) should be compared to test 14 (8.5 l/min flow rate), on the LTES point of view. On the other hand, if one wanted to analyze the integrated LTES to plant system, should compare tests having the same inlet flow rate (test 28 compared to test 11).
In Figure 6.60 the energy stored for every hour of the charging phase of the four tests are reported. The tests have a very similar behaviour, only in the first hour the difference is bigger, this may be caused by the different flow rate inside the single roll-bond.

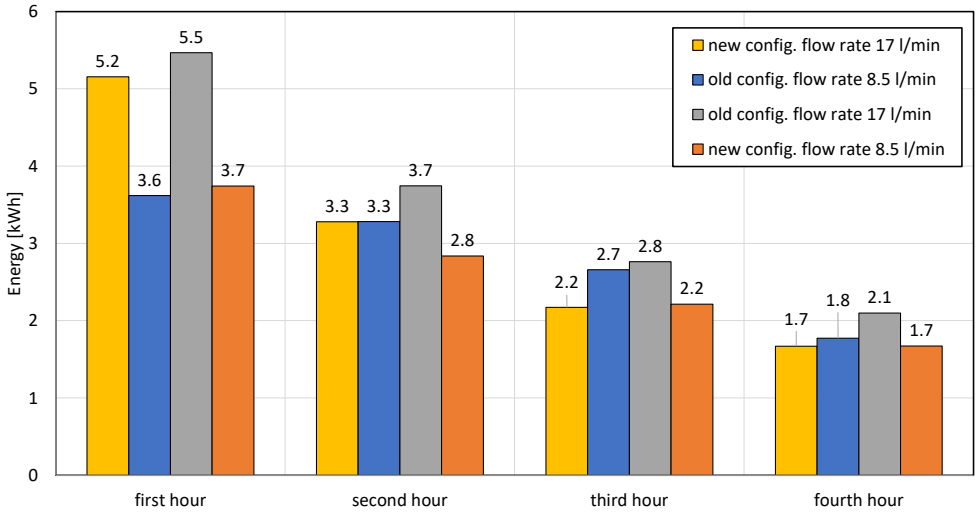

Figure 6.60: Energy stored every hour for test 11 (old configuration and flow rate 17 l/min), 14 (old configuration and flow rate 8.5 l/min), 27 (new configuration and flow rate 8.5 l/min) and 28 (new configuration and flow rate 17 l/min); the inlet water temperature was kept constant at 2 °C

In Figure 6.61 a comparison between test 14 and 28 is reported. Test 14 has the parallel of series water configuration and a flow rate of 8.5 l/min, instead for test 28 the roll-bonds are connected all in parallel and the flow rate was 17 l/min. In the first hour of charging with the new configuration allows to store 30% more energy, for the following hours the difference in energy stored is negligible.

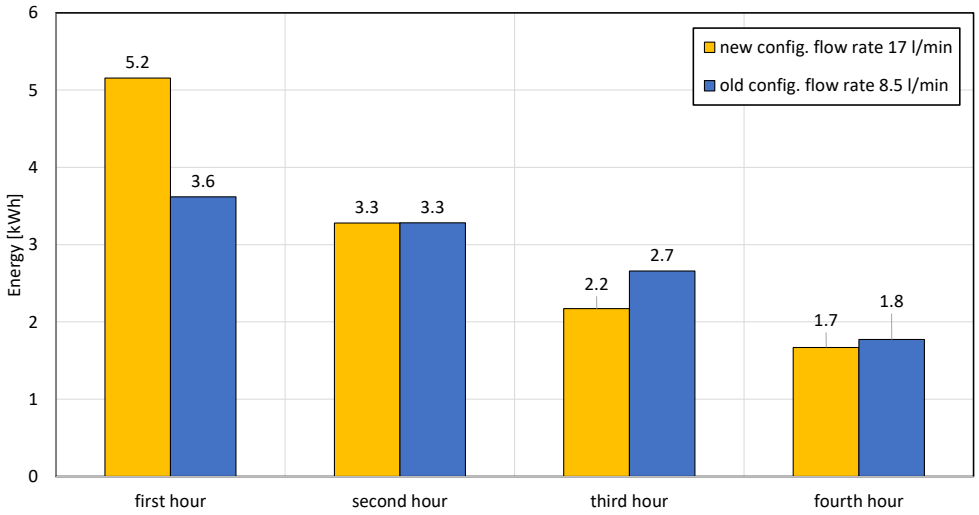

Figure 6.61: Energy stored every hour for test 14 (old configuration and flow rate 8.5 l/min) and 28 (new configuration and flow rate 17 l/min)

7 Numerical analysis

In this part of the work the system has been numerically studied in order to evaluate some other configurations that are not possible to try in the lab, this part of the study was done together with PhD student Shengqi Zhang.

7.1 Physical model

Initially a 2D model was created for the simulations, this way the computational power required is lower. However the experimental tests were very long (even more than 10 hours) thus the time required for every simulation is still pretty long. On the left of Figure 7.1 the physical model is reported. As already stated the model is two-dimensional, it is a slice of the system between a pair of roll-bonds. The connection method of the roll-bonds has been discussed in Chapter 3, there are 8 pairs of roll-bond connected in parallel, instead the roll-bonds of each pair are connected in series. Thus, assuming the water flow rate is the same for every pair and that they are all perfectly equal, it is enough to study the behaviour of the system between the roll-bonds of a pair. There is only half of the roll-bond on the left and on the right, in the middle there is the PCM. The dimensions of the model can be seen in Figure 7.1 (left) and are the same as the real system, on the right of Figure 7.1 the mesh can be seen. The two roll-bonds on the sides are meshed in green, instead the PCM in the middle is meshed in purple/blue. The mesh size increases from the sides to the middle, the size along the height of the PCM is kept constant in order to limit the number of elements used.

7.1.1 Boundary and initial conditions

The boundary conditions are symmetry on the left and right side, adiabatic at the top and at the bottom. Symmetry means $\frac{\partial T}{\partial n} = 0$, where T is the temperature and n is the normal vector perpendicular to the plane of symmetry. Instead adiabatic means there is no heat or mass transfer through the boundary. The experimental data was used

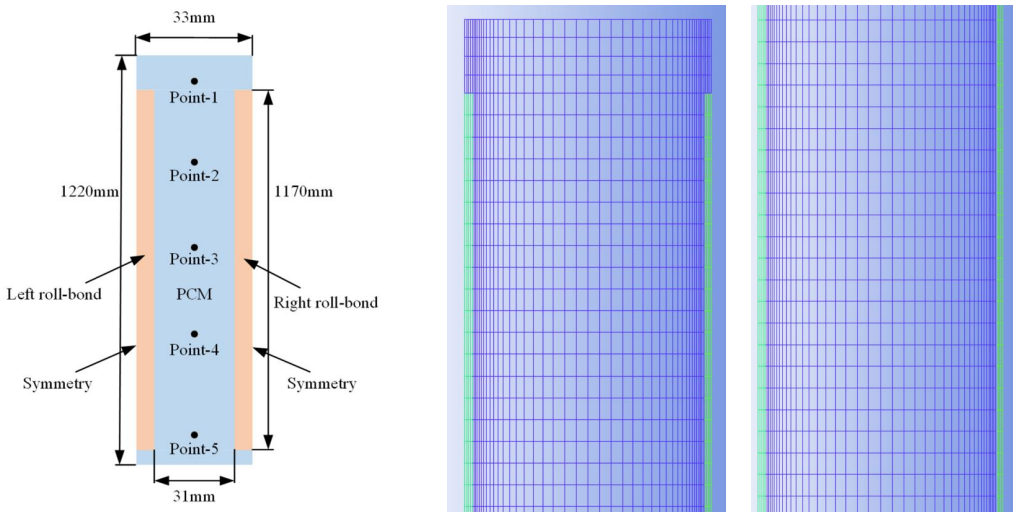

Figure 7.1: Model (not to scale) used for the simulations (left) and mesh of the same model (right)

for the initial conditions of the simulations. Further, the temperature of the left roll-bond was set equal to the inlet water temperature from the experimental data, instead the right roll-bond was set the same as the outlet water temperature.

7.2 Governing equations

For the numerical analysis the commercial CFD software ANSYS FLUENT was used. In order to investigate the behaviour during phase change of the PCM the "Solidification and Melting Model" was used. The SIMPLE scheme was used in order to solve the pressure-velocity coupling, instead PRESTO! was used for the pressure correction. For the zone that is changing phase (labeled mushy zone) the model uses the enthalpy-porosity approximation, this zone is considered porous and the liquid fraction is set as the porosity. The liquid fraction indicates the amount of liquid in each cell volume, this is calculated for all the cells in the domain, the liquid fraction can vary between 0 (PCM is solid) and 1 (PCM is liquid).

7.2.1 Continuity equation

$$\frac{\partial u}{\partial x} + \frac{\partial v}{\partial y} = 0 \tag{7.1}$$

where the u is the x-direction velocity
and the v is the y-direction velocity

7.2.2 MOMENTUM EQUATION

$$\frac{\partial(\rho u)}{\partial t}+\frac{\partial(\rho u u)}{\partial x}+\frac{\partial(\rho u v)}{\partial y}=-\frac{\partial P}{\partial x}+\frac{\partial}{\partial x}\left(\mu\frac{\partial u}{\partial x}\right)+\frac{\partial}{\partial y}\left(\mu\frac{\partial u}{\partial y}\right)+S_u \tag{7.2}$$

$$\frac{\partial(\rho v)}{\partial t}+\frac{\partial(\rho u v)}{\partial x}+\frac{\partial(\rho v v)}{\partial y}=-\frac{\partial P}{\partial x}+\frac{\partial}{\partial x}\left(\mu\frac{\partial v}{\partial x}\right)+\frac{\partial}{\partial y}\left(\mu\frac{\partial v}{\partial y}\right)+S_v \tag{7.3}$$

S_u and S_v are the momentum source items

$$S_u=-Au \tag{7.4}$$

$$S_v=-Av+\rho g\alpha(T-T_{ref}) \tag{7.5}$$

The reference temperature $T_{ref}=282.15$ K, α is the thermal expansion coefficient of the PCM, g is the gravitational acceleration, ρ is the density, ε is a small computational constant, μ is the viscosity.

$$A=-C_{mushy}\frac{(1-f)^2}{f^3+\varepsilon} \tag{7.6}$$

C_{mushy} is the mushy zone constant,
f is the liquid fraction of the PCM and is defined as follows:

$$\begin{cases}0 & T<T_s\\ \dfrac{T-T_s}{T_l-T_s} & T_s\le T\le T_l\\ 1 & T_l<T\end{cases} \tag{7.7}$$

7.2.3 ENERGY EQUATION

$$\frac{\partial(\rho h)}{\partial t}+\frac{\partial(\rho v h)}{\partial x}+\frac{\partial(\rho v h)}{\partial y}=\frac{\partial}{\partial x}\left(\lambda\frac{\partial T}{\partial x}\right)+\frac{\partial}{\partial y}\left(\lambda\frac{\partial T}{\partial y}\right)+S_h \tag{7.8}$$

S_h is the energy source term. For the HTF $S_h = 0$, instead for the PCM $S_h = -\rho L_p \frac{\partial f}{\partial t}$.
Enthalpy h is defined as follows:

$$\begin{cases} \int_{T_{ref}}^{T} c_p dT & T < T_s \\ \int_{T_{ref}}^{T_s} c_p dT + fL_p & T_s \leq T \leq T_l \\ \int_{T_{ref}}^{T_s} c_p dT + \int_{T_l}^{T} c_p dT & T_l < T \end{cases} \tag{7.9}$$

7.3 Thermophysical properties of PCM, HTF, Fins

The thermophysical properties of the roll-bond and HTF are reported in Table 7.1, instead for the properties of the PCM refer to Table 3.1. As already explained the roll-bond is made out of aluminium sheets, thus the thermophysical properties are similar to that of pure aluminium. For the PCM the specific heat in the simulations was set as piecewise linear according with temperature change.

Property	HTF (water)	Roll-bond
Density (kg m^{-3})	998.2	2719
Specific heat (J kg^{-1} K^{-1}	4182	871
Thermal conductivity (W m^{-1} K^{-1})	0.6	202.4
Dynamic viscosity (Pa s)	0.001003	-

Table 7.1: Thermophysical properties for HTF and roll-bond

7.4 Numerical procedure

The model was discretised using ANSYS-ICEM by structure grids and it is reported in Figure 7.1 (on the right). Instead the governing equations were discretised using the Finite Volume Method. The solution was considered to be converged when the residuals of continuity and momentum were less than 10^{-6} and energy equations were less than 10^{-9} at each time step. The maximum number of iteration for each time step was set to 30.
Three sets of time steps (0.1s, 0.2s and 0.5s) and three sets of grid numbers (5382, 20352 and 40672) were studied. A grid number of 20352 and time step of 0.2s are enough to ensure the calculation accuracy.

7.5 Numerical Validation

In order to validate the numerical model the numerical results were compared to the experimental data, this can be seen in Figures 7.2, 7.3, 7.4, 7.5.

7.5.1 Temperatures

In Figure 7.2 and 7.3 a comparison between the average temperatures of the planes of the experimental data (continuous line) and the temperatures at different heights of the numerical simulation (dashed line) for test 2 are reported. The same comparison was done also for test 3, as reported in Figure 7.3

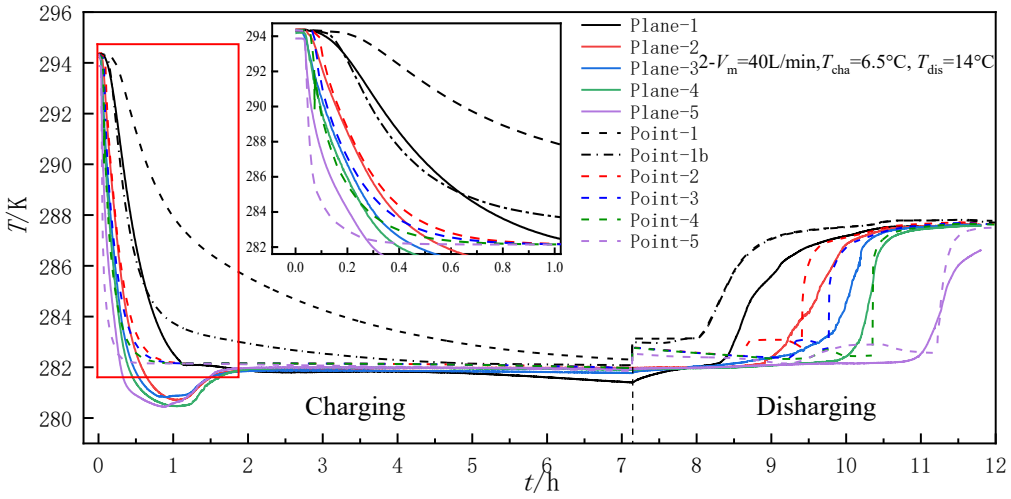

Figure 7.2: Validation test 2

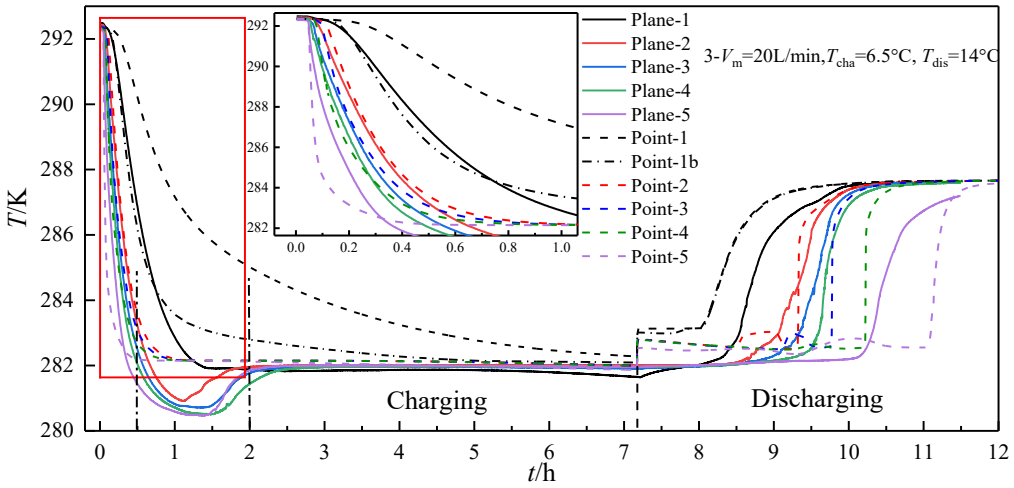

Figure 7.3: Validation test 3

For both Figures 7.2 and 7.3 it can be seen that the numerical results are very close to the experimental data with the exception of plane 1. The first plane, as already stated (see Figure 6.23), in the experimental data is not representative. The difference in results is due to the impossibility of numerically modeling the subcooling phenomenon, this is also why there is a difference in the energy stored as reported in Figures 7.4 and 7.5.

7.5.2 Energy stored

In Figures 7.4 and 7.5 the numerical results are validated with the experimental data of test 2 and 3 considering the energy stored. The red line describe the energy stored in the simulations, instead the black line depict the energy stored in the experimental tests. The energy stored in the experimental results have a slope change due to

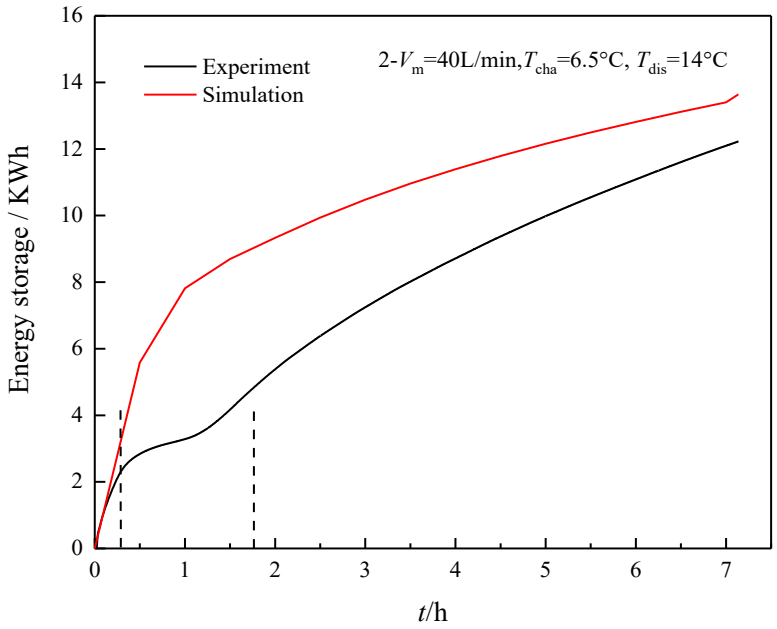

Figure 7.4: Comparison of energy stored from experimental and numerical results (test 2)

the subcooling phenomenon, this can not be modeled in the simulations. Thus, the difference between the two curves in Figures 7.4 and 7.5.

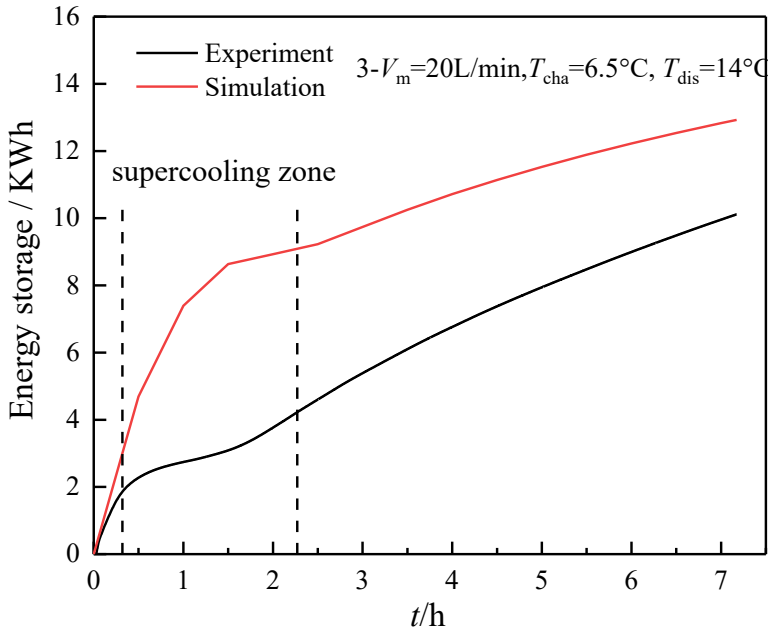

Figure 7.5: Comparison of energy stored from experimental and numerical results (test 3)

8

Numerical results

8.1 Different circuiting

In Figure 8.1 the liquid fraction inside the PCM domain during the solidification process (charging phase) is reported. It can be seen, as was assumed during the experimental results, that the solid start to forms from the roll-bond to the center. The same can be seen for the new water circuitation (complete parallel) in Figure 8.2, thus the circuiting has little to no influence, this is also confirmed in the liquid fraction graph comparison in Figure 8.3 and 8.4.

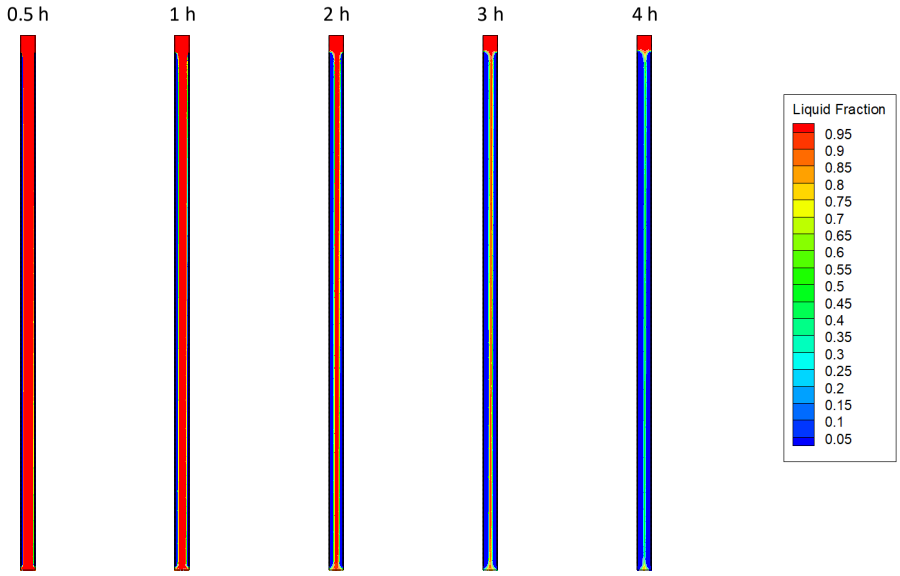

Figure 8.1: Liquid fraction in the PCM zone with the configuration of parallel of series.

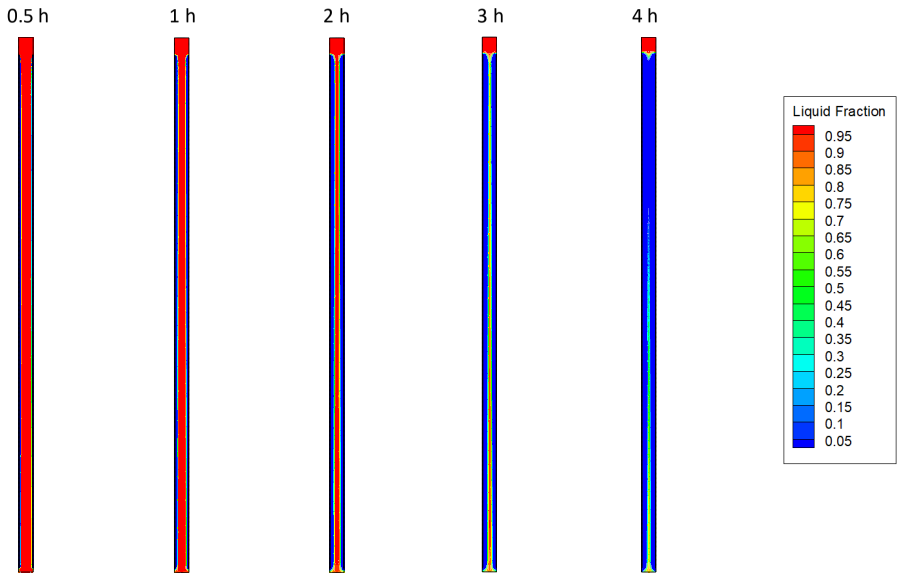

Figure 8.2: Liquid fraction in the PCM zone with the complete parallel configuration.

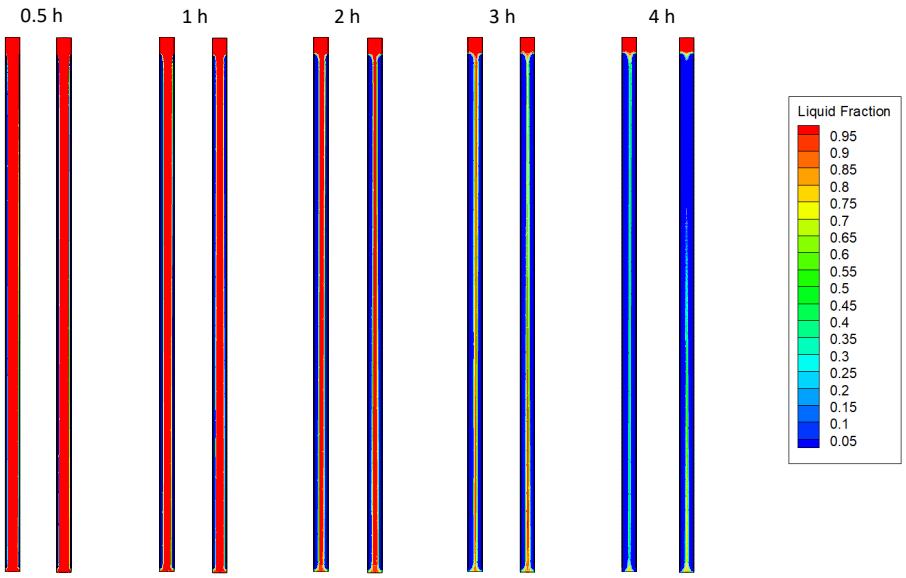

Figure 8.3: Side by side comparison between the two configurations (parallel of series and complete parallel).

In Figure 8.4 the liquid fraction comparison between the two configurations in the simulation is reported. Liquid fraction is a good indicator for the charging effectiveness and speed. It can be seen that the difference is limited exactly like the experimental results about the water configuration (6.61).

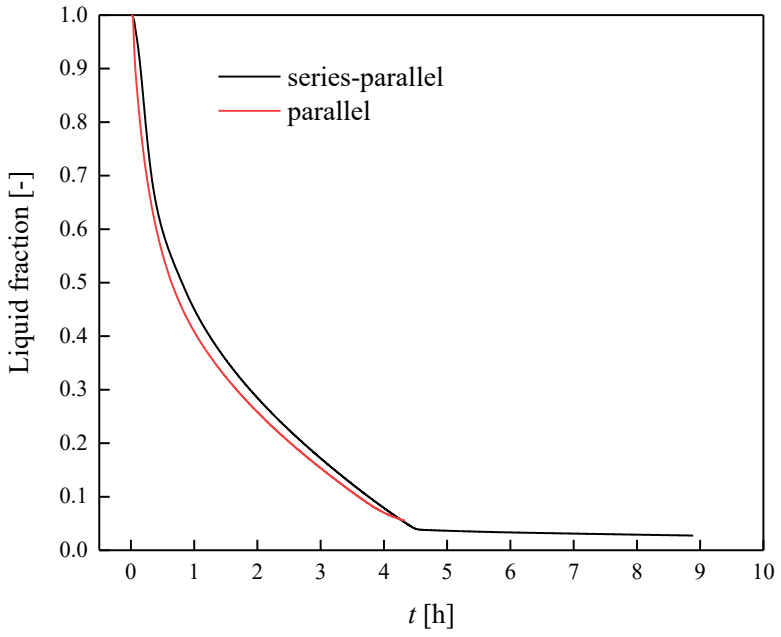

Figure 8.4: Liquid fraction comparison between the two configurations for the charging phase.

8.2 Distance optimization

It was decided to numerically study the influence of the distance between the roll-bonds, the distance in the previous simulations was 31 mm and in this section also the 25, 28, 34 and 37 mm distances were evaluated. In Figure 8.5 the influence of the distance between the roll-bonds for the charging phase is reported. The influence in the discharging phase is reported in Figure 8.6. It can be seen that for both the charging and discharging phases a smaller distance between the roll-bond can significantly reduce the time required to charge and discharge the system, this can also be seen in Figure 8.7.

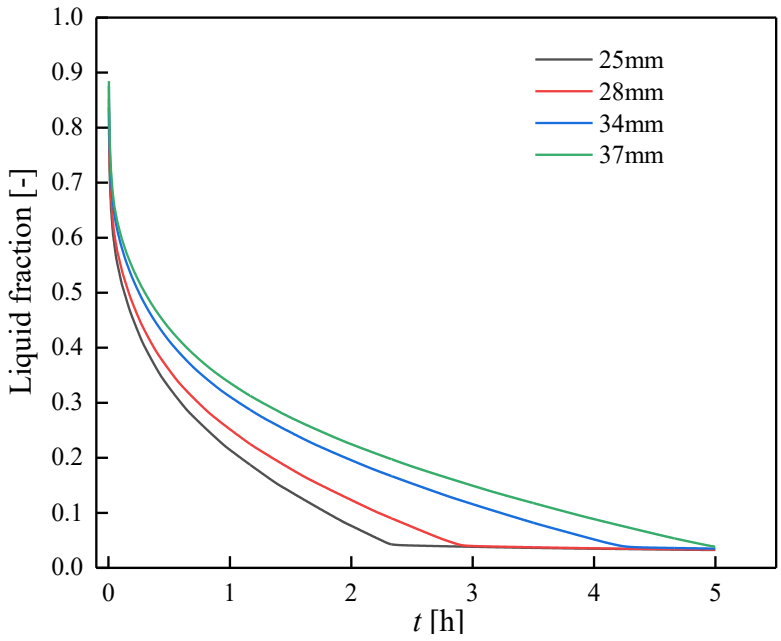

Figure 8.5: Influence of the distance between the roll-bonds in the charging phase

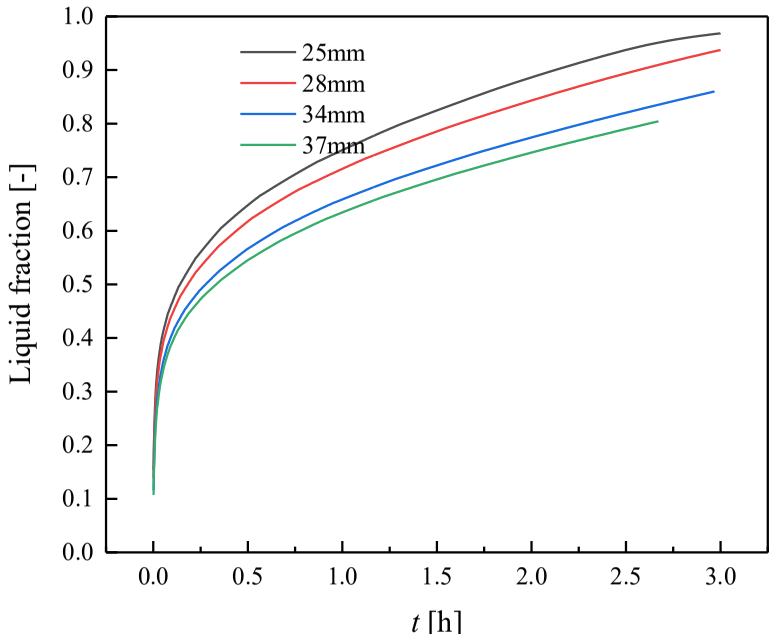

Figure 8.6: Influence of the distance between the roll-bonds in the discharging phase.

In Figure 8.7 a side by side comparison between the 31 mm and 25 mm distances is reported. The solidification process is faster with a smaller distance between the roll-bonds.

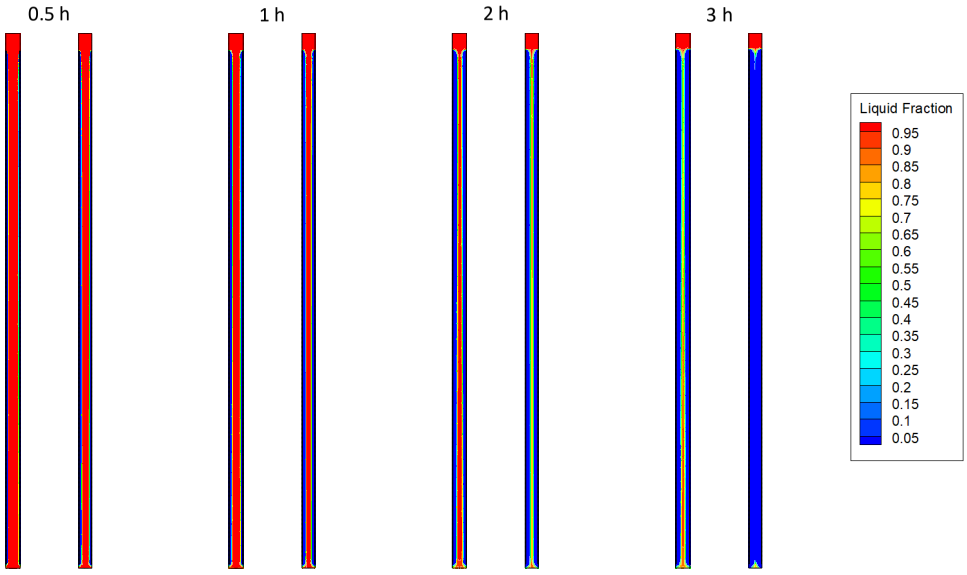

Figure 8.7: Comparison of 31 mm and 25 mm distances between the roll-bonds.

Missing data

There are some thermophysical properties of the PCM that are missing, such as the thermal expansion coefficient and the viscosity of the PCM. These can greatly influence the accuracy of the simulations.

9 Conclusions

In this work a PCM based latent thermal energy storage for air-conditioning applications was experimentally and numerically studied. The focus of the work was to build the experimental setup in order to evaluate the system behaviour under several working conditions. To reach this goal, a large number of thermocouples were embedded in the tank to monitor the temperature field and data was recorded by means of a dedicated acquisition system (IPR, acquisition system, labview program). Also a numerical model was used to study others configurations that could not be done experimentally.

The main observations made are as follows:

- It was observed that the system takes more than 8 hours to complete the charging and discharging phases. So some optimization should be done in order to shorten the system's charging and discharging times.
- In order to reduce the time required for charging the system, the inlet water temperature was decreased to 2 °C, even if the AC efficiency decreases as reported in the Equation 1.3.2. Furthermore if the inlet water temperature needs to decrease even more, pure water can no longer be used but some glycol needs to be added in order to decrease the freezing temperature of the mixture.
- It was observed that for both the charging and discharging phases the inlet water temperature has a greater influence than the water flow rate. So it is suggested to carefully select it.
- The swapping between inlet and outlet water manifolds resulted in no difference between the two configurations. This was confirmed by the roll-bond design's symmetry.
- Instead the different circuiting (complete parallel) of the water inside the roll-bonds slighty improves the energy stored during the first hour. This is because the heat transfer resistance is in the PCM side.
- It was found that the 2D simulations adequately describe the behaviour of the real system. The two water circuiting were also numerically studied and compared and the results are very similar to the experimental results.

- The distance between the roll-bonds was studied in the simulations, this has a big influence on charging and discharging times, thus this parameter should be optimized. This is not easy to do experimentally, thus numerical simulations can help a lot.
- In the tested geometry, roll-bond plates are located a few centimeters from the bottom of the tank. This lead to an area at the bottom of the tank where the heat transfer happens through convection in the melted material and conduction in the alluminium structure that holds the roll-bond plates, thus it is very slow. Indeed a part of the energy stored in the PCM can not be extracted in a reasonable amount of time.

Some suggested future developments are listed below:

- Experimental measurements of viscosity and thermal expansion coefficient of the PCM should be done in order to improve the accuracy of the simulations.
- Simulations of the 3D system should be run to better depict the real system and the newer roll-bond configuration (complete parallel).
- The optimization of the tank geometry, (for instance the height to width ratio) should be taken into consideration.
- The roll-bond design and the water path in the roll-bond should also be improved in order to increase the heat transfer from the water to the PCM.
- The effects of the number of roll-bonds and distance between roll-bonds should be studied.
- Different materials should be tested to adapt the LTES to other system requirements.
- Next, the interaction between the LTES and the heat pump should be carefully investigated, to optimize the whole system efficiency.

References

[1] "International energy agency iea," www.iea.org.

[2] "Global renewables outlook: Energy transformation 2050," *International Renewable Energy Agency, Abu Dhabi*, 2020.

[3] "United nations," https://www.un.org/en/climatechange/paris-agreement.

[4] P. K. Adom, W. Bekoe, F. Amuakwa-Mensah, J. T. Mensah, and E. Botchway, "Carbon dioxide emissions, economic growth, industrial structure, and technical efficiency: Empirical evidence from ghana, senegal, and morocco on the casual dynamics," *Energy, 47:314-325*, 2012.

[5] L. F. Cabeza and M. Chàfer, "Technological options and strategies towards zero energy buildings contribuiting to climate change mitigation: A systematic review," *Energy buildings, 219 (2020) 110009*, 2020.

[6] G. Pinto, Z. Wang, A. Roy, T. Hong, and A. Capozzoli, "Transfer learning for smart buildings: A critical review of algorithms, applications, and future perspectives," *Advances in Applied Energy, 5 (2022) 100084*, 2022.

[7] G. Chiesa, D. D. Vita, A. Ghadirzadeh, A. H. M. Herrera, and J. C. L. Rodriguez, "A fuzzy logic iot lighting and shading control system for smart buildings," *Automation in Construction, 120 (2020) 103397*, 2020.

[8] J. Drgoňa, J. Arroyo, I. C. Figueroa, D. Blum, K. Arendt, D. Kim, E. P. Ollé, J. Oravec, M. Wetter, D. L. Vrabie, and L. Helsen, "All you need to know about model predictive control of buildings," *Annual Reviews in Control, 50 (2020) 190-232*, 2020.

[9] "Innovation outlook: Thermal energy storage," *International Renewable Energy Agency, Abu Dhabi*, 2020.

[10] H. Jouhara, A. Żabnieńska Góra, N. Khordehgah, D. Ahmad, and T. Lipinski, "Latent thermal energy storage technologies and applications: A review," *International Journal of Thermofluids, 5-6 (2020) 100039*, 2020.

[11] S. Chandel and T. Agarwal, "Review of current state of research on energy storage, toxicity, health hazards and commercialization of phase changing materials," *Renewable and Sustainable Energy Reviews, 67 (2017) 581-596*, 2017.

[12] E. Oró, A. de Garcia, A. Castell, M. Farid, and L. Cabeza, "Review on phase change materials (pcms) for cold thermal energy storage applications," *Applied Energy, 99 (2012) 513-533*, 2012.

[13] C. Veerakumar and A. Sreekumar, "Phase change material based cold thermal energy storage: Materials, techniques and applications - a review," *International Journal of Refrigeration, 67 (2016) 271-289*, 2016.

[14] L. Fan and J. Khodadadi, "Thermal conductivity enhancement of phase change materials for thermal energy storage: A review," *Renewable and Sustainable Energy Reviews 15 (2011) 24-46*, 2011.

[15] M. Al-Maghalseh and K. Mahkamov, "Methods of heat transfer intensification in pcm thermal storage systems: Review paper," *Renewable and Sustainable Energy Reviews 92 (2018) 62-94*, 2018.

[16] P. Sivasamy, A. Devaraju, and S. Harikrishnan, "Review on heat transfer enhancement of phase change materials (pcms)," *Materials Today: Proceedings 5 (2018) 14423-14431*, 2018.

Acknowledgments

I would like to thank the professors: Claudio Zilio, Giulia Righetti and Simone Mancin that allowed me to work in the thermotechnics laboratory for my master's thesis. A big thanks also goes to Sergio Storato for helping with the experimental tests done in the lab.
I also want to thank my family: my mom Luciana and dad Alberto, my brothers Riccardo and Fabrizio for all the help they gave me and putting up with me. A special thanks goes to my grandma Romana and my uncle Stefano that always supported me even if they were far away in South Africa, also a big thanks goes to all my family that stills lives there. I also want to say a big thank you to all my friends, the Malleogra's group with Simone (Pietro, Pietro Simonelli), Matteo (Berlaffa), Federico (Speed, Fed), Denis (Tennis, Lović) and Marco (Feddy, Il quadrato, Farco, Gardologo). I want to give credit to Matteo Berlato for how much he helped me in my second year of the master degree, especially for "Meccanica delle Vibrazioni (disperazioni)", and for the countless hours spent on zoom studying together when we were in lockdown and at the library when lockdown ended.
A big shout out goes to all the friends that I had fun with on the endless train trip each day on the "minuetto" from Thiene to Vicenza and back. To all my university friends I want to say thank you for making these last few years unforgettable. It is impossible for me to name everyone but I want to thanks all my friends that have been there during this though journey.
Finally I have to give credit to myself for never giving up and reaching this incredible goal.